MINIATURIZING IRON DETERMINATIONS: ADAPTING THE DPD-Fe
CHEMISTRY TO A MICRO-SEQUENTIAL INJECTION ANALYSIS PLATFORM

A THESIS SUBMITTED TO THE GRADUATE DIVISION OF THE UNIVERSITY
OF HAWAIʻI AT MĀNOA IN PARTIAL FULFILLMENT OF THE REQUIREMENTS
FOR THE DEGREE OF

MASTER OF SCIENCE

IN

OCEANOGRAPHY

DECEMBER 2016

By

Gabrielle A. Weiss

Thesis Committee

Christopher I. Measures, Chair

Jaromir (Jarda) Ruzicka

Eric H. DeCarlo

## DEDICATION

This thesis is dedicated to my family: Sheryl Grabow-Weiss, Michael Weiss, Aleen (Nini) Grabow, and Helen Grabow. Without your continued love and support I never could have followed my dreams to become an oceanographer and finished this thesis. This thesis is also dedicated to Kaitlin Prugger. You were the sunshine in the laboratory every day and even though we lost you far too early, every obstacle I encountered during this thesis could be overcome by thinking of you and what sassy remark you would make if you were here. I miss you and think of you everyday and this work is in your memory.

## ACKNOWLEDGEMENTS

# TABLE OF CONTENTS

# LIST OF TABLES

# LIST OF FIGURES

# CHAPTER 1: Introduction

Iron (Fe) is the fourth most abundant element in Earth's crust by weight (5.6%); however concentrations of Fe in seawater are extremely low, ranging from subnanomolar to nanomolar levels as a result of the low solubility of Fe in seawater and its biological uptake (Johnson et al., 1997). In well oxygenated, pH~8 seawater the relevant Fe species are Fe(II) and Fe(III), with Fe(III) being the dominant, thermodynamically stable, and relatively insoluble species. The Fe(II) species is soluble in seawater but is not thermodynamically stable in oxygenated seawater at pH~8 (Johnson et al., 1997; Wells et al., 1995). The limited solubility of Fe in seawater means that Fe concentrations can be elevated in the immediate proximity of sources but decline rapidly away from the source. Thus, mapping the distributions of Fe can be useful in identifying Fe inputs.

Fe in seawater can be further characterized operationally by size fraction using filtration. Fe in seawater can be characterized by filtration as particulate Fe (pFe >0.4µm or >0.2µm) or dissolved Fe (dFe <0.2µm or <0.4µm; the latter of which is further characterized as truly soluble (sFe <0.02µm) or colloidal (cFe =0.02µm-0.2µm) size fractions. Characterizing the dFe fraction in seawater is further complicated by the fact that Fe is usually complexed with inorganic and organic ligands that exist in both the colloidal (0.02-0.2um) and the truly soluble (<0.02um) size fractions. Characterizing the dFe fraction in seawater is also complicated by the different stabilities of Fe(II) and Fe(III) species as either free ions or as complexes in seawater. Inorganic Fe binding ligands such as hydroxide

complexes in seawater allow for multiple inorganic Fe(III) complexes to exist at seawater pH (pH~8.1; $Fe(OH)_2^+$, $Fe(OH)_3^0$, $Fe(OH)_4^-$, Fe(III) free ion); the sum of which are often referred to as Fe(III)'. However, inorganic Fe binding ligands do not improve the overall solubility of Fe(III) in seawater over the theoretical solubility of Fe(III)' in abiotic, pH 8, oxygenated seawater ($\sim10^{-8}$ to $\sim10^{-10}$M dFe) (Bruland & Rue, 2001). Between 95-99.9% of dissolved Fe(III) in seawater has been observed to be complexed by organic ligands, which are thought to greatly increase the overall solubility of Fe(III) above the theoretical solubility of inorganic Fe(III) in oxic, pH~8 seawater (Rue & Bruland, 1995). Conversely, the speciation of inorganic Fe(II) in the ocean is dominated by the free hydrated Fe(II) species with the remainder of the Fe(II) complexed by carbonate species (Millero et al., 1995). Fe(II) is more soluble in seawater than Fe(III) but is also less stable, with oxidation of Fe(II) to Fe(III) occurring on the timescale of minutes in surface waters at pH ~8 (Wells et al., 1995). Thus, the speciation of dFe in surface seawater is dominated by Fe(III)-organic complexes. Since it is thought that dFe is the bioavailable fraction of Fe in seawater, dFe receives the most interest in the oceanographic community (Lis et al., 2015; Morel et al., 2008; Shaked & Lis, 2012; Wells et al., 1995).

The discovery of vast regions of the surface ocean replete with nitrate and phosphate but with low chlorophyll a and depleted in dFe, referred to as High Nutrient Low Chlorophyll (HNLC) regions, led to the hypothesis that Fe may be a critical micronutrient for phytoplankton growth (Martin & Fitzwater, 1988; Hudson & Morel, 1990). This hypothesis was confirmed by several shipboard Fe addition incubation experiments with HNLC waters, where primary production was

observed to increase in those incubations containing Fe additions (Martin & Fitzwater, 1988; Martin et al., 1990).  Additionally, incubation experiments with HNLC waters confirmed that the increase in primary production resulting from Fe additions to the seawater also reduced the concentration of dissolved inorganic carbon (DIC) in the ambient environment, and thus $pCO_2$ (Martin et al., 1990; Martin et al., 1993; Martin, J. H. & S. E. Fitzwater, 1988).

These observations led John Martin to propose the 'Iron Hypothesis' in 1990, which suggested that the uptake of DIC by phytoplankton in HNLC regions fertilized with Fe could mitigate future rising atmospheric $CO_2$ concentrations.  The 'Iron Hypothesis' further suggested that the increased dust flux during glacial periods could have fertilized the ocean with Fe, thereby increasing levels of primary productivity and $CO_2$ uptake.  The increase in primary production and therefore DIC uptake from the ambient seawater requires that some atmospheric $CO_2$ diffuse into surface waters to maintain equilibrium.  Thus, increased dust fluxes during glacial periods and the subsequent feedback loops could be partially responsible for the lower atmospheric $CO_2$ concentrations observed during the last glacial maximum (Martin, 1990; Martin et al., 1990).  This hypothesis spurred intense interest in mapping out dFe distributions throughout the oceans and several large scale Fe fertilization experiments (IRONEX, IRONEXII, SOIREE, SOFeX, and others) were conducted in HNLC waters to gain an understanding of how Fe fertilization affects carbon export in the ocean (Aumont & Bopp, 2006;Bidigare et al., 1999; Bishop et al., 2004; Buesseler et al., 2005; Coale et al., 1998; Martin et al., 1994).

The desire to map out dFe distributions requires the ability to make accurate, high-resolution Fe measurements at low concentrations, which has presented a challenge to oceanographers. The ubiquity of Fe in the ambient environment makes clean sampling, handling, and analysis of seawater critical for accurately measuring true Fe concentrations (Johnson et al., 1997; Measures et al., 2012). Furthermore, developing analytical methods capable of measuring Fe at picomolar to nanomolar levels that do not potentially contaminate samples has required extensive research efforts. Ship based methods capable of accurately measuring Fe levels in open ocean seawater have only been developed over the past two decades and are still undergoing refinement to improve their limits of detection (LOD) and sensitivities (Johnson et al., 1997; Measures et al., 2012). However, of the methods available for Fe determinations in seawater at open ocean levels (LOD <0.1nM dFe), no platforms or instruments developed thus far have the properties required for autonomous deployment such as small size, low power requirements, infrequent/minimal maintenance, full automation and data recording.

This thesis presents an alternative method for dFe measurements in seawater developed by adapting the existing N,N-Dimethyl-p-phenylenediamine (DPD)-Fe(III) chemistry to a novel platform, the micro-sequential injection analysis (μSIA) platform. The chemistry used is based on the DPD-Fe(III) methodology developed for Flow Injection Analysis (FIA) based dFe analyses by Measures et al. (1995) and uses the spectrophotometric signal from the reaction between Fe(III) and DPD in the presence of hydrogen peroxide ($H_2O_2$) originally reported by Hirayama & Unohara (1988). In this method Fe(III) oxidizes DPD and hydrogen

peroxide reoxidizes the reduced Fe(II) resulting from the DPD oxidation back to Fe(III), thus increasing the analytical signal produced.  This method then allows for the determination of total dFe (Fe(II) + Fe(III)) to be measured by this method.  The µSIA-LOV platform that this chemistry has been adapted to has many of the properties necessary for autonomous deployment and *in-situ* monitoring  (Grand et al., 2011; Oliveira et al., 2015).  The development of a fully autonomous instrument for *in-situ* dFe determinations in seawater would provide a means to study the temporal variability of Fe sources and sinks on time scales that are not feasible with ship-based determinations.

## 1.1 The Oceanic Fe Cycle

The distribution of dFe in the ocean varies both spatially and temporally reflecting the variability of external Fe sources to the ocean, internal regeneration and removal processes.  External sources of Fe to the ocean include aeolian deposition, hydrothermal vent fluids, and land runoff.  A fraction of the total external Fe that enters the ocean as pFe will undergo dissolution becoming dFe. Processes that remove Fe from the ocean include biological uptake and particle scavenging.  In the latter case dFe adsorbs to particulate matter and is subsequently buried in sediments (Boyd & Ellwood, 2010; Hawkes et al., 2013; Johnson et al., 1997; Kalnejais et al., 2010).

Dissolved Fe typically has a nutrient-like vertical profile in the upper 1000m of the open ocean, with depleted dFe concentrations in surface waters increasing with depth.  In surface waters, dFe concentrations are typically at sub-nanomolar

levels (<0.2nM) resulting from biological uptake in the euphotic zone (Johnson et al., 1997; Moore & Braucher, 2007). In the intermediate waters from below the euphotic zone down to the oxygen minimum zone (OMZ), the remineralization of settling biogenic material releases dFe to the surrounding waters (Boyd et al., 2005). This results in the concentration of dFe increasing with depth, often reaching a maximum value in the OMZ.

Below the OMZ in the open ocean, the vertical profile of dFe is more characteristic of a scavenged-type element, with the concentration of dFe declining slightly and then maintaining a relatively constant concentration with depth. The concentration of dFe below the OMZ results from the continued but much smaller release of dFe from the diminishing flux of particulate material balanced by the scavenging of ligand stabilized dFe and its burial as pFe in sediments (Boyd & Ellwood, 2010).

The dominant source of external Fe to open ocean surface waters is aeolian deposition and the subsequent partial dissolution of Fe bearing minerals, which elevates dFe concentrations in surface waters (Jickells et al., 2005; Johnson et al., 1997; Moore & Braucher, 2007; Watson et al., 2000). The resulting levels of dFe in the open ocean surface waters are a result of a balance between dissolution of Fe from aeolian deposition, uptake by the biological community, and export of pFe from the surface waters (Jickells et al., 2005; Johnson et al., 1997; Wells et al., 1995). In surface waters, the turnover time of dFe in the biological pool is driven by the size of the biological community, the amount of bioavailable Fe in ambient seawater, the cellular Fe:C requirements of organisms present, and the rate of pFe export from the

mixed layer (Boyd et al., 2005; Boyd & Ellwood, 2010; Johnson et al., 1997; Sunda & Huntsman, 1997; Sunda & Huntsman, 2015; Wells et al., 1995). For example, in HNLC surface waters, the turnover of the dFe pool occurs on the timescales of days to weeks as a result of the high biological demand for dFe (Boyd et al., 2005; Wells et al., 1995).

Apparent oxygen utilization (AOU), which indicates the extent of *in situ* respiration, is often observed to correlate with dFe concentrations when remineralization is the dominant process contributing dFe to the deeper water column. However, the slope of the AOU/dFe relationship can differ spatially, reflecting the various sources and compositions of the particulate organic matter (POM) undergoing remineralization (Fitzsimmons et al., 2013; Rijkenberg et al., 2014; Sunda & Huntsman, 1997; Sunda & Huntsman, 2015).

Within the intermediate waters, the main process removing dFe from the water column is the scavenging of dFe on to particulates; however, the relatively high concentrations of dFe seen in intermediate waters suggest that the process of remineralization out competes the scavenging process at these depths (Boyd & Ellwood, 2010; Rijkenberg et al., 2014).

Furthermore, as the scavenging of dFe increases with time, this process would explain the inter-ocean fractionation of dFe in deep-waters, which are characterized by high dFe concentrations (0.6-0.8nM) in the North Atlantic, declining to lower concentrations (0.4-0.6nM) in the North Pacific (Boyd & Elllwood, 2010; Boyle, 1997; de Baar & de Jong, 2001; Moore & Braucher, 2007; Wu et al., 2001).

Thus, the distribution of dFe in the deep ocean reflects the balance between the supply of dFe by remineralization, the stabilization of a fraction of dFe thereof by Fe binding ligands, and the scavenging of dFe (Boyd & Ellwood, 2010; Bruland & Rue, 2001; Jickells et al., 2005; Rue & Bruland, 1995).

Exceptions to these open ocean distributions can result from spatially and temporally varying sources and processes such as upwelling, proximity to land, and hydrothermal venting. For example, open ocean upwelling, such as in the central and equatorial Pacific, and deep winter mixing at high latitudes bring relatively dFe enriched waters (0.4-0.8nM) from below the mixed layer into surface waters. Thus, seasonal upwelling and deep winter mixing replenish dFe stocks in the mixed layer that have been depleted during the summer when stratification of the mixed layer limits the extent of diapycnal mixing (Jickells et al., 2005; Johnson et al., 1997; Watson et al., 2000).

In coastal regions, external sources of nutrients and Fe such as riverine discharge, sediment resuspension, remineralization, and upwelling support large phytoplankton communities in the immediate proximity of the sources (Boyd & Ellwood, 2010; de Baar & de Jong, 2001; Moore & Braucher, 2007; Elrod et al., 2004). However, ~95% of the riverine dFe flocculates during estuarine mixing and is scavenged, resulting in large horizontal dFe gradients from the coast to offshore (Sholkovitz et al., 1978). Thus, despite the relatively high dFe concentrations associated with the coastal ocean, advection of surface coastal water to the upper open ocean (0-250m depth) does not provide a significant source of dFe to open ocean surface waters (Boyd & Ellwood, 2010).

Hydrothermal venting also provides localized inputs of dFe and pFe and can result in ambient concentrations on the order of 100nM dFe close to the source. While these inputs are highly localized and would be expected to be rapidly scavenged, recent research by Fitzsimmons et al. (2015) suggests that despite the decline of dFe concentrations with distance from hydrothermal sources, the dFe may be stabilized in the colloidal phase allowing for much longer distance transport of dFe than previously thought. Additionally, the potential for these more persistent hydrothermal Fe inputs to influence surface water dFe distributions in upwelling zones far removed from vent sites is currently of interest to the scientific community (Boyle et al., 2005; Fitzsimmons et al., 2015; Tagliabue et al., 2010; Wu et al., 2011).

## 1.2 Current Methods for dFe Determinations

Inductively Coupled Plasma – Mass Spectrometry (ICP- MS) is one of the most extensively used techniques for shore-based determinations of dFe in seawater samples and is often used to verify the accuracy of ship based dFe determinations. However, the size and gas requirements for ICP-MS instrumentation prohibit its use on ships. Methods for the determination of Fe in seawater that can be used at sea include but are not limited to either batch or FIA based colorimetric analyses using the Ferrozine reagent (Stookey, 1970) or the DPD reagent (Hirayama & Unohara, 1988; Measures et al., 1995), and chemiluminescence using luminol (King et al., 1995; Kinnan, 2003; Oliveira et al., 2015). Additionally, Cathodic Stripping Voltammetry (CSV) (Obata & van den Berg, 2001; Rue & Bruland,

1995) can be used to determine the overall concentration of dFe and the speciation of Fe in samples. However, currently all of these methods require a preconcentration step to achieve Fe concentrations consistent with the detection limits of these methods (Johnson et al., 2007; Oliveira et al.; 2015).

Resin columns with metal chelating functional groups provide a means for sample preconcentration and can also be used to remove Fe from reagents. However, preconcentration methods often require manipulation of the sample pH since samples are frequently acidified to pH ~1.7 to release ligand bound Fe and resins such as 8-Hydroxyquinoline (8-HQ) need a pH ~ 5.2 solution in order to achieve quantitative adsorption (Landing et al., 1986; Measures et al., 1995).

The recent development of metal- chelating resins such as nitrilotriacetic acid (NTA) that can quantitatively recover Fe(III) from seawater in the pH range 1.3-3.5 and Fe(II) + Fe(III) above pH 6 may provide a means for preconcentration without requiring raising the pH of acidified samples (Lohan et al., 2005).

While the use of chelating resins increases the sensitivity of analyses, the addition of a preconcentration step increases the volume of sample needed as well as the amount of time per analysis. Thus, a technique for the determination of dFe in seawater that can reach adequate detection limits without preconcentration would enhance analytical throughput as well as avoid any uncertainty that may arise from manipulating the sample pH and the capacity of the chelating resin to retain the various Fe species.

## 1.3 Proposed Method for dFe Determinations

The increasing availability of autonomous platforms for oceanographic research such as moorings, gliders, and floats provides opportunities to develop new methodologies and instruments that can be deployed on these platforms to obtain high temporal and/or spatial resolution data sets. The limitations posed by autonomous platforms such as small size and limited power are driving the miniaturization of analytical platforms. In addition, the limited ability to service deployed instruments requires that analytical methodologies are robust and experience little wear and tear over extended periods of use.

Current FIA based methods have large space requirements, high power requirements, consume large volumes of reagents which generates large volumes of waste, and require frequent replacement of peristaltic tubing, and are thus unsuitable for autonomous platforms.

A relatively new platform, the micro Sequential Injection Analysis- Lab On Valve (μSIA –LOV), however, has many of the properties required for deployment on autonomous platforms. The μSIA- LOV is small in size (~ 16cm x 16 cm x 20cm), requires little power, uses extremely small volumes of reagent solutions (on the order of ~10μL), and therefore generates very small volumes of waste (on the order of ~1ml/ analysis including rinse steps)(see *Chapter 2: Experimental*). The objective of this work was to develop a μSIA-LOV based method for the determination of dFe in seawater by adapting the DPD-Fe(III) methodology developed for FIA based dFe analyses by Measures et al. (1995) to the μSIA-LOV platform.

**CHAPTER 2: Experimental**

## 2.1 General Description of the µSIA Platform

The micro-sequential injection analysis (µSIA) platform, shown in **Figure 2.1**, consists of a 1ml high precision glass barrel syringe pump with a three-way distribution valve connected to a 6- port multi-position valve (MPV)(Vici®) with a lab-on-valve® (LOV) manifold mounted on the MPV face. The LOV manifold allows for multiple solutions to be accessed and to be aspirated or dispensed by the syringe pump and has an integrated flow cell. To aspirate samples and reagent into the system the LOV ports are equipped with 0.8mm I.D. PTFE tubing and the carrier line utilizes 1.6mm I.D. tubing (Optimize Technologies, Oregon City, OR). In addition to external solution lines, a cylindrically wrapped holding coil (PTFE, 0.8mm I.D., 1mL internal volume) is used to hold the sample and reagent mixture prior to analysis. The holding coil acts as a buffer, preventing solutions from coming into contact with the syringe pump, which is a potential source of contamination (see section *3.1 Results and Discussion: The µSIA Platform*).

Solutions are monitored by visible spectrophotometry using a USB4000 UV-VIS spectrophotometer (Ocean Optics, Dunedin, Fl) equipped with a Megabright Xlamp white LED light source (CREE Inc., Durham, NC). The spectrophotometer and light source are connected to the flow cell of the LOV manifold using optical fibers with PEEK (polyether ether ketone) terminations to produce a 9.5cm long flow cell with a total internal volume of 47.5µL.

The µSIA platform and data collection are controlled using FIAlab for Windows 5.9.312 software (FIAlab Instruments) installed on a Macbook Pro (Apple, Cupertino, CA) running Windows 8 (Microsoft, Redmond, WA) through VMware Fusion 6.0.3 (VMware Inc., Palo Alto, CA).  Data collected using the FIAlab software are plotted and analyzed using Matlab R2011b (MathWorks, Natick, MA) after minimal processing in the FIAlab software (see section *3.1: The µSIA- LOV Platform, Signal Monitoring in FIAlab Software*).

## 2.2 The DPD-Fe(III) Chemistry

The DPD-Fe(III) chemistry used to determine dFe concentrations in seawater with the µSIA platform was originally developed as a batch method by Hirayama & Unohara (1988).  This methodology relies on the catalytic oxidation of N, N-Dimethyl-p-phenylenediamine (DPD) to a colored semiquinone derivative (DPDQ) by Fe(III) as shown in **Figure 2.2**.  The Fe(II) produced in this reaction is subsequently reoxidized to Fe(III) by $H_2O_2$.  The reaction occurs in a buffered 0.6M ammonium acetate ($NH_4Ac$) solution, ensuring it is within the optimal pH range ($\sim$5.5-6.0) for the DPD oxidation reaction (Hirayama & Unohara, 1988; Measures et al., 1995).  The catalytic nature of the reaction improves the sensitivity of the method since each Fe atom can continuously recycle, thereby oxidizing more DPD. However, this also requires reproducible timing of reagent and sample additions and signal monitoring in order to ensure accurate results, making this method more suitable for an automated system.

The batch DPD method chemistry was adapted to a continuous flow platform, Flow Injection Analysis (FIA), by Measures et al. (1995). The FIA platform uses computer automation, which improves the reproducibility of the method, but the peristaltic pumps used can result in variable flow rates as tubes age and the need to have continuously flowing reagents produces large volumes of waste. The FIA method has been used successfully for shipboard Fe determinations; however, for the reasons stated above, the platform is unsuitable for deployment on autonomous platforms (Lohan et al., 2006; Measures et al., 1995). Thus, the adaptation of the method to the μSIA platform that uses a high precision pump and utilizes discrete volumes rather than continuously flowing solutions provides the ability to increase automation, reduce service requirements, reduce waste production, and improve precision; properties that are needed for platforms with the potential to be on unmanned platforms.

One main disadvantage of μSIA relative to FIA, though, is that the discrete aspiration of samples and reagents into the μSIA system results in shorter transport distances and less opportunity for reagent and sample solutions to mix than is observed with FIA (see *Chapter 3: Results and Discussion*). In FIA the continuously flowing reagent and sample streams merge with one another at confluence points, which results in increased turbulence and increased mixing; which does not occur in μSIA. However, since μSIA pumping rates and the sequencing of the aspirated solutions are under computer control, extensive variations of these parameters can be investigated to assess their effect on mixing between sample and reagent solutions without reconfiguring the platform.

Additionally, the use of continuously flowing peristaltic pumps in FIA makes it simpler to clean the contaminant Fe from the DPD reagent. In FIA, the DPD and other reagents are passed through metal adsorbing columns to remove the associated Fe and metal contaminants in real time (Measures et al., 1995). However, with the μSIA platform, cleaning reagents in line was not feasible and an offline DPD cleaning protocol was developed (see section *3.3 The System Blank & Interferences*).

**Reagents.** Due to the prevalence of Fe in the ambient environment, trace metal clean procedures were implemented to minimize the possibility of contamination. All sample and solution handling as well as μSIA analyses were carried out in a Class-100 laminar flow hood and solutions were prepared using ultra high purity (UHP) water, 18.2MΩ-cm (Barnstead International, Dubuque, IA). The μSIA tubing was cleaned with 0.5% (v/v) trace metal clean HCl (Q-HCl) and the syringe pump was flushed with UHP water at the beginning and end of each day. All bottles were made of high density polyethylene and were pre-cleaned by soaking in a 10% (v/v) HCl acid bath overnight for >12hrs and then rinsed a minimum of three times with UHP water. New bottles, prior to their first use, were initially soaked with soap for 24 hours followed by 30% (v/v) aqua regia at 60°C for 24 hours. These bottles were then rinsed three times with aqua regia and three times with UHP water and left to soak in a 10% (v/v) Q-HCl acid bath until needed. Prior to use, pipette tips were rinsed three times with 30% (v/v) Q-HCl and three times with UHP water.

**Stock Solutions.** Trace Metal Clean Hydrochloric acid (Q-HCl, 6M)

Commercial 12M hydrochloric acid, (HCl)(Fisher Scientific, Certified A.C.S. Plus, Pittsburgh, PA), was purified for use by dilution to 6M with UHP water and a single distillation in a quartz-finger sub-boiling still within a fume hood to produce 6M Q-HCl (Measures et al., 1995). All Q-HCl was handled within the laminar flow hood following purification.

*Glacial Acetic Acid ($CH_3COOH$). Commercial grade glacial $CH_3COOH$, ~17M, (Fisher scientific, Certified A.C.S. Plus, Pittsburgh, PA), was purified by a single distillation in a quartz-finger sub-boiling still within a fume hood to produce ~17M Q-$CH_3COOH$ using the same procedures and equipment as Measures et al. (1995). The strength was verified by titration following distillation.*

*Ammonium Hydroxide ($NH_4OH$).* Reagent grade ~15M $NH_4OH$ (Fisher Scientific, Certified A.C.S., Pittsburgh, PA) was purified using passive isopiestic distillation and diluted using UHP water to produce a high purity Q-$NH_4OH$ solution of ~4.9M (Measures et al., 1995).

*Ammonium Acetate Buffer ($NH_4Ac$) with Hydrogen Peroxide ($H_2O_2$).* $NH_4Ac$ buffer (2M, pH 6.3) was prepared by mixing the appropriate amount of Q-$NH_4OH$ with Q-$CH_3COOH$. To each 1L of 2M $NH_4Ac$ buffer, 2.4mL of 5%(w/w) Brij®-35 (Sigma Diagnostics, St. Louis, MO) and 1.26mL of triethylenetetramine (TETA) (Fluka, St. Gallen, Switzerland) were added. Nine milliliters of this solution were further diluted for daily use with 8mL of UHP water and 13mL $H_2O_2$ (Perdrogen® 30% (w/w); Sigma- Aldrich, St. Louis, MO) to yield a final concentration of 0.6M

NH$_4$Ac buffer with 13% (w/w) H$_2$O$_2$. Stock H$_2$O$_2$ was stored in the fridge to minimize degradation.

*N, N Dimethyl-p-phenylenediamine dihydrochloride (DPD).* The 0.4mM DPD reagent was made daily by dissolving 24mg of the solid commercial DPD reagent (≥99% assay, Sigma- Aldrich, St. Louis, MO) into 30mL of UHP water (acidified to 24mM with 120μL of 6M Q-HCl). The solid DPD reagent and daily DPD solution were stored in the dark when not in use to prevent photo-oxidation.

*Dissolved iron standards (dFe standards).* A stock certified reference material (1000μg Fe/L)(VWR, West Chester, PA) was diluted into acidified UHP water containing 24mM Q-HCl to produce intermediate concentration standards (~500nM dFe). Daily working standards were prepared from these by the addition of up to 1.0mL of the intermediate standard into low Fe seawater, which had been filtered through a 0.2μm Acropak capsule and acidified to pH 1.7-1.8 with Q-HCl. Working standard concentrations ranged up to +40nM dFe above the initial filtered seawater value.

All solutions and samples were stored in pre-cleaned high-density polyethylene bottles (as described above) and all solutions were handled within a class-100 laminar flow hood.

**2.3 Detection Techniques**

The µSIA platform can be used to perform either flow or reaction-based determinations. Flow based-determinations, where the reacting solutions pass through the flow cell, can be accomplished for any absorbance-based reaction. However, reaction-based determinations, where the progress of the reaction within the flow cell is monitored as a function of time, require that the reaction is either slow, far from reaching equilibrium, or is catalytic in nature. In flow-based determinations in µSIA, the sample and reagent solutions are aspirated into a holding coil and the mixed plug of sample and reagents is then pushed through the flow cell, resulting in an absorbance peak, similar to that obtained from continuous flow methods, as shown in **Figure 2.3B**. This is referred to as the stopped- in-holding coil (SHC) method. The µSIA platform also allows the reacting plug of solution to be stopped in the flow cell so that the progress of a reaction can be monitored as a function of time. This is referred to as stopped-in- flow cell analysis (SFC). An example of the absorbance signal generated by SFC is shown in **Figure 2.3C**. This technique results in a linear increase in absorbance over time as the reaction proceeds (providing the reaction rate is constant) and results in a reaction progress curve. An advantage of using the SFC analysis is that a line can be fitted to the large number of points generated during the reaction progress, providing a more precise estimate of sample absorbance than the peak based absorbance determination of the SHC technique, where only a few points at the top of a peak are used to calculate the sample absorbance.

Another added benefit of the SFC protocol is that the changes in absorbance can be normalized to the initial conditions within the flow cell using a reference scan to establish the initial light intensity in the flow cell with the reacting plug of solution in the flow cell (see *FIAlab Data Acquisition and Processing* below). This approach eliminates potential artifacts associated with refractive index gradients amongst the stacked solutions with varying matrices within the flow cell. Since the refractive index of the sample and reagent solutions differ, the ability of light to be transmitted through the sample and reagent solutions also differs. The formation of refractive index gradients between the sample and reagent solutions results from their mixing and with the axial dispersion in the holding coil, these gradients can produce lenses, which distort the transmission of light through the flow cell. This is referred to as the Schliren effect, which can alias the absorbance signal as demonstrated in **Figure 2.4** (Dias et al., 2006).

With both detection techniques in the μSIA method, a parabolic lens is formed within the flow cell as a result of pushing the mixtures into the flow cell. The presence of this lens significantly alters the light intensity passing through the flow cell, focusing the light, which results in higher light transmission than when the flow cell is filled with UHP water. Thus, to avoid saturation of the pixels in the spectrophotometer when using the SFC protocol, in which the light intensity reaching the detector was too high and resulted in flat- topped peaks during a voltage scan, the integration time was decreased until no saturation was observed during a determination while monitoring the voltage. Once the optimal integration time was established, the reference scan effectively 'zeroed' the absorbance across

all wavelengths to the conditions in the flow cell so that only the change in absorbance over time was measured (see *FIAlab Data Acquisition and Processing below*) (Dias et al., 2006).

**2.3.1. FIAlab data acquisition and processing.** FIAlab 5.0 software is used to control the μSIA platform and to record the digital output from the USB4000 spectrophotometer. The USB4000 signal detection is based on a charge coupled/transfer device (CCD) with >3600 pixels across the wavelengths 200-1100nm, allowing for simultaneous signal detection across these wavelengths. During a measurement, a scan is taken across all pixels. Since multiple pixels correspond to a given wavelength, consecutive pixels can be averaged during a scan using the FIAlab software setting called "Detectors to Average", where detectors refers to the pixels of the CCD array. In this method, three consecutive pixels were averaged for each wavelength during a scan. The amount of time (in milliseconds) that the pixels in the CCD array collect light for a single scan is referred to as the "Integration Time" and in this method, the integration time was set to 8ms, meaning that each pixel collected light for 8ms during a single scan. The frequency of data points recorded in the FIAlab software can be set between 0.25-4Hz. Data were recorded at 4Hz to obtain higher-resolution data.

Since the FIAlab software recorded one data point every 250ms and the integration time for each scan of the CCD array pixels was 8ms, multiple scans were averaged to produce the single data point recorded by the FIAlab software. In the software this function is referred to as "Samples (scans) to Average", and could be used to average the scans made during the 250ms time period for each data point.

Since it took 8ms for a single scan, in theory 31 scans could be averaged over a 250ms time period; however, 28 scans were averaged providing additional time for the USB4000 and FIAlab software to communicate and record the data. Using calibration coefficients specific to the spectrophotometer used, the FIAlab software converted the voltages to absorbance values to produce the final data set. A summary of the spectrophotometer settings is shown in **Table 2.1**.

Prior to starting a determination, a series of calibration scans are made. Initially, a dark scan (no light), as seen in **Figure 2.5A**, is made with DI water in the flow cell to evaluate electrical noise and stray light across all wavelengths. The dark scan indicates if the detector is working properly and provides an indication of any problematic areas of the wavelength spectrum. Following the dark scan, a discrete reference scan of DI water (normally the highest transmission), **Figure 2.5B**, is made to establish the relative light intensity across all wavelengths. Since this includes voltage contributions seen in the dark scan, the reference scan also normalizes any contributions from ambient light and electrical noise. The reference scan is necessary because the light intensity from the white LED light source varies across the wavelengths as shown in **Figure 2.5B**, where the shorter wavelengths (~450nm) saturate prior to the rest of the visible spectrum.

The amount of light reaching the detector can be adjusted by changing either the intensity of the light source or by varying the integration time setting in the software. In practice, it is easier and more precise to adjust the integration time in the software because a physical thumb wheel is used to adjust the light output of the LED light source, which is much less precise than changing the integration time

setting in the computer. After optimizing the integration time, a reference scan is then made to ensure that there is no saturation. In the event that the FIAlab software encounters saturation at any wavelength, the software will automatically change the integration time to reduce the light intensity without informing the user. This can result in inconsistent conditions between sample and standard runs. Thus, as previously discussed it is necessary to monitor the reaction as voltages first to ensure that no saturation occurs, which is evident from flat- topped peaks. If saturation is observed, the integration time must be decreased until no saturation is observed during an analysis.

As previously mentioned, for the stopped-flow protocol used in this method, a reference scan was made with the reacting mixture in the flow cell to zero the detector prior to measuring the reaction progress. Variations in light output across all wavelengths while monitoring the reaction were then normalized using a reference wavelength, which was chosen in a relatively stable region of the spectrum unaffected by the absorbance of the reaction product (DPDQ), as shown in **Figure 2.6**. To normalize the signal, the absorbance at the reference wavelength (620nm) was continually subtracted from the absorbance at the reaction wavelength (514nm). Thus, the absorbance values that make up the reaction progress curve are relative absorbance values and not absolute absorbance values.

## 2.4 The Finalized µSIA Protocol

The protocol for the determination of dFe using the µSIA platform consists of the following steps. First, the syringe pump and holding coil were filled with DI water aspirated from port 6 **(Figure 2.1)**. Next, the valve on the syringe pump was switched to waste 2 and 300µL of DI water were dispensed directly from the syringe pump to waste 2 and then the syringe pump valve was switched back to the LOV. Next, the MPV was switched to port 4 to aspirate 50µL of the $NH_4Ac$ & $H_2O_2$ solution, then the MPV was switched to port 5 to aspirate 80µL of sample, then the MPV was switched to port 3 to aspirate 20µL of the DPD solution, and finally the MPV was switched back to port 5 to aspirate another 50µL of the sample solution. Once all solutions had been aspirated the MPV was switched to the flow cell, the flow was reversed, and 140µL of solution were dispensed to the flow cell by the syringe pump at 15µL/s. After the reacting solution had entered the flow cell and stopped, the MPV was switched to waste, a reference scan was taken to zero the absorbance and then the absorbance was recorded for a continuous 60 second period using the SFC monitoring protocol. After the 60 second stopped flow period, the MPV was switched back to the flow cell and 500µL of solution from the holding coil were pushed through the flow cell at 250µL/s to rinse the flow cell after the analysis.

# Chapter 3: Results and Discussion

The objectives of the experiments described herein were to improve the figures of merit including the sensitivity, precision, accuracy, and limit of detection for the μSIA-based method. The proposed μSIA method provides a simplified, fully automated system for the determination of dFe in seawater with a LOD=0.1nM. The system is optimized for the analysis of acidified seawater samples (pH 1.7-1.8) without preconcentration or matrix removal.

Developing the μSIA- LOV based method required significant modifications of the previous continuous flow based method due to key differences in flow dynamics between the two platforms. Specifically, the limited mixing that occurs in μSIA required optimization of the reagent and sample aspiration sequence as well as modification of the reagent concentrations and sample acidification. Optimization of the μSIA system focused on minimizing the method blank, improving the extent of mixing between reagents and sample solutions, and optimizing the reagent concentrations for the method. Additionally, to improve the sensitivity and precision of the method, the technique for signal detection was changed from peak based absorbance measurements, which are used in FIA, to reaction progress based measurements achieved using the SFC technique (see section *3.1.1 μSIA Detection Protocols* below).

The μSIA- LOV system was used onboard the R/V Falkor for the rapid detection of hydrothermal plumes at Loihi Seamount, HI based on dFe concentrations in discrete seawater samples. Samples from this cruise were also

determined on shore using the optimized μSIA- LOV method to validate the system's ability to accurately quantify dFe and these values were compared with ICP-MS determinations of another group's samples from the same cruise (Olivier Rouxel, pers. comm.).

## 3.1 The μSIA- LOV Platform

The μSIA- LOV platform configuration for this study was the same as presented in Grand et al. (2011). The μSIA- LOV platform was configured to minimize potential Fe contamination from the ambient environment while maximizing sensitivity and analytical throughput. The components of the system (tubing, fiber optic terminations, LOV) were chosen with these considerations in mind and the system was kept in a Class-100 laminar flow hood to prevent airborne contamination of samples and reagents. The configuration of the sampling ports and flow cell in the LOV were previously shown in **Figure 2.1.** The LOV manifold replaces the face-plate of a 6-port multi-position valve (MPV), the rotation of which facilitates the aspirating and dispensing of solutions directly into and out of the LOV and its integrated flow cell through the various LOV ports. The syringe pump was used to drive the carrier solution, which in turn controlled the flow of solutions into and out of the holding coil. A carrier solution of deionized water (DI) was used to fill the syringe pump, the adjacent 1mL capacity of the holding coil, and the flow cell prior to and after each analysis. The purpose of the 1mL capacity holding coil filled with carrier solution between the syringe pump and the sample and reagent solutions was to keep the sample and reagents from coming into contact with the

potentially Fe-contaminating glass syringe pump.  In addition to the DI carrier solution, the DPD reagent, $NH_4Ac$ & $H_2O_2$ reagent, and sample were aspirated through their respective channels of the LOV into the holding coil **(**see **Figure 2.1)**.

Methods using the μSIA- LOV platform for analyte determinations are based on the sequential aspiration of reagent and sample solutions into a holding coil.  As solutions are aspirated into the holding coil they begin to mix (see **Figure 3.1.1**) and after all solutions are aspirated, the flow is reversed and mixing continues as the syringe pump dispenses the solution from the holding coil into the flow cell for signal monitoring.  In the case of the DPD-Fe method, the mixed $NH_4Ac$ & $H_2O_2$ reagent is aspirated into the holding coil first, followed by the sample and finally the acidified DPD reagent.  The absorbance of the resulting DPDQ compound is monitored at 514nm.

The absorbance in the flow cell is detected using two optical fibers placed end to end within the flow cell channel of the LOV (see **Figure 2.1**).  One fiber was connected to a white LED light source and the other fiber was connected to a USB4000 UV-VIS spectrophotometer detector (Ocean Optics, Dunedin, Fl.).  To improve sensitivity, the original LOV flow cell length of 3.75cm was extended using additional PEEK tubing and fittings to 9.5cm with a new total internal volume over which absorbance measurements were integrated of 47.5μL.  Absorbance measurements from the spectrophotometer were digitized at 4Hz and recorded with the FIAlab software.

**3.1.1 μSIA detection protocols.** In μSIA, two different protocols can be used to measure the reaction product depending on where the reaction product forms in the system. These two techniques, referred to as Stopped in Holding Coil (SHC) and Stopped in Flow Cell (SFC), are possible because of the ability to stop and start the flow of sample and reagent mixtures in μSIA in a very reproducible manner.

*SHC*. In the SHC protocol, sample and reagent solutions are aspirated into the holding coil where the flow is stopped and the reaction between sample and reagents occurs for a set amount of time. The reaction product is then pushed from the holding coil through the flow cell resulting in a peak shaped absorbance. This is similar to the monitoring system that is used in the FIA based method (Measures et al., 1995). However, in μSIA the precision (~5-10%) and sensitivity (LOD=1.5nM) resulting from the SHC protocol were not adequate for developing a method capable of measuring typical surface open ocean levels of dFe (<0.2nM dFe)(Johnson et al., 1997; Moore & Braucher, 2007).

*SFC*. In the SFC protocol, the sample and reagent solutions are aspirated into the holding coil after which the flow is immediately reversed and the reacting sample and reagent mixture is moved into the flow cell. The formation of the reaction product is then monitored as the change in absorbance as a function of time resulting in a reaction progress curve. The exact volume of the reacting solution that is moved into the flow cell is carefully controlled. This is to ensure that the zone of solution with the optimal ratio of the reagents to one another mixed into the sample zone, characterized by the fastest reaction progress, is in the flow cell for

27

monitoring. The SFC protocol resulted in improved precision (<1% RSD) and greater sensitivity (LOD=0.1nM) for the method.

**3.1.2 Signal monitoring.** As previously discussed in section *2.3 Detection Techniques*, in order to zero the absorbance it is necessary to perform a reference scan prior to making an absorbance determination. The technique used to zero the absorbance differs between the two protocols.

*Stopped in holding coil (SHC)*. While the $NH_4Ac$ & $H_2O_2$, sample, and DPD solutions were stopped in the holding coil to react for 60s and the flow cell was filled with DI water, a discrete reference scan across all wavelengths was made to zero the absorbance. This effectively normalized the absorbance of the sample and reagent mixture to a DI water baseline. After 60s had elapsed, the flow was reversed and the solution in the holding coil was pushed through the flow cell. The absorbance peak generated resulted from the formation of the DPDQ as well as any additional absorbance signals that may have arisen from refractive index gradients entering the flow cell in comparison to baseline conditions in the flow cell filled with DI water (**Figures 2.6 & 3.1.2**)(see section *2.3 Detection Techniques)*. The maximum absorbance (peak height) was then plotted versus the concentration of dFe in the standard to produce a calibration curve. The peak height from unknown samples was then used to determine the concentration of dFe using the calibration curve.

*Stopped in flow cell (SFC).*  For reaction chemistries that are slow or are catalytic, SFC is an alternative technique for analyte determination by monitoring the progress of the reaction in the flow cell as a function of time.

In the SFC technique, the sample and reagent mixture was moved immediately into the flow cell after aspiration, and a discrete reference scan was taken.  This yielded a baseline for normalizing the absorbance signal to the solution matrix, which included any refractive index gradients within the flow cell.  The absorbance signal was then monitored (514nm) as a function of time for 60s producing a reaction progress curve (**Figures 3.1.3, 3.1.4**).

Since the DPD-Fe chemistry is catalytic, the absorbance signal continues to increase linearly with time as long as no reagent is limiting and the absorbance signal is still within the linear rage.  A line can be fitted to this increasing absorbance signal and the slope of the line (the reaction progress curve) can be plotted as a function of the concentration of dFe in the standards to create a calibration curve, which can then be used for the determination of dFe in unknown samples.

For both the SHC and SFC protocols, the analytical cycle was repeated four times for each sample or standard.  The absorbance signal from the first analytical cycle was always observed to be significantly lower than the signal from the subsequent three analytical cycles and was therefore used as a priming/conditioning step to introduce fresh reagent and sample solutions into the system for the following three analytical cycles.  The average absorbance signal from the last three cycles was used for quantifying the absorbance signal and the

standard deviation between the SFC reaction progress slopes from the last three runs was calculated as a measure of reproducibility.

**3.1.3 Signal monitoring in FIAlab software.** In the case of the DPD-Fe chemistry, the formation of DPDQ can be observed at 514 and 550nm wavelengths, this method used the 514nm wavelength to monitor the reaction. The absorbance at 620nm was always flat and not affected by DPDQ production and showed little noise during analyses. The absorbance at 620nm was also representative of continuous changes in flow cell conditions that affected all wavelengths and used as a reference wavelength (see **Figure 2.6**). When a mixed sample, DPD, NH$_4$Ac, and H$_2$O$_2$ solution entered the flow cell the refractive index of the solution was much greater than that of DI water; which also resulted in an increased absorbance at all wavelengths. In the FIAlab software, correcting the absorbance signal was achieved by simply subtracting the absorbance value at the reference wavelength from the absorbance measured at the primary wavelength, Absorbance(514nm)-Absorbance(620)(**Figure 3.1.5**). This correction was made regardless of the detection technique (SHC or SFC), as both were subject to continuous shifts in the spectral baseline.

The FIAlab software could be used to further analyze a set of standards and samples and process the data to create calibration curves and calculate the sample concentration by uploading a sample definition file in which standards and their concentrations were defined. When using SHC protocol, the software could be used to find the local peak maxima, and in the case of SFC it could be used to calculate the slope of the absorbance profile over time. A drawback of the FIAlab software was

that it did not permit either selection of sub-regions of the absorbance profile in which to find the peak maxima, or in the case of SFC, did not permit defining a sub-region of the data over which to fit the line. Thus, if there were regions of signal instability or noise spikes in the run, these could lead to errors in the calculated peak heights or slopes. For example, when using the SHC technique, an absorbance peak formed from refractive index gradients prior to or following the absorbance peak from the colored DPDQ solution entering the flow cell (**Figure 3.1.2**). Since the FIAlab software finds the maximum absorbance value over the entire run, it may in turn be from such an interference. Furthermore, most absorbance peak based methods such as FIA require that a baseline be calculated prior to and/or following the arrival of the absorbance peak to correct the absorbance peak height for the background absorbance signal unrelated to the reaction being monitored. However, the version of FIAlab software that was used did not include a baseline correction step to account for background absorbance in the flow cell.

With the SFC technique, the first ~10s of the absorbance profile has a slightly different slope than the rest of the profile (**Figures 2.6, 3.1.5**). This has also been observed using the SFC technique with other analytical methods; however, the exact reason remains unknown (J. Ruzicka, pers. comm.). After ~10s had elapsed, the time course of the absorbance profile became linear. The FIAlab software, however, does not allow this first part of the run to be excluded from the line fitting process and there is no option in the FIAlab software to use a running mean of the data to minimize noise in the absorbance profiles and remove any anomalous spikes.

The final data set generated by the FIAlab software consists of the 620nm corrected absorbance values for each of the two wavelengths monitored (514nm and 620nm) and their time points. The reference wavelength (620nm) has the time recorded and all absorbance values are listed as zero since the absorbance at 620nm was subtracted from each of the wavelengths monitored, including the absorbance signal from the reference wavelength, 620nm.

**3.1.4 Data processing with Matlab.** To overcome the deficiencies in the FIAlab software, Matlab was used to process and analyze corrected SFC and SHC absorbance profiles. Matlab processing of the data also allowed for greater user control of the data processing.

For the SHC technique, with a peak width of 14seconds, a four- point moving average was first applied to the 4Hz data, producing a data point every second, minimizing the effects of high frequency noise and outliers (**Figure 3.1.6**). A four-point moving average was chosen because it allowed for noise reduction while still maintaining the overall shape and height of the raw absorbance data. Next, using the smoothed, corrected five seconds of the absorbance profile prior to the arrival of the absorbance peak a baseline was calculated. No baseline value was calculated from the absorbance signal following the absorbance peak. The baseline value was then subtracted from the entire absorbance corrected sample run data. From the baseline corrected data, the maximum value of the absorbance and the time point at which it occurred were identified by the Matlab software and a second order polynomial was fit to a set number of points (defined by the user) around the absorbance maximum of the peak. This was accomplished using Matlab's built-in

function, 'polyfit', which could fit any order polynomial to a data set. A second order polynomial was used to fit the peak maxima as a parabola was observed to be the best approximation of the shape of the absorbance peak, this was also observed for Zn peaks (**Figure 3.1.7**) (M. Grand, pers. comm.). The peak maximum was then determined from the fitted polynomial. Thus, the maximum absorbance can be determined in this manner even if it was not recorded during the continuous signal monitoring. Using a fitted polynomial also helped to eliminate outliers or noise that might have existed at or around the absorbance maximum in the raw data, providing a more precise means to evaluate the absorbance peaks resulting from the SHC technique (**Figure 3.1.7**). SHC data that were processed in this way will now be referred to as corrected absorbance maxima.

Calibration curves were constructed in Excel by plotting the individual standards' average corrected absorbance maxima against the concentration of the standard. A line was fitted to the average corrected absorbance maxima data as a function of standard concentrations, producing a standard curve. The calibration curve was then used to determine the concentrations of dFe in unknown samples.

For SFC, (**Figure 3.1.8**), the constant reaction rate leads to a linear increase in absorbance over time meaning more points can be averaged to reduce the effect of noise and outliers than in SHC. For SFC, the FIAlab corrected absorbance values and their corresponding time points are imported into Matlab, and the data are smoothed using a 20-point running average (5 second average). The Matlab function 'polyfit' is then used to fit a straight line to the smoothed SFC absorbance values between elapsed time 10s and 60s and also to provide the coefficients for the

fitted line.  The coefficients of the fitted line are then used to calculate y-values using time as the x- values to plot the fitted line on top of the smoothed SFC absorbance data.  This process ensures that the line fitted to the SFC data is characteristic of the data and the $R^2$ value for the line fit to the data is calculated (**Figure 3.1.8**).

Matlab was used to process the SFC data and construct calibration curves. From the last three analytical cycles of each standard or sample run, the average reaction progress slope, average $R^2$, and the standard deviation between the slopes of the fitted lines were calculated.  Calibration curves were produced by plotting the average slope of the reaction progress curve of each standard against its Fe concentration.  Samples were run in the same manner as standards and the average calculated slope for each sample was used with the calibration curve to determine the unknown concentration of dFe in the sample.

**3.1.5 Conclusions in signal monitoring and data processing.**  The SHC technique proved extremely useful for visualizing the extent of mixing in the holding coil but was not sensitive enough for Fe determinations in the open ocean and suffered from interferences in the absorbance profile from refractive index gradients due to matrix gradients passing through the flow cell.  In contrast, the SFC technique was free from the major interferences that limit the sensitivity of the SHC method and provided a more accurate measure of the absorbance signal that resulted from the concentration of dFe in samples and standards.  The ability to fit a line to many points along the SFC profile improved the accuracy of the curve fit to the absorbance profile and further improved the precision of the method as compared to using the few points at the top of an absorbance peak as a measure of

peak height with SHC.  Thus, the SFC technique was adopted for monitoring the absorbance signal when making Fe determinations.

## 3.2 Optimization of Chemistry and Related Factors

Adapting the DPD-Fe methodology to the µSIA platform first required understanding the inherent differences between µSIA and FIA, such as the extent of mixing, the number of solutions that can enter the system, and reagent blanks. Because of these differences, the chemistry required reoptimization for use in µSIA.

The µSIA platform is an automated method where the solutions aspirated into the holding coil effectively dilute one another in the mixing process.  The concentrations of sample and reagent solutions participating in a reaction are a function of the initial reagent and sample concentrations and the extent of mixing (see section *3.2.1. Mixing* below).  The extent of mixing that occurs is a function of the distance travelled by each solution aspirated, and thus is a function of the aspirated volume of each solution, the aspiration order, and the overall volume of solutions aspirated.  Therefore, the individual concentrations of the reagent solutions participating in the reaction will be less than the concentrations of the individual reagent solutions entering the LOV, where solutions have yet to undergo mixing.

The key to optimizing µSIA is to mix sufficient amounts of the reagent solutions into the sample solution zone in the holding coil to maximize the reaction without diluting the sample more than is necessary.  Since more than one reagent is required for the DPD- Fe(III) method, it was also critical to find the optimal ratio of

reagent concentrations to one another mixed in the sample solution zone to maximize the reaction. This was done empirically. Since the DPD- Fe(III) reaction is catalytic, the analyte (Fe) is not consumed in the reaction; however, the reagents are. By monitoring the catalytic reaction as a function of time and variable reagent concentrations, the reagent limiting the rate at which DPD oxidizes to DPDQ (either $H_2O_2$ or DPD) could be determined, which will now be referred to as the rate-limiting reagent. As discussed below (see section *3.2.4 Reagent Concentrations*), the optimal reagent ratio was observed to occur when neither the DPD nor the $H_2O_2$ were rate-limiting during the time period that the reaction was being monitored.

To optimize the DPD-Fe chemistry for μSIA, the extent of mixing was investigated first to find the best order to aspirate the sample and reagent solutions into the holding coil so as to maximize mixing and minimize the reagent blank associated with the DPD reagent (see below, *Aspiration Sequences: Order*). The volumes of the sample and reagent solutions were then investigated to minimize the reagent volume while maintaining the optimal ratio of the DPD reagent to the $NH_4Ac$ & $H_2O_2$ reagent (see section *3.2.3 Aspiration Sequence: Volumes* below). Using the optimized aspiration order and volumes, the concentrations of the reagents were then investigated and optimized.

Once the overall aspiration sequence (aspiration order, volumes, and reagent concentrations) was optimized, the contributions to the overall method blank were investigated. Surprising results from these experiments revealed that a non-Fe blank was responsible for ~50% of the overall method blank (see section *3.3 The System Blank & Interferences* below). This could explain complications that arose

during the optimization of the overall aspiration sequence with regards to the relationship between reaction progress curves and sensitivity (see section *3.2.4 Reagent Concentrations* below).

**3.2.1. Limitations of the μSIA -LOV platform.** *Mixing.* The limited extent of mixing possible in μSIA is one of the key difference between the μSIA and the FIA methodology, where mixing is essentially complete partially as a result of the longer travel distances that the reagent and sample mixture experiences. Furthermore, the presence of confluence points in FIA, where sample and reagent solutions merge into a carrier stream results in greater turbulence, thereby improving mixing. Mixing in μSIA is limited by the short travel distance of solutions, which occurs through the sequential aspiration of sample and reagent solutions into the holding coil. Mixing continues when the flow is reversed and the solution in the holding coil is dispensed to the flow cell. Because there are no confluence points in μSIA, mixing is a function of the travel distance of solutions.

For example with the μSIA platform used for this study, the entire holding coil capacity (1mL) is initially filled only with carrier solution (DI water) prior to any reagents or samples being aspirated. The first solution aspirated into the holding coil is in contact with the DI water carrier solution. As the solution is aspirated into the holding coil, an equal volume of the DI water carrier is displaced from the holding coil to the syringe pump. While the first solution is being aspirated it begins to mix with the carrier solution in the holding coil. A parabolic flow profile forms as a result of faster flow rates at the center of the tubing than along the walls of the tubing, where flow is slower due to friction (**Figure 3.2.1**). When the second

solution is aspirated it begins to mix with first solution at the interface between the two solutions. As the parabolic flow profiles form, each plug of solution aspirated mixes with the previously aspirated solution, a fraction of which is still present along the walls of the holding coil tubing. The lateral mixing that results from this purely laminar flow is referred to as axial dispersion (**Figures 3.1.1, 3.2.1**).

The extent of mixing is further improved from purely laminar flow conditions by wrapping the holding coil in a cylindrical shape, which promotes radial dispersion. Radial dispersion is further improved during the flow reversal that occurs in μSIA once all solutions have been aspirated into the holding coil (**Figures 2.1, 3.1.1**). By reversing the flow of solutions in the holding coil, the previously parabolic flow profile resulting from axial dispersion takes on the shape of an ellipse, resulting from effective radial and axial dispersion in the center of the mixed sample and reagent solution zone (**Figure 3.1.1**).

***The lab on valve (LOV).*** With the FIA-based DPD- Fe chemistry three individual reagents are required; $H_2O_2$, $NH_4Ac$ buffer, and acidified DPD. However, for the μSIA- based method, the LOV used could not accommodate aspirating all of the reagents and the sample solution separately because there are only two LOV ports available for reagent solutions and one port for the sample solution (**Figure 2.1**). Furthermore, only three solutions can adequately mix within the μSIA platform since there is only one holding coil. Therefore, it was necessary to reduce the number of reagent solutions by finding a mixture of two of the three required reagents that could be aspirated into the LOV as a combined reagent solution. This

required investigating the interactions between the various reagents and the potential reagent blanks that might result.

*Reagent interactions.* The interactions between the $NH_4Ac$ buffer solution, $H_2O_2$ solution, and acidified DPD solution were investigated to find the most stable reagent combination that could be used. Investigating the stability of the reagent mixtures was necessary as a result of contaminant Fe in the DPD reagent, which could oxidize the DPD reagent when reagent combinations were at pH>3. Furthermore, investigating the stability of $H_2O_2$ solutions at pH>4.7 was necessary as the decomposition of $H_2O_2$ is known to increase with increasing pH as indicated by the manufacture's specification sheet (Sigma- Aldrich, St. Louis, MO).

In the FIA based method, the DPD reagent is prepared in acid solution (pH <3) to prevent the oxidation of DPD by contaminant Fe in the reagent and then is cleaned in-line by mixing it with the $NH_4Ac$ buffer immediately before passing the mixture through an 8-HQ resin column which removes the Fe (see section *3.3 The System Blank & Interferences* below) (Measures et al., 1995). It is necessary to raise the pH of the DPD as the column will only remove Fe(III) in the pH range 3-4.2 but will remove Fe(II) and Fe(III) in the pH range 5.2-6.0 (Obata et al., 1993). Since in-line reagent cleaning was not feasible with the μSIA platform, the DPD used for optimizing the chemistry was not precleaned. However, the presence of Fe in the DPD reagent made combining two reagent solutions for μSIA complicated as any contaminant Fe associated with the DPD reagent as Fe(III) would oxidize the DPD reagent to DPDQ above pH ~3; effectively decreasing the concentration of the DPD reagent over time and increasing the method blank (King, 1972). Thus, the

interactions in reagent combinations were investigated to determine the relative stability of each reagent in various reagent mixtures and to evaluate the potential reagent interactions that could result in increased reagent blanks.

Reagents were considered 'stable' if there was no observed change in the sensitivity and LOD of the method over a 24-hour period. This was established by evaluating the change in the sensitivity of the method and the blank signal that resulted when comparing 24-hour old mixed reagents with freshly prepared ones. A reagent combination was considered 'relatively stable' if the observed change in sensitivity occurred slowly over a relatively long period of time and the LOD of the method maintained a constant value even as sensitivity changed. For example, a decline in the sensitivity of the method of less than 50% over 12 hours, with a constant LOD of 0.1nM with time would indicate that this is a 'relatively stable' reagent mixture.

A reagent combination was considered unstable when the change in sensitivity occurred rapidly, often on the order of 10% loss in sensitivity per hour.

*DPD & NH$_4$Ac.* The DPD reagent was prepared in 24mM HCl to prevent oxidation of the DPD compound prior to its interacting with the sample and the NH$_4$Ac & H$_2$O$_2$ solutions. Mixing the DPD reagent with the pH 6.3, 0.6M NH$_4$Ac buffer solution resulted in a raised pH ($\sim$5) of the mixed reagent and the immediate production of DPDQ was apparent from the rapid visible change in the color of the reagent mixture from clear to bright pink. The rapid formation of DPDQ in the batch DPD and NH$_4$Ac mixture means that the DPD reagent was being consumed, reducing the concentration of DPD over a short period of time (few hours) as it was oxidizing

to DPDQ.  Thus, since the concentration of the DPD reagent declined rapidly as a function of time when mixed with $NH_4Ac$, this reagent mixture was not considered to be stable and was not a feasible way to introduce these two reagents into the μSIA-LOV as a single mixed reagent solution.

*DPD & $H_2O_2$.*  The combination of acidified DPD and $H_2O_2$ reagent solution was observed to slowly turn from clear to pink with time, indicating that DPD was oxidizing to DPDQ at the mixture pH of ~3.5; (note that the pH of solutions containing $H_2O_2$ cannot be accurately measured with a glass electrode).  This oxidation was also confirmed by a 50% decrease in the slope of a 0.4nM Fe sample reaction progress curve over a period of 2 hours.  Since the $H_2O_2$ was also being consumed by the reoxidation of Fe(II), both the concentration of DPD and $H_2O_2$ in the reagent mixture were declining as a function of time.  This reagent combination was considered highly unstable.

*$NH_4Ac$ & $H_2O_2$.*  The most stable reagent combination found was a mixture of the $NH_4Ac$ reaction buffer (pH 6.3) with the 30% (w/w) $H_2O_2$ solution.  The $H_2O_2$ solution is stable at pH ~4.7 and when the pH of the solution was raised by adding the $NH_4Ac$ buffer to the $H_2O_2$ solution and the formation of bubbles in the mixed reagent solution was observed over a 12-hour period suggesting that evasion of oxygen from the solution was occurring.  However, the decline in the $H_2O_2$ concentration in the mixed reagent solution was relatively slow and was observed to result in only a 40% decline in the sensitivity of the method over a 12-hour period, with a linear decline in sensitivity over the first 8 hours.  This 40% decline in sensitivity was reproducible and occurred over a long enough time period that the

overall change in sensitivity could be corrected for.  After approximately an 8-hour period, the decline in sensitivity was observed to plateau. Thus, despite this reagent mixture being only 'relatively stable' from the loss of $H_2O_2$ with time; the combination of the $NH_4Ac$ & $H_2O_2$ reagents was the most stable reagent combination and the loss of peroxide with time was highly reproducible.  Furthermore, the blank signal declined as sensitivity decreased resulting in an unchanged LOD of ~0.1nM for the μSIA method using both fresh $NH_4Ac$ & $H_2O_2$ and 24-hour old $NH_4Ac$ & $H_2O_2$ reagent mixtures.  Thus, the observed change in the sensitivity of the method and the blank signal did not affect the overall detection limit of the method over this time period.

It is important to note that for this method the $H_2O_2$ used was Sigma-Aldrich stabilized $H_2O_2$.  It was found to be necessary to use stabilized $H_2O_2$ when combining it with the $NH_4Ac$.  Hydrogen peroxide is reported to be stable below pH ~4.5-4.7. When $H_2O_2$ without stabilizers was used no DPDQ was observed to form in the reaction.  This was likely a result of rapid degradation of the $H_2O_2$ occurring in the $NH_4Ac$ & $H_2O_2$ mixture at the pH of 6.1 (Petri et al., 2011).

*Spiking samples and standards.*  Since no reagent combination was deemed to be truly stable, spiking the sample (in the form of acidified seawater standards) with the $H_2O_2$ reagent was investigated.  The results produced were highly variable with the greatest sensitivity being observed immediately after the sample was initially spiked.  As an example, the slope of a 0.4nM dFe seawater sample's reaction progress curve declined by ~50% over 12 hours for seawater samples, but interestingly remained constant for a standard made in DI water.  This suggests that

the $H_2O_2$ was probably being consumed in reactions with organic material in the seawater.  In contrast, DI water standards, which had low organic matter content, retained the same sensitivity over 12 hours

*Final reagent mixtures.*  Based on the observations from the reagent interactions and sample spiking experiments above, the combination of the $NH_4Ac$ (pH 6.3) reaction buffer and the $H_2O_2$ solution (30% w/w) was chosen as the reagent combination to be used.  Despite the decrease in sensitivity over time, the drift in sensitivity was highly reproducible and the LOD of the method remained constant.

With the $NH_4Ac$ & $H_2O_2$ reagents combined, the acidified DPD reagent and sample solution were aspirated into the µSIA -LOV independently.  Thus only three aspirated solutions were required to mix in the holding coil for the method (**Figures 2.1, 3.1.1**).

**3.2.2 Aspiration order**.  The limited mixing that is encountered with µSIA and the fact that this will vary depending on the relative aspiration positions and viscosities suggests that the order in which samples and reagents are aspirated also plays a critical role in optimizing the methodology.  The order of the aspiration sequence was investigated to determine the optimal order in which to aspirate sample and reagent solutions (see section *3.2.1 Limitations of the µSIA Platform: Reagent Interactions* above).

Initial experiments using dyes focused on investigating the extent of mixing across the three separate plugs of solution.  The first experiment, using DI water to simulate sample and reagent solutions aspirated **(Figure 3.2.2)**, demonstrated that

there was sufficient dispersion within the holding coil for two reagent solutions and one sample solution to partially mix, with the well-mixed region shown in the shaded box in **Figure 3.2.2**. In this experiment three 50μL DI water plugs of solution were aspirated into the holding coil to simulate the aspiration of reagent and sample solutions. Each of these plugs of solution in turn had bromocresol purple added to them to permit separate SHC analyses to visualize the extent of dispersion of each dyed plug of solution with its neighbor. Observation of the overlap between solutions in the holding coil (pink shaded region in **Figure 3.2.2**), confirmed that mixing across three zones of solutions in the holding coil was feasible with DI water; however, this did not include any of the effects resulting from the differences between sample and reagent solution viscosities on the extent of mixing.

The order in which the sample and reagent solutions were aspirated was also investigated to minimize reagent interactions that increase the blank signal while improving the sensitivity of the method to dFe in samples. To reduce the interactions between the DPD and the $NH_4Ac$ & $H_2O_2$ reagent solutions that increase the blank signal (**Figure 3.2.3**), only aspiration sequences in which these reagents were separated by the sample were investigated (**Figure 3.2.4**). In this scheme, the reagents could only interact after they have mixed with the sample solution in the holding coil. These sequences were observed to significantly reduce the reagent blank compared to having the DPD and $NH_4Ac$ & $H_2O_2$ reagents aspirated adjacent to each other (**Figure 3.2.3**).

Consequently, two specific aspiration sequences were then investigated in aspiration order:  A) DPD - Sample - $NH_4Ac$ & $H_2O_2$ mixture and B) $NH_4Ac$ & $H_2O_2$ mixture – Sample– DPD (**Figure 3.2.4**).  Since the viscosity of the solutions aspirated into the holding coil will affect the extent of mixing possible, it was necessary to understand the differences in mixing between these two aspiration sequences as a function of the sample and reagent solution viscosities.  Mixing was visualized using dyed plugs of the sample, DPD, and $NH_4Ac$ & $H_2O_2$ solutions.  To eliminate any potential interference from the colored DPDQ reaction product, acidified DI water was used instead of the acidified DPD reagent.  One by one the DI water (representing the DPD reagent), sample, and $NH_4Ac$ & $H_2O_2$ solutions were dyed for individual SHC runs and the resulting absorbance peaks were recorded for both aspiration sequences **(Figure 3.2.5)**.  All solutions were buffered to a pH of 4.3 to ensure that the bromocresol purple dye was indicative of dispersion and not pH gradients within the sample and reagent mixture.

These experiments revealed that the aspiration order $NH_4Ac$ & $H_2O_2$ solution-Sample-DPD (**Figure 3.2.5.B**) allowed for greater overlap of the sample and reagent solutions in the holding coil at higher concentrations than was observed with the opposite aspiration sequence (**Figure 3.2.5.A**).  This is indicated by the area and height of overlap between the sample and reagent peaks that are dyed, shown in the pink shaded region (**Figure 3.2.5, A & B**).  The height of the shaded region is reflective of the relative concentrations of the sample and reagent solutions in the zone where the sample and reagent solutions mix.

The higher concentrations of sample and reagent solutions mixing in the aspiration sequence $NH_4Ac$ & $H_2O_2$- Sample- DPD means that the sample had undergone less dispersion, and thus more of the sample would be present to react with the reagents. Furthermore, the $NH_4Ac$ & $H_2O_2$ reagent was dispersed throughout the sample zone and was still at a relatively high concentration in the zone where the reagents and sample mix. This is because the $NH_4Ac$ & $H_2O_2$ reagent was aspirated first, and therefore travelled the farthest and underwent the most dispersion in the holding coil.

With the reverse aspiration sequence the buffer solution was aspirated last and, as shown in **Figure 3.2.5,** resulted in far less dispersion of the buffer solution, likely resulting in a sample and reagent mixture in the holding coil that was below the optimal pH range. Furthermore, the high viscosity of the $NH_4Ac$ & $H_2O_2$ reagent makes dispersion difficult with short travel distances. This suggested that the aspiration sequence $NH_4Ac$ & $H_2O_2$- Sample - DPD (**Figure 3.2.4**) was the better aspiration sequence to ensure that the sample and reagent mixture was buffered to the optimal pH range (pH 5.5-6.0) for the reaction to take place and was chosen as the optimal order to aspirate the sample and reagent solutions (Measures et al., 1995).

**3.2.3 Sample and reagent volumes.** Since there are, in theory, a limitless number of combinations possible with regards to varying the individual volumes of the sample and reagent solutions aspirated in the μSIA methodology, steps were taken to simplify the optimization process. To allow for the comparison of aspiration sequences with variable reagent and sample volumes, the total aspirated

volume of solutions was kept constant at 170μL, so that the overall extent of mixing in the holding coil was the same. To further simplify the optimization of the reagent and sample volumes, the volume of the $NH_4Ac$ & $H_2O_2$ reagent aspirated was kept at 50μL and the sample and DPD reagent volumes were varied. Thus, to keep the total aspirated volume the same, increasing the volume of the sample solution aspirated occurred at the expense of the volume of the DPD reagent aspirated.

The SFC technique for signal monitoring was used to investigate the effects of varying the sample and DPD reagent volumes aspirated on the sensitivity of the method. Seawater standards were run using the aspiration order $NH_4Ac$ & $H_2O_2$-Sample- DPD and varying the volumes of the sample and DPD reagent solutions to produce calibration curves for each volume change. The slopes of the calibration curves produced were then indicative of the sensitivity of the method to varying the aspirated volumes. However, changing the volumes of the DPD and sample solutions aspirated shifts the position of the zone of solution with the optimal reagent ratio that needs to be in the flow cell for SFC absorbance monitoring.

Thus, after changing the aspiration volumes but prior to running a full set of standards, a low Fe seawater sample (~0.4nM dFe) was first run using the new aspiration volumes and monitored using the SHC technique to produce a peak shaped absorbance signal (**Figure 3.1.6**). The position of the peak maximum corresponded to the zone of solution in the holding coil with the optimal reagent ratio. Using the flow rate at which the mixed solution from the holding coil was dispensed to the flow cell and the time it took for the peak maximum to enter the

flow cell, the volume of the mixed solution that needed to be dispensed into the flow cell for the SFC technique could be calculated (**Figure 3.1.4**).

Using the volume calculated above, a SFC program was run using the same low Fe seawater sample. The exact volume of the mixed sample and reagent solution to be dispensed from the holding coil to the flow cell was then varied in 10μL increments over a range of 60μL to find the volume that resulted in the highest sensitivity (**Figure 3.1.4**).

The optimal volume of the mixed sample and reagent solution dispensed to the flow cell was then used to run a full set of dFe standards (+0nM to +5nM dFe) and construct calibration curves.    Calibration curves were also produced for dispensing the optimal volume +/- ~20μL of the mixed sample and reagent solution to the holding coil to ensure that the optimized volume was characterized by the highest sensitivity.  The resulting calibration curves were then used to characterize the sensitivity, blank, and LOD of each aspiration sequence to the variations of the volumes of the DPD reagent and the sample solution, and to ensure that the optimal zone of mixed solution was in the flow cell.  The overall method blank was calculated as the intercept of the calibration curve divided by the slope of the calibration curve.

It was found that the addition of 20μL of carrier solution (DI water) aspirated following the DPD reagent improved the mixing of the DPD reagent into the sample and $NH_4Ac$ & $H_2O_2$ mixture in the holding coil by increasing the overall travel distance of the aspirated sample and reagent solutions. The calibration curves

characterizing this aspiration sequence as a function of the volume of the mixed sample and reagent solution dispensed to the flow cell are shown in **Figure 3.2.6**.

Starting with volumes of NH$_4$Ac & H$_2$O$_2$ (50μL)- Sample (50μL)- DPD (50μL)- Carrier (20μL); the volume of the sample and DPD reagent solution plugs were varied. Based on the slopes of the calibration curves from this experiment it was apparent that dispensing 140μL of the solution in the holding coil into the flow cell for SFC absorbance monitoring resulted in the greatest sensitivity for this aspiration sequence and volumes. Furthermore, dispensing 140μL of solution into the flow cell resulted in a low overall method blank, as indicated by the calibration curve intercept, when compared to dispensing 160μL of solution into the flow cell (**Figure 3.2.6**). This was likely a result of higher concentrations of H$_2$O$_2$ in the flow cell during analyses, thereby allowing for more contaminant Fe to be recycled (in the 160μL case) during the oxidation of the DPD reagent. Furthermore, since the concentration of peroxide is also correlated to the non-Fe blank of the system, it is likely that the higher blank signal is from both Fe contamination in the DPD reagent and the non-Fe blank increasing with higher concentrations of H$_2$O$_2$ (see section *3.3 Blanks*).

One of the main factors that determined the sensitivity of the μSIA based method was the volume of sample used relative to all other reagents, as is the case with FIA (Ruzicka & Hansen, 1988). This is because aspirating a larger volume of sample introduces a greater amount of the analyte to react with reagents. Since the DPD reagent is contaminated with dFe, further optimization of aspiration volumes focused on decreasing the volume of the DPD reagent aspirated to minimize the

associated Fe blank contribution and increasing the volume of the sample solution aspirated. Thus, each time the volume of the DPD reagent aspirated was decreased, the volume of the sample solution aspirated was increased by the same amount to improve the sensitivity of the method to dFe in the samples.

The next aspiration sequence investigated was $NH_4Ac$ & $H_2O_2$ (50µL)- Sample (70µL)- DPD (30µL)- Carrier (20µL- DI water) (**Figure 3.2.7**). This aspiration sequence resulted in a 20-30% decline in sensitivity compared to when the sample and DPD volumes aspirated were 50µL each. However, it is worth noting that this also resulted in a three-fold decrease in the overall method blank, thereby resulting in an improved LOD.

The overall blank of the method could be further reduced by increasing the sample volume aspirated from 70µL to 80µL and decreasing the volume of the DPD reagent aspirated from 30µL to 20µL (**Figures 3.2.7, 3.2.8**). To improve mixing and further minimize the potential blank from the DPD reagent, the 20µL of carrier solution (DI water) aspirated following the DPD reagent solution was replaced by 50µL of acidified sample for a final aspiration sequence of $NH_4Ac$ & $H_2O_2$ reagent (50µL)- Sample (80µL)- DPD (20µL)- Sample (50µL). By increasing the volume of the plug of solution aspirated last in the sequence, the overall mixing was improved by increasing the travel distance of all reacting solutions in the holding coil. Acidified sample replaced the DI water carrier solution in an attempt to keep the plug of the DPD solution aspirated surrounded by acidified solutions to minimize the potential for oxidation of the DPD reagent prior to adequately mixing with the sample and the $NH_4Ac$ & $H_2O_2$ solutions. Acidified sample was used rather than

acidified DI water to improve sensitivity by increasing the amount of analyte from the sample in the holding coil and to minimize the addition of potential contaminant Fe from the DI water.

Prior to finalizing the sample and reagent volumes, the volumes of the DPD and the $NH_4Ac$ & $H_2O_2$ reagents were investigated independently to determine if dispersion during mixing was significantly diluting reagent concentrations, thereby limiting sensitivity. To investigate the dilution of the DPD reagent during dispersion, calibration curves were produced from two aspiration sequences with variable DPD reagent volumes; 1) $NH_4Ac$ & $H_2O_2$ reagent (50µL)- Sample (80µL)- DPD (20µL)- Sample (50µL) & 2) $NH_4Ac$ & $H_2O_2$ reagent (50µL)- Sample (80µL)- DPD (70µL) (**Figure 3.2.9**). As demonstrated in **Figure 3.2.9**, the difference in sensitivity between two aspiration sequences with variable DPD volumes was ~13%, with slightly higher sensitivity when using 70µL of the DPD reagent. However, the overall method blank associated with the aspiration sequence using 70µL of DPD was approximately three times higher (16.7nM) than the overall method blank associated with using only 20µL of DPD (5.9 nM dFe). The decrease in the method blank when using only 20µL of the DPD reagent was primarily a result of having less of the DPD reagent and the associated contaminant Fe in the flow cell. Furthermore, the relatively consistent sensitivity suggested that dispersion of the 20µL plug of 0.45mM DPD solution did not dilute the reagent to the point of limiting the sensitivity of the method and was chosen as the optimal volume of the acidified DPD reagent at this concentration of DPD (0.45mM).

As previously mentioned, the concentrations of the reagents actually present in the reaction zone is a function of the original concentrations of the reagents, the volume of the reagents aspirated, and the overall distance the aspirated solutions travel. Thus, at lower DPD concentrations with the same $NH_4Ac$ & $H_2O_2$ reagent, dispersion could dilute the DPD reagent to the point of limiting the rate of reaction; which is discussed in section *3.2.4 Reagent Concentrations* below.

Similarly, the volume of the $NH_4Ac$ & $H_2O_2$ reagent aspirated was investigated to determine if the 50µL of the $NH_4Ac$ & $H_2O_2$ reagent maintained a high enough concentration of both $NH_4Ac$ & $H_2O_2$ during mixing or whether sensitivity was improved by increasing the aspirated volume of the $NH_4Ac$ & $H_2O_2$ reagent to 100µL. To aspirate 100µL of $NH_4Ac$ & $H_2O_2$ reagent, an additional 50µL of carrier solution had to be dispensed to waste from the holding coil prior to aspirating the sample and reagent solutions to accommodate the extra volume aspirated. Two aspiration sequences; 1) $NH_4Ac$ & $H_2O_2$ (100µL) – Sample (80µL) – DPD (70µL) and 2) $NH_4Ac$ & $H_2O_2$ (50µL) – Sample (80µL) – DPD (70µL), were used to analyze seawater standards (+0-5nM dFe). Calibration curves were produced to characterize the sensitivity and overall method blank associated with the aspiration sequences and respective volumes of solutions (**Figure 3.2.10**). The difference in sensitivity between the two aspiration sequences was ~3%; thus, aspirating an additional 50µL of $NH_4Ac$ & $H_2O_2$ did not improve the overall sensitivity of the method. However, the overall method blank was 16% higher when aspirating 100µL of the $NH_4Ac$ & $H_2O_2$ solution as compared with aspirating only 50µL of the $NH_4Ac$ & $H_2O_2$ solution. The increase in the overall method blank was likely a result

of the linear increase in both the contaminant Fe blank from the DPD reagent as well as the non-Fe blank associated with the method. Higher concentrations of $H_2O_2$ would allow for more of the contaminant Fe to be recycled following the oxidation of the DPD reagent, thereby increasing the signal from contaminant Fe. Furthermore, the non-Fe blank associated with the method likely increased with increasing $H_2O_2$ concentrations as this non-Fe blank was found to be a function of the concentration of $Cl^-$ and $H_2O_2$ in samples and reagents (see section *3.3 The System Blank & Interferences*). Thus, the volume of the $NH_4Ac$ & $H_2O_2$ aspirated for the method was kept at 50μL.

The optimized final aspiration sequence and volumes, $NH_4Ac$ & $H_2O_2$ mixture (50μL)- Sample (80μL)- DPD (20μL)- Sample (50μL), was used to investigate the independent effects of changing either the concentration of the DPD reagent or the concentration of the $H_2O_2$ in the 0.6M $NH_4Ac$ buffer solution on the sensitivity and blank of the method.

**3.2.4 Reagent Concentrations.** Optimization of reagent concentrations focused on investigating the effects of variable reagent concentrations on the sensitivity and overall blank of the μSIA-based method for the determination of dFe in seawater samples. The concentration of the DPD reagent and the $H_2O_2$ concentration in the 0.6M $NH_4Ac$ buffer solution were investigated separately keeping other components constant and using the aspiration sequence $NH_4Ac$ & $H_2O_2$ solution (50μL)- Sample (80μL)- DPD (20μL)- Sample (50μL). 140μL of the mixed sample and reagent solution were dispensed to the flow cell for SFC monitoring over a 60 second period. Standard curves using +0nM, +1nM, +2nM,

+3nM, and +5nM dFe seawater standards were produced each time the concentration of a reagent was changed. The trends in the sensitivity and the overall blank could be observed from the slope and intercept values from the calibration curves, respectively, as a function of changing either the concentration of the DPD reagent or the $H_2O_2$ concentration in the $NH_4Ac$ & $H_2O_2$ reagent mixture.

$H_2O_2$. The effect of changing the $H_2O_2$concentration in the $NH_4Ac$ & $H_2O_2$ reagent on the sensitivity of the method was investigated first. The concentration of the $H_2O_2$ in the $NH_4Ac$ & $H_2O_2$ reagent mixture was varied while the concentration of $NH_4Ac$ in the mixture was held constant at 0.6M $NH_4Ac$ and the concentration of the DPD reagent was kept at 0.07mM DPD in 24mM HCl. As demonstrated in **Figure 3.2.11**, the optimal sensitivity was achieved with 13% $H_2O_2$ (w/w) (12% $H_2O_2$ (v/v)) in the $NH_4Ac$ & $H_2O_2$ reagent mixture and, as shown in **Figure 3.2.12**, the method using 13% $H_2O_2$ (w/w) had the lowest calculated method blank. Above 13% $H_2O_2$ (w/w), the sensitivity of the method began to decline (**Figure 3.2.11**) and the method blank began to increase (**Figure 3.2.12**).

The apparent increase in the method blank above 13% $H_2O_2$ (w/w) was a result of the declining sensitivity of the method to dFe despite a linear increase in the +0nM standard SFC reaction rate progress curve with increasing concentrations of $H_2O_2$ in the $NH_4Ac$ & $H_2O_2$ reagent. As previously mentioned, this is a result of the increasing non-Fe blank associated with the method and will be discussed further in section *3.3 The System Blank & Interferences*. The increase in the non-Fe blank limits the linear working range of the method for dFe standards. This results in a decline in the sensitivity of the method to dFe as the non-Fe contribution to the blank

increases and the overall method blank increases. For example, at 13% $H_2O_2$ (w/w) the sensitivity of the method was $1.03 \times 10^{-4}$ arbitrary slope units/nM and the intercept of the calibration curve had a reaction rate progress curve slope value of $5.136 \times 10^{-4}$. By dividing the calibration curve intercept's reaction rate progress curve slope value by the calibration curve slope the method blank could be calculated, which in this case was 4.99nM dFe.

Above 13% $H_2O_2$ (**Figure 3.2.11**), sensitivity declined with increasing $H_2O_2$ concentrations and at 17% $H_2O_2$ the sensitivity had declined to $6.32 \times 10^{-5}$ arbitrary slope units/nM Fe. Because the intercept value had increased to $5.627 \times 10^{-4}$ the calculated overall method blank increased to 8.91nM dFe (**Table 3.2.1**). However, the calculated dFe intercept as a measure of the overall method blank includes both Fe and non-Fe blank contributions, which were found to be related to the concentration of $Cl^-$ in solution and this will be discussed in detail in section *3.3 The System Blank & Interferences*. Thus, 13% $H_2O_2$ (w/w) was determined to be the optimal concentration for dFe analyses using ~0.07mM DPD in 24mM HCl.

***DPD***. Using a 0.6M $NH_4Ac$ & 13% $H_2O_2$ (w/w) reagent mixture, the same aspiration sequence and volumes ($NH_4Ac$ & $H_2O_2$ reagent (50µL)- Sample (80µL)- DPD (20µL)- Sample (50µL)) were used to evaluate the effects of changing the concentration of the DPD reagent on the sensitivity and overall blank of the method. Concentrations of the DPD reagent evaluated ranged from 0.04mM DPD to 0.8mM DPD in 24mM HCl.

The effects of changing the DPD concentration on the sensitivity and the calculated dFe intercept of the method are shown in **Figure 3.2.13** and **Figure**

**3.2.14**, respectively.  As demonstrated in **Figure 3.2.13**, there was a linear increase in sensitivity as a function of the concentration of the DPD reagent.  At low DPD concentrations (0.038-0.4mM DPD) both 10% and 13% $H_2O_2$ in the $NH_4Ac$ reagent yielded the same sensitivity.  This suggested that DPD was the rate-limiting reagent at concentrations below 0.4mM DPD.  At concentrations greater than 0.4mM DPD, the greater improvement to sensitivity with the 13% $H_2O_2$ (w/w) and 0.6M NH4Ac solution as compared to the 10% $H_2O_2$ and $NH_4Ac$ solution suggested that, above 0.4mM DPD, the 10% $H_2O_2$ (w/w) reagent became the rate-limiting reagent.

   *Reoptimizing the $H_2O_2$ concentration with 0.4mM DPD*.  To ensure that the 13% $H_2O_2$ in the $NH_4Ac$ & $H_2O_2$ solution was the optimal concentration to use with the optimized 0.4mM DPD reagent; (it had previously been optimized with 0.07mM DPD) the effect of the concentration of $H_2O_2$ was reinvestigated using the same aspiration sequence, $NH_4Ac$ & $H_2O_2$ reagent (50μL)- Sample (80μL)- DPD (20μL)-Sample (50μL).

   As demonstrated in **Figure 3.2.15**, the maximum sensitivity was achieved at a concentration of 13% $H_2O_2$ (w/w) and sensitivity remained constant at higher $H_2O_2$ concentrations.  The method blank calculated from calibration curves remained constant below 13% $H_2O_2$ (**Figure 3.2.16**).  At concentrations greater than 13% $H_2O_2$ the calculated method blank increased; which was a result of the continuous linear increase in the non-Fe blank with increasing concentrations of $H_2O_2$ (**Figure 3.2.17**) although the sensitivity was constant at concentrations greater than 13% $H_2O_2$ (**Figure 3.2.15**).  Furthermore, **Figure 3.2.18** demonstrates that with 0.4mM DPD, the optimal precision and sensitivity was achieved with 10-

15% $H_2O_2$, where the LOD is at its lowest value and constant. As shown in **Figures 3.2.15-3.2.18**, 13% $H_2O_2$ (w/w) in the $NH_4Ac$ & $H_2O_2$ reagent with 0.4mM DPD for analyses resulted in maximum sensitivity (**Figure 3.2.15**) in a stable region and a low LOD in a stable region (**Figure 3.2.18**). Thus, small changes in the concentration of $H_2O_2$ would not affect the sensitivity of the method and the LOD was likely at the highest signal: noise ratio possible for the spectrophotometer used.

A concentration of 0.4mM DPD was chosen as the optimal concentration of DPD as it was observed to be the point between the DPD reagent being the rate-limiting reagent and the $H_2O_2$ being the rate-limiting reagent. Based on the results shown in **Figures 3.2.13** & **3.2.14**, it is apparent that at a DPD concentration of ~0.4mM and greater than 10% but less than 13% $H_2O_2$ in the $NH_4Ac$ & $H_2O_2$ solution is optimal for the best sensitivity while minimizing the reagent blank.

### 3.3 The System Blank & Interferences

With the μSIA method the overall method blank was a function of contaminant Fe from the μSIA platform, from the DPD reagent, as well as from any potential interfering ions or compounds that were capable of oxidizing the DPD reagent to DPDQ.

In the FIA based method, a continuous absorbance baseline is monitored to characterize the background absorbance that may result from reagent interactions, Fe contamination in reagents, and Fe contamination from the analytical platform (Measures et al., 1995). This baseline is used to determine the overall method blank in the absence of dFe from samples in FIA. However, as a result of the sequential flow in μSIA, the μSIA based measurements have no continuous baseline to

characterize the background absorbance that might have resulted from contaminant Fe, reagent interactions (see section *3.2.1 Limitations of the μSIA Platform: Reagent Interactions*), or other interfering compounds that were capable of oxidizing the DPD reagent to DPDQ.

Thus, in the μSIA method, each stopped-flow absorbance profile measurement using the SFC technique was a function of the sum of the dFe in the sample or standard solution and any of the potential contaminants. This overall blank was calculated from the intercept value of the calibration curve divided by its slope (**Figure 3.3.1**).

Since obtaining Fe free seawater to make seawater standards was extremely difficult, filtered (0.2μm) Kaneohe Bay seawater was used for standards. Therefore, the overall method blank calculated as described above included the contribution from dFe in the Kaneohe bay seawater used to make standards. To separate the dFe concentration of the Kaneohe bay seawater from the blank, the SAFe-S community reference sample (0.093nM dFe) was run using the same SFC monitoring protocol. The SAFe-S standard dFe concentration was below the detection limit of the method (0.1nM dFe), and therefore could be assumed to be effectively zero and could be used to measure the overall method blank. Thus, the difference between the overall method blank calculated from the intercept of the Kaneohe Bay standard curve and the SAFe-S sample was the concentration of dFe in the Kaneohe bay seawater (~0.4nM dFe).

Thus, every time samples and standards were run using the μSIA based method for the determination of dFe, the SAFe-S reference sample was also run to estimate the blank and the dFe concentration of the Kaneohe Bay seawater.

**3.3.1 Contributions to the Overall Method Blank.**  The contributions to the overall method blank were investigated in an attempt to identify the main sources of the overall method blank and subsequently minimize their contributions to the overall blank.

***The Contaminant Fe Blank.***  *Fe Contamination from the μSIA Platform.*  The μSIA-LOV platform itself can contaminate sample and reagent solutions if the reacting solutions come in contact with the glass barrel syringe pump.  As previously discussed in section *3.1 The μSIA Protocol*, at least 750μL of DI water were used to separate the reacting solutions entering the holding coil from the syringe pump.  Furthermore, the holding coil tubing and the flow cell were flushed thoroughly with DI water and no carryover was observed between analyses.  Thus, it was highly unlikely that the μSIA platform itself contributed significantly to the overall method blank.

***Fe Contamination in Reagents***.  Fe contamination in the reagents used was thought to be the primary source of the overall method blank using the DPD-Fe(III) chemistry. Measures et al. (1995) found that Fe contamination in the DPD reagent was primarily responsible for their elevated baseline absorbance signal and that an in-line metal chelating resin to remove Fe from the DPD reagent significantly reduced the baseline absorbance.  Since the μSIA system does not have a continuous absorbance baseline like FIA, the Fe contamination from the DPD reagent also

contributes to the overall method blank and is included in every SFC absorbance profile. Thus, removing Fe from the DPD reagent was investigated to reduce the overall method blank.

*DPD Cleaning*. Current FIA methods using the DPD-Fe(III) chemistry clean the DPD reagent in- line using peristaltic pumps to pass the DPD solution through a metal chelating resin containing 8-HQ. In FIA, the stock DPD reagent is acidified to pH ~2, below the pH range in which DPD can oxidize to DPDQ (pH 3-6), to prevent oxidation of the stock DPD solution. The acidified DPD reagent enters the FIA system and mixes at a confluence point in an ice bath with the pH 6.3 $NH_4Ac$ buffer solution to raise the pH of the DPD solution to pH ~5, within the pH range at which metals adsorb to the 8-HQ resin (Landing et al., 1986; Measures et al., 1995). The ice bath slows the oxidation of DPD to DPDQ until the solution can pass through an 8-HQ column within a few seconds of mixing. Because the DPD solution is cleaned immediately prior to use in-line it does not require acidification to stabilize it after cleaning.

Unfortunately, with the μSIA platform it is not feasible to clean the DPD reagent in-line. Thus, offline cleaning of the DPD reagent was investigated.

To batch clean the DPD reagent offline for μSIA the procedure was very similar to the in-line cleaning procedure used for FIA. Using a peristaltic pump, acidified DPD (pH <2) was mixed an ice bath with ~0.3M $NH_4Ac$ buffer solution (pH 6.3) to raise the pH of the DPD solution to pH ~5 and was passed through an 8-HQ column to remove Fe and was then collected into a bottle containing Q-HCl to reduce the pH<2, which stabilizes the DPD until it is used. The DPD prepared in this

way will be referred to as 'clean' DPD, whereas DPD that was not passed through an 8-HQ column will be referred to as 'dirty' DPD.

The results from cleaning the DPD reagent are shown in **Figure 3.3.2,** which shows that this procedure significantly reduced the overall method blank from 10nM to 5nM (**Figure 3.3.2**, **Figure 3.3.3**). However, numerous attempts to further remove Fe from the DPD reagent by using multiple 8-HQ columns in series proved unsuccessful, with the lowest calculated dFe intercept always remaining around ~5nM dFe. This suggested that there was either a limit to the amount of Fe that could be removed from the DPD reagent using the 8-HQ resin, or that something other than Fe in the DPD reagent was responsible for the remaining blank signal.

To determine if the 5nM dFe blank observed when using clean DPD was from Fe in the DPD reagent, ethylenediaminetetraacetic acid (EDTA) was added to the clean DPD reagent and seawater sample for analyses using the SFC protocol. Spiking the DPD reagent and the sample solution with EDTA ensured that Fe or any other metals in the DPD solution or in the sample and reagent solutions that can complex with EDTA will be unable to oxidize the DPD. Thus, the SFC reaction progress curve that resulted from using EDTA spiked sample and reagent solutions could be used to characterize the overall method blank in the absence of Fe from samples and standards (**Figure 3.3.3**). Furthermore, to provide a measure of the overall method blank in the absence of oxidation of the DPD reagent, L-ascorbic acid was used to spike samples and the DPD reagent to act as a sacrificial reductant.

As shown in **Figure 3.3.3**, cleaning the DPD reagent significantly reduced the rate of DPD oxidation. This was a result of removing the contaminant Fe in DPD

reagent and the reaction progress slope was observed to decline by ~50% when EDTA was added to the clean DPD reagent (**Figure 3.3.3**).  Thus,  ~50% of the signal observed when using the clean DPD reagent was unrelated to the oxidation of the DPD compound by Fe or other metals that could be complexed by EDTA.  In the presence of L-ascorbic acid the reaction progress curve was flat, suggesting that the reaction signal in the presence of EDTA was a result of the DPD reagent being oxidized to DPDQ but by a compound or ion other than Fe (**Figure 3.3.3**).  This also confirmed that the SFC signal in the presence of EDTA was from the oxidation of DPD and was not a potential artifact from changes in the refractive index gradients in the flow cell during SFC monitoring or from using an inappropriate reference wavelength to correct absorbance measurements.

Furthermore, during the experiments investigating cleaning the DPD reagent, it became apparent that the amount of HCl added to the clean DPD significantly affected the overall method blank as well as that from the EDTA complexed sample (non-Fe blank) (**Figure 3.3.4**).  This further suggested that in the presence of EDTA the blank signal was likely related to the amount of HCl in the cleaned DPD reagent.

**3.3.2 The Non-Fe Blank.**  The overall method blank in the presence of EDTA with the clean DPD reagent acidified to different pHs is shown in **Figure 3.3.4** and a negative linear relationship between both the overall method blank and the pH of the clean DPD solution as well as a negative linear relationship between the blank and the pH of the clean DPD solution in the presence of EDTA can be observed. Furthermore, as shown in **Figure 3.3.4**, the overall method blank and the blank in the presence of EDTA converged when the pH of the DPD solution was ~pH 5, which

resulted from using the clean DPD solution with the least amount of HCl added (~50μL).

Alfthan and Jarvis (1928) first reported that DPD could be used for the determination of free chlorine in water. Palin (1945) found that the DPD reagent could determine free chlorine and chloramines at pH 4-6 but was subject to interferences from Fe when the solution pH was below 6. Petri et al. (2011) suggested that the oxidation of $Cl^-$ by $H_2O_2$ degradation products ($OH^-$ + $OH\bullet$) produced free chlorine radicals, which could subsequently oxidized DPD to DPDQ (Alfthan and Jarvis, 1928; Palin, 1945; Tarvin et al. 1934). In μSIA, the oxidation of $Cl^-$ probably occurs in the mixing coil when the $Cl^-$ from seawater, acidified samples, and acidified DPD mixed with the $NH_4Ac$ & $H_2O_2$ reagent mixture. The largest contribution of $Cl^-$ is from the seawater sample itself (~0.5M $Cl^-$); however, the cleaned DPD reagent acidified to low pH (<2) could also have up to ~0.3M $Cl^-$ in solution from acidifying the cleaned DPD reagent (pH ~5) with HCl to stabilize it for later use.

To determine if chloride ion concentrations were responsible for to the non-metal blank, the SFC signal as a function of the concentration of $Cl^-$ in the presence of EDTA was observed and is shown in **Figure 3.3.5**. This figure clearly demonstrates that the slope of the SFC reaction progress curve in the presence of EDTA (i.e. the absence of Fe) was positively correlated with concentration of the chloride ion in solution. Thus it seems likely that the free chlorine species are in fact oxidizing the DPD reagent to DPDQ even in the absence of Fe at the reaction pH (~5.5).

The DPD-Fe(III) chemistry is based on the Fenton reaction in which Fe(II) is oxidized to Fe(III) (see equation 1).

$$Fe(II) + H_2O_2 \rightarrow Fe(III) + OH^- + OH\bullet \qquad (1)$$
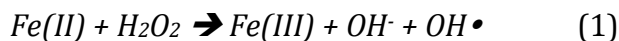
Thus, for every one Fe(II) ion oxidized to Fe(III), one hydroxyl radical is produced, which would react with $Cl^-$ producing a free chlorine radical, resulting in a blank signal that did not result from Fe(III) oxidizing the DPD reagent (Petri et al., 2011). In the presence of Fe and other metals, the rate of $H_2O_2$ decomposition increases and could theoretically change the concentration of $H_2O_2$ in solution thereby affecting the reaction. However, the high concentration of $H_2O_2$ used for this method (~13% (w/w), 3M) with extremely low concentrations of Fe in samples (<5nM) suggest that the increased rate of $H_2O_2$ decomposition in the presence of Fe from samples does not appreciably change the concentration of $H_2O_2$ participating in the reaction for this method. This assertion is also supported by the high level of precision and reproducibility of the method.

## 3.4 Validation of the µSIA Based Method

The method was validated using the SAFe community reference samples, shown in **Table 3.4.1**. The SAFe D1 and D2 samples were analyzed during the reanalysis of seawater samples from Loihi in the shore-based laboratory. The SAFe-S surface sample (dFe=0.093nM) is below the current method detection limit to obtain any reliable value and the concentration of dFe in the SAFe D1 sample (dFe=0.67nM) is too close to the current limit of detection for accurate determination of dFe in the sample. In contrast, the higher concentration SAFe sample D2 (0.933nM) was accurately determined by the µSIA method, suggesting

that the method is accurate for dFe determinations at concentrations greater than or equal to approximately 1nM dFe.

The method was further validated using samples from the R/V Falkor Cruise to Loihi Seamount in June/July 2014. The concentration of dFe in samples from Loihi was determined using the μSIA-based method and is compared to ICP-MS values provided by Olivier Rouxel (pers. comm.). **Figure 3.4.1** shows that there is good agreement between the dFe concentrations determined by μSIA and by ICP-MS. Furthermore, comparison of the μSIA Fe values and ICP-MS Fe values for all samples with concentrations of dFe>1.0nM show a linear relationship with a slope of 0.953 suggesting good agreement between the two methods as shown in **Figure 3.4.2**.

This further suggests that using the SAFE S sample to correct dFe determinations for blank contributions from Fe and free chlorine is an adequate means to evaluate the method blank. The high correlation between the values determined by μSIA and the values determined by ICP-MS also suggests that using the SAFe S sample to account for the method blank reduces any potential offset between the methods resulting from the positive interference of free chlorine.

**3.5. Loihi**

Hydrothermal systems involve the percolation of seawater into the seafloor where it is heated from contact or proximity to magma. Thus, hydrothermal venting often occurs along mid ocean ridges where two lithospheric plates diverge and magma moves up from the mantle to the seafloor (Tivey, 2007). However, hydrothermal activity can also occur at hot spots, where a plume of magma from the mantle rises and weakens the lithosphere and localized volcanic activity occurs. This type of volcanic activity can occur away from plate boundaries as is observed at the Hawaiian Hot Spot, which is the source of the volcanic activity currently observed at Loihi Seamount (Sakai et al., 1987).

When seawater percolates into the seafloor and is heated by magma, gas and element exchanges occur with the ambient environment. For example hydrothermal fluids can become acidic from the outgassing of volatile gasses (such as $CO_2$) in the magma, as well as from exchange of metal cations such as $Mg^{2+}$ into surrounding rocks and the leaching of protons (Seyfried & Mottl, 1982). This acidic water rises as it warms and interacts with the wall rock, leaching metals, and finally is vented through chimneys or by diffuse flows from cracks in the seafloor. This process is referred to as hydrothermal activity. The altered fluids emanating from the seafloor are referred to as hydrothermal fluids and can be enriched with high levels of dissolved metals (Edmond et al., 1979a; Edmond et al., 1979b; Hedenquist & Lowenstern, 1995; Von Damm, 1995).

**3.5.1 Hydrographic Setting.** Loihi seamount is an intra-plate hot-spot volcano located ~30km south east of the Big Island of Hawaii, HI, the summit is at a depth of ~970m (**Figure 3.5.1**). Loihi contains a series of previously active vent sites, now in the form of pits due to their collapse during a series of seismic events in 1996. Diffuse venting from the flanks of Loihi has also been reported (Malahoff et al., 2006). Variations in the chemical composition of the hydrothermal effluent was observed to vary drastically prior to and following the 1996 seismic events, with elevated Fe/Mn ratios following the seismic events in 1996, providing insights into the extent of temperature and $CO_2$ moderation of hydrothermal vent fluids present at various locations in the vicinity of Loihi seamount. Specifically, prior to 1996, high concentrations of dissolved metals were reported such as dFe (~13uM), Mn (4-700nM); however, following the 1996 seismic events, the concentrations of dissolved metals declined with dFe levels ~200nM and dMn ~30nM in 2001. A detailed synopsis of observations at Loihi since the early 1980's can be found in Malahoff et al. (2006).

The water column at depth of and in the vicinity of Loihi is characterized by anomalously high concentrations of Fe and Mn (~200nM dFe, ~20nM dMn) resulting from the hydrothermal processes occurring at this site. The relative concentration of Fe and Mn in hydrothermal end-member waters is a function of the temperature of the water-rock interactions as well as the extent of leaching metals from the surrounding wall rock resulting from the acidic nature of the hydrothermal fluids as a result of high concentrations of dissolved $CO_2$ in the seawater, which are referred to as $CO_2$ moderated fluids (Malahoff et al., 2006; Seyfried & Mottl, 1982).

The vent water is diluted by ambient seawater to form a neutrally buoyant plume enriched in Fe, Mn, and [3]He, which has been detected over 450km away at station ALOHA (Boyle et al., 2005).

**3.5.2 Methods.** Seawater samples were collected from the water column within 8km of Loihi Seamount, Big Island, Hawaii (155.267W, 18.89N) during a research cruise aboard the R/V Falkor from June 25- July 6, 2014 (**Figure 3.5.1**). A total of 15 CTD casts were conducted over this period; eight of which were sub-sampled for μSIA dFe analysis, yielding a total of 72 samples. The number of discrete depths sampled during each cast varied between 6 and 12 due to the large volumes of water required for other parameters being determined. Samples were collected using the shipboard rosette consisting of an SBE32 carousel with 24-10L Niskin bottles equipped with an SBE 9plus CTD. The CTD rosette and frame used were not trace metal clean as is required for open ocean trace metal analyses where concentrations of dFe are often at sub-nanomolar levels.

Subsamples from the CTD rosette were collected through an acid- leached 0.2um Acropak-500™ capsule filters (Supor® (PES), Pall Corp.). Separate AcroPaks™ were used for filtering seawater from within the enriched dFe plume and for use with low Fe seawater samples to minimize any potential carryover between high Fe and low Fe samples. Prior to each subsample collection, the Acropaks™ were flushed with a minimum of 500mL seawater from the corresponding Niskin bottle being sampled. Once flushed, 125mL samples were collected into trace metal clean HDPE sample bottles that were rinsed 3 times with the sample. Immediately following collection 0.5mL of 6N Q-HCl was added to the samples to achieve a final

concentration of 24mM HCl and they were left for >24 hours to dissociate any organically bound Fe prior to analysis. Acropaks were stored in a refrigerator between uses to prevent biological growth.

In an attempt to minimize Fe contamination from the internal Teflon coated stainless steel springs used to close the Niskin bottles, they were removed and bare metal parts were coated with two-part marine epoxy and allowed to dry for 48 hours prior to being reinstalled.  However, exposed steel was observed on the springs after the second cast of the cruise and over the course of the cruise the extent of exposed steel increased and the springs were observed to be noticeably rusting in multiple spots.  In addition to this source of contamination, the CTD wire beyond the first 1000m was heavily rusted, providing an additional potential source of Fe contamination to the water column.

Thus, while the samples obtained from this cruise are not of trace metal clean sampling quality, they are still of use for mapping the distribution of the hydrothermal plume of dFe around Loihi, where dFe concentrations are on the order of 100nM dFe.  However, all samples are likely to be contaminated to some extent, but the observed values in surface waters where there are low levels of Fe can be used to estimate the likely extent of plume sample contamination, which was ~1nM dFe.

Seawater samples from Loihi were reanalyzed with the optimized µSIA method in the shore based laboratory.  Samples from Loihi with concentrations greater than 5.0nM dFe were diluted with the same seawater used to make daily standards (filtered, acidified Kaneohe Bay seawater (see section *3.3 The System*

*Blank & Interferences*).  The concentration of dFe in the Kaneohe Bay seawater was determined as the difference between the values of the SAFe S community reference sample and the Kaneohe bay seawater determined by assuming that the the SAFe S community reference sample (0.093nM), which was below the LOD of this method (0.1nM dFe).  The SAFe S sample could also be used to approximate the blank of the method and could be used to assess the instrumental and reagent blank of this method.  This value could then be subtracted from the intercept value of standards that had been prepared by adding Fe to Kaneohe Bay seawater to yield a value of ~0.4nM for the Kaneohe Bay water (see secton *3.3 Blanks*).

**3.5.3 Results.**  Results from Loihi Seamount samples are shown in **Figures 3.5.1-3.5.9**.  Two transects are used to present the data in **Figure 3.5.1**.

*SW to NE Transect.* **Figures 3.5.2** and **3.5.3** show the turbidity and dFe concentrations, respectively, from the SW to NE transect.  Two turbidity maxima with similar values can be observed in **Figure 3.5.2** at ~1150m and ~1250m and the turbidity maximum at ~1250m corresponds to elevated concentrations of dFe (50-150nM) as shown in **Figure 3.5.3.**  However, the turbidity maximum at ~1150m corresponds to a lower concentration of dFe (<70nM).  The upper plume waters at ~1150-1170m correspond to a neutral density of 27.60 kg/m$^3$ and the deeper plume at ~1250m corresponds to a neutral density of 27.66 kg/m$^3$.

*SE to NW Transect.*  **Figures 3.5.4** and **3.5.5** show the turbidity and dFe concentrations, respectively, from the SE to NW transect.  A single turbidity maximum can be observed at ~1170m (**Figure 3.5.4**) and corresponds to elevated

concentrations of dFe but does not correspond to the maximum concentration of dFe observed in samples at that depth (**Figure 3.5.5**).

 ***Surface Sections.*** To better understand the flow direction of the hydrothermal fluids sampled at Loihi, surface plots along neutral densities were used to observe the upper ($\sim$1150m) and lower ($\sim$1250m) hydrothermal plumes separately. **Figures 3.5.6** and **3.5.7** show the distribution of turbidity and dFe where neutral density is 27.60 kg/m$^3$, and shows the distribution of dFe where neutral density is 27.60 kg/m$^3$. In both figures the flow path of the plume at $\sim$1150m appears to be from NE to SW. The flow path of the hydrothermal fluid was evaluated by looking at the relative concentrations of dFe on the surface plot. It was assumed that the station with the highest dFe concentration observed was closest to Loihi and that concentrations of dFe would remain elevated along the flow path relative to ambient seawater, with concentrations of dFe declining as the hydrothermal plume moves further away from the source.

 Surface plots of the distribution of turbidity and dFe concentrations where neutral density is 27.66 kg/m$^3$ ($\sim$1250m) are shown in **Figures 3.5.8** and **3.5.9**. As shown in **Figure 3.5.8**, the plume at 27.66 kg/m$^3$ shows only a very small increase in turbidity with a maximum at station 4. Along this density layer the concentration of dFe is also elevated but the maximum concentration ($\sim$120nM dFe) does not correspond to the maximum turbidity at station 3, but is at a maximum value at station 16, implying that this hydrothermal plume is moving from SE to NW.

 Thus, based on the depth distribution of turbidity it appears that the hydrothermal plumes observed along these two neutral density layers are from

different sources. The plume at 27.60 kg/m$^3$ corresponding to ~1150m depth is characterized by high turbidity and high concentrations of dFe and moves to the south-southwest. In contrast, the plume at 27.66kg/m$^3$ corresponding to ~1250m depth is characterized by low turbidity and elevated concentrations of dFe and appears to move to the north-northwest.

Two manuscripts describing dFe concentrations at station ALOHA (~450km to the northwest of Loihi) by Boyle et al. (2005) and Fitzsimmons et al. (2015) report elevated concentrations of dFe at ~1200m. The elevated concentrations of dFe detected at station ALOHA were thought to result from the distal transport of dFe at depth from Loihi (Fitzsimmons et al., 2015). Thus, in order for hydrothermally derived Fe from Loihi to reach station ALOHA at depth (~1200m) the hydrothermal plume is either moving to the east-northeast around the Island of Hawaii and then moving to the northwest (**Figure 3.5.10**). Alternatively, the hydrothermal plume from Loihi may move south-southwest until reaching the southern edge of Hawaii Island and then flow north, northwest along the island chain. This water would then move northeast between Oahu and Kauai Islands through the Kaieiewaho Channel providing a mechanism for Fe from Loihi to reach station ALOHA. Data from deep ADCP moorings (400m-1400m) off Kaena Point, Oahu, HI show a predominant northward flow suggesting that a feasible route exists for a hydrothermal plume that flows along the southwest boundary of the Hawaiian Islands to move north through the Kaieiewaho Channel and appear at station ALOHA (Doug Luther, pers. comm.).

More research is necessary to understand the deep-water currents around the Hawaiian Islands and to identify the actual trajectory of the hydrothermal plume dispersing from Loihi and whether or not the elevated concentrations of Fe and He-3 observed at depth at Station ALOHA could originate from hydrothermal activity at Loihi. Nonetheless, the µSIA method can be used to trace dFe anomalies from the hydrothermal plume at Loihi, providing another tracer to better understand the movement of deep-water currents around the Hawaiian Islands.

## 3.6 Conclusions

A new system for the determination of dFe in seawater at concentrations ≥1nM has been developed and successfully used to measure the concentration of dFe in hydrothermal plumes at Loihi Seamount. More work is required to lower the limit of detection of the method and minimize the blank contributions from Fe in the DPD reagent and the blank contribution from free chlorine to measure open ocean surface water dFe concentrations accurately (<0.2nM dFe).

The recent development of new µSIA platform configurations such as those equipped with two syringe or two discrete syringe-type pumps and two holding coils makes on-line sample preconcentration and on-line reagent cleaning feasible in µSIA, as well as facilitating improved mixing between samples and reagents by means of a confluence point in the LOV. Thus, with a more advanced µSIA platform and LOV more than three solutions are able to mix and each reagent could be aspirated into the LOV separately, which means that the $H_2O_2$ and $NH_4Ac$ reagents would not need to be mixed into a single reagent solution. Thus, the concentration

of $H_2O_2$ will not decline with time as a result of mixing with the $NH_4Ac$ to a pH above the stability of $H_2O_2$. Furthermore, the pH and concentration of the $NH_4Ac$ buffer can be increased to buffer the sample reagent mixture to the optimal pH range since the $H_2O_2$ is not mixed with the buffer, and thus the decline in the concentration of $H_2O_2$ is not of concern since it is aspirated separately.

Since the two main sources of the method blank are Fe in the DPD reagent and free chlorine oxidizing the DPD reagent, lowering the overall method blank and improving the limit of detection would likely be possible through pre-concentrating the sample. This would improve measurements by removing the seawater matrix thereby decreasing the blank contribution from chloride ions in the seawater. Furthermore, by including an in-line DPD cleaning procedure, the overall method blank could be further lowered and no HCl would have to be added to the clean DPD reagent, effectively lowering the blank contribution from free chlorine.

**TABLES**

| Sampling Rate (Hz) | Integration Time (milliseconds) | Samples (Scans) to Average | Detectors to Average |
|---|---|---|---|
| 4 | 8 | 28 | 3 |

**Table 2.1. Settings in FIAlab for the Spectrophotometer.** (See text for details).

| %$H_2O_2$ in $NH_4Ac$ & $H_2O_2$ reagent | Calibration Curve Intercept's SFC Rx Rate Progress Slope Value | Calibration Curve Slope | Calculated dFe Blank (nM dFe) (Intercept/ calibration slope) |
|---|---|---|---|
| **13% $H_2O_2$** | $5.14*10^{-4}$ | $1.03*10^{-4}$ | 4.99 |
| **17% $H_2O_2$** | $5.63*10^{-4}$ | $6.32*10^{-5}$ | 8.91 |

**Table 3.2.1. Comparing calculated dFe values as a function of $H_2O_2$ concentration**. The +0nM dFe standard reaction rate progress curve (arbitrary slope units/nM dFe) as well as the full suite of standards (+0 to +5nM dFe) is monitored to produce calibration curves. The dFe intercept is calculated by dividing the +0nM reaction rate progress slope by the slope of the calibration curve.

| SAFe Reference Sample | Concentration Determined by μSIA | Standard Deviation | Consensus Concentration of Reference Sample | Number of Measurements |
|---|---|---|---|---|
| SAFe D1 | 0.319 nM | 0.143 nM | 0.67 +/- 0.04 nM | 9 |
| SAFe D2 | 0.924 nM | 0.327 nM | 0.933 +/- 0.023 nM | 10 |

**Table 3.4.1.** Comparison of dFe values determined for SAFe samples using the μSIA method with reported consensus values.
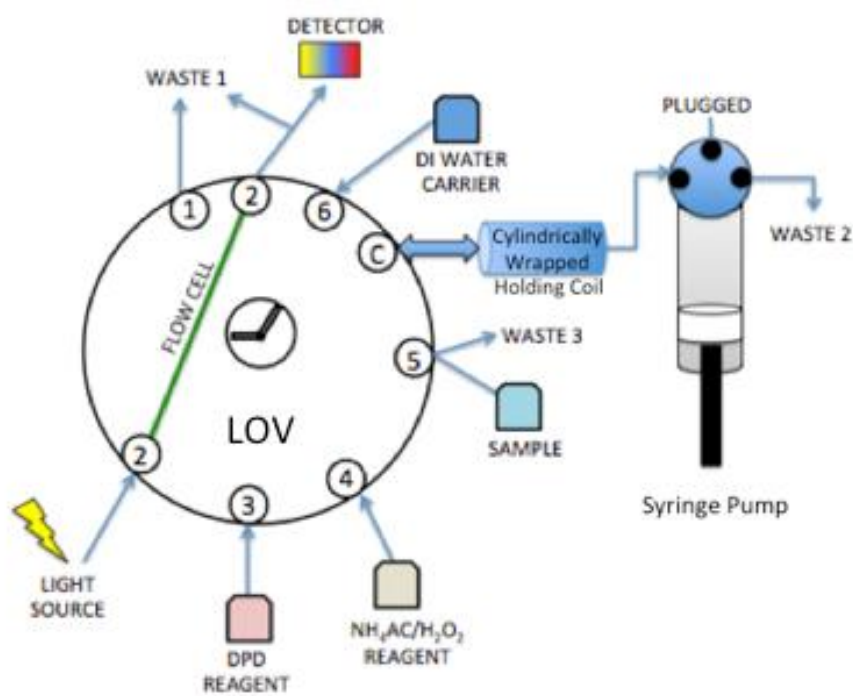
**Figure 2.1:** Diagram of the μSIA-LOV platform used for dFe determinations.
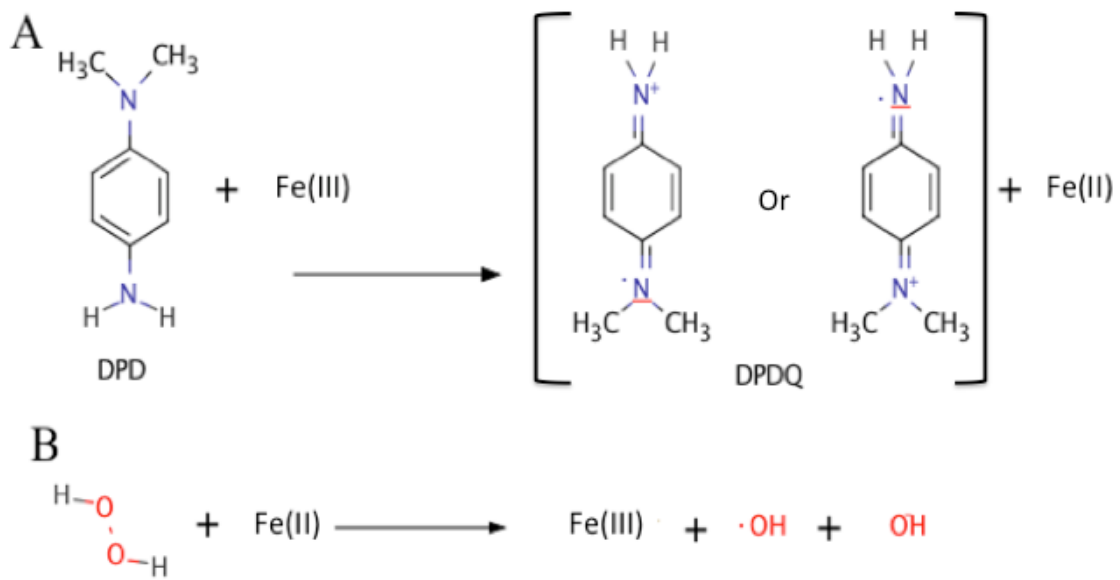
**Figure 2.2.** Schematic of the catalytic oxidation of DPD by Fe(III) (A), and (B) the reoxidation of Fe(II) by $H_2O_2$ (see text for details).
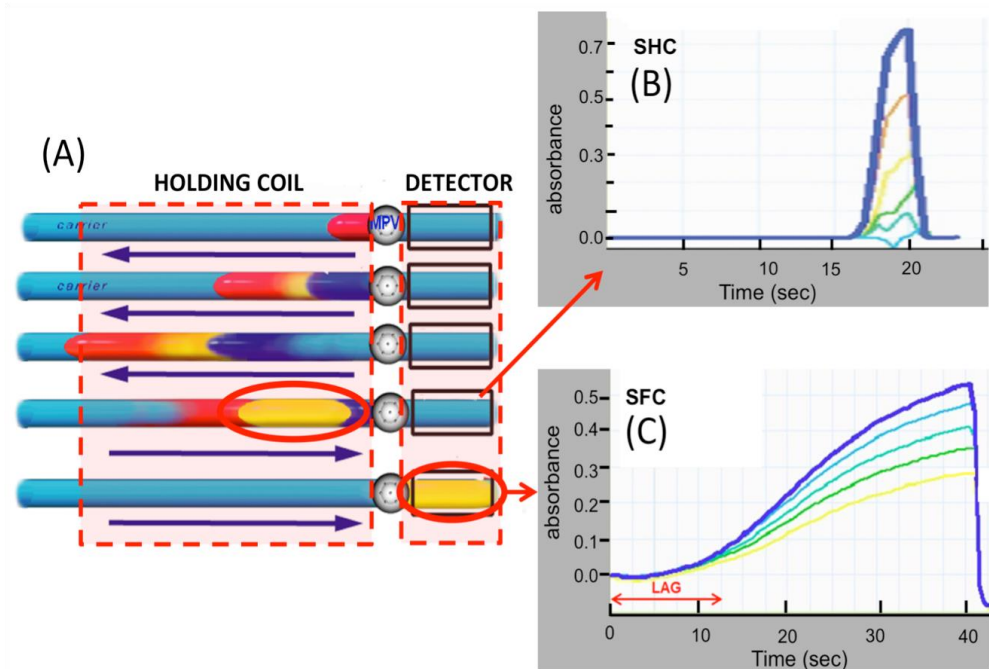
**Figure 2.3. A)** Schematic of mixing between plugs of solution in the holding coil. **B)** Typical absorbance signal resulting from the SHC protocol (see text for details) **C)** Typical absorbance signal from the SFC protocol (see text for details) *Figure from Ruzicka (2009).*
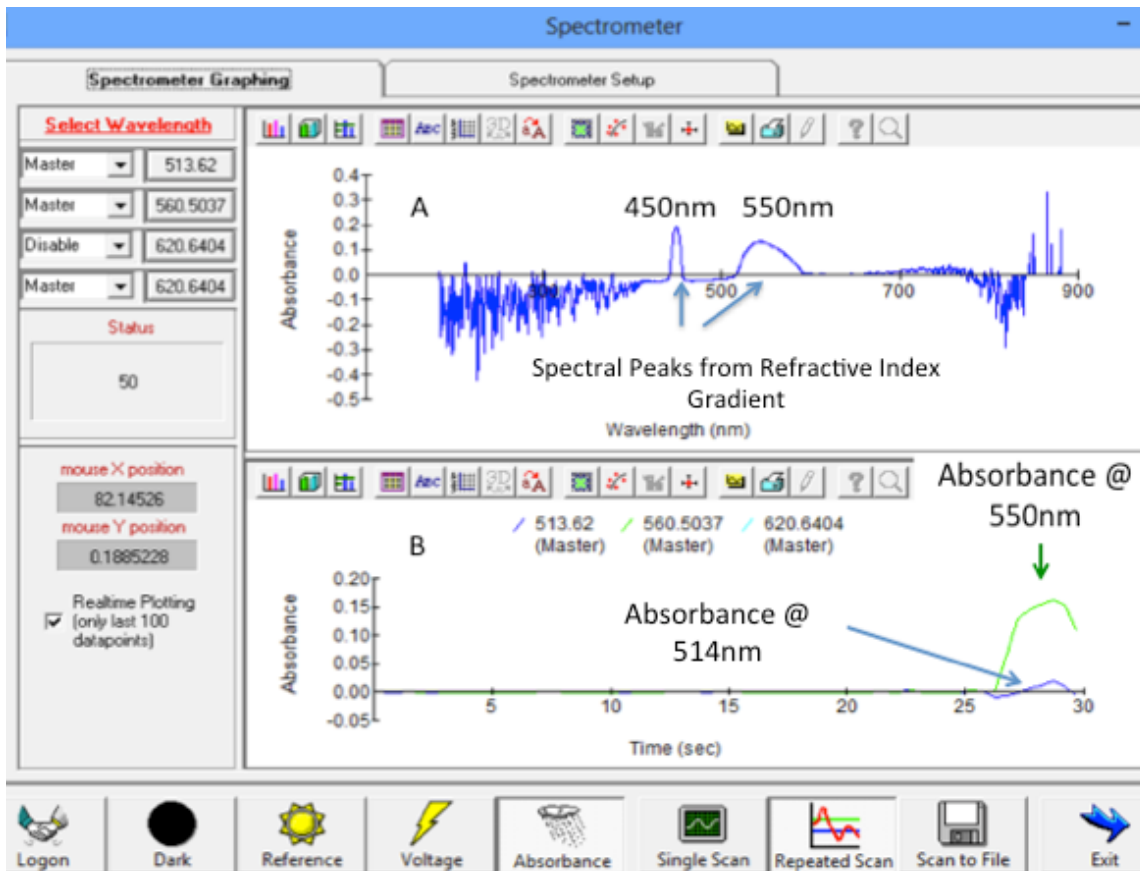
**Figure 2.4. A)** The effect of the refractive index gradient on absorbance across all wavelengths for a sample/reagent mixture without DPD during the SHC protocol (see text for details).  **B)** The effect of the refractive index gradient on absorbance at 514nm and 550nm (SHC protocol) (see text for details).
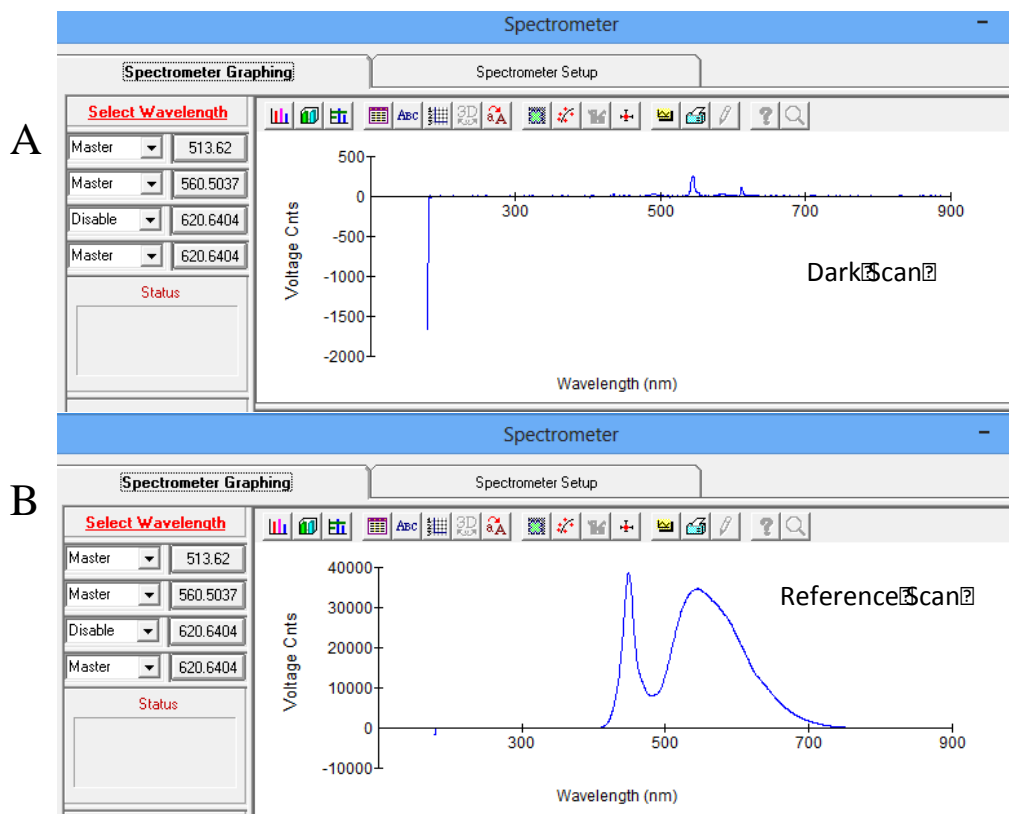
**Figure 2.5. A)** Dark scan (light source off) voltage counts as function of wavelength with UHP water in the flow cell. **B)** The corresponding reference scan with the light source on, see text for details.
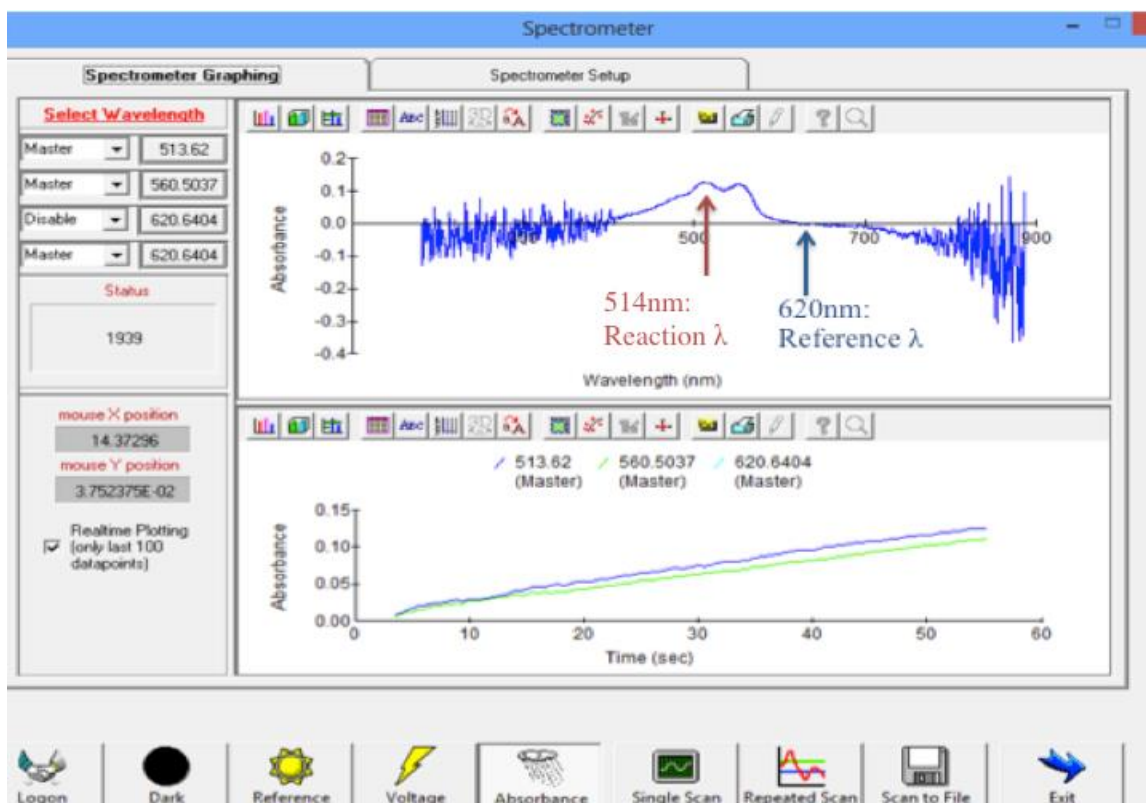
**Figure 2.6. Top)** The absorbance spectra of DPDQ as a function of wavelength, showing peaks at 514nm and 550nm and the reference peak location at 620nm (see text for details). **Bottom)** A typical SFC reaction progress curve showing the increase in absorbance from the production of DPDQ with time (see text for details).
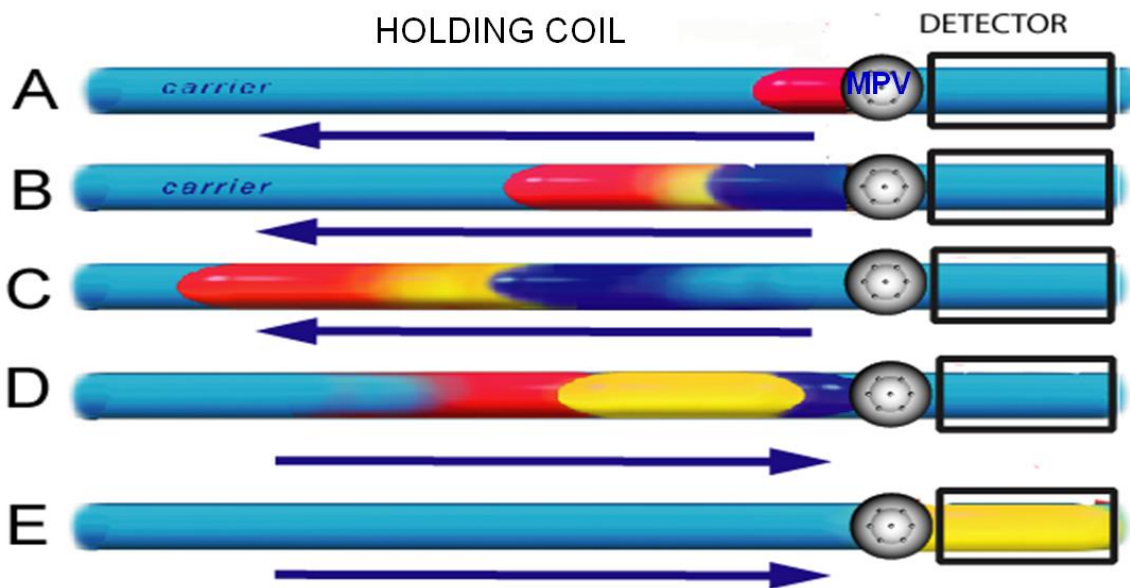
**Figure 3.1.1.  Schematic of the interaction of sample and reagent plugs during the reaction sequence.**  A) Aspiration of a sample plug.  B) Formation of the reaction product (yellow) between the sample solution (red) and the reagent solution (blue).  C) Dispersion in the holding coil resulting from aspirating solutions sequentially.  D) Flow reversal following formation of the reaction product.  E) Monitoring the reaction product in the flow cell.  *Figure Courtesy of Jarda Ruzicka, flowinjectiontutorial.com.*
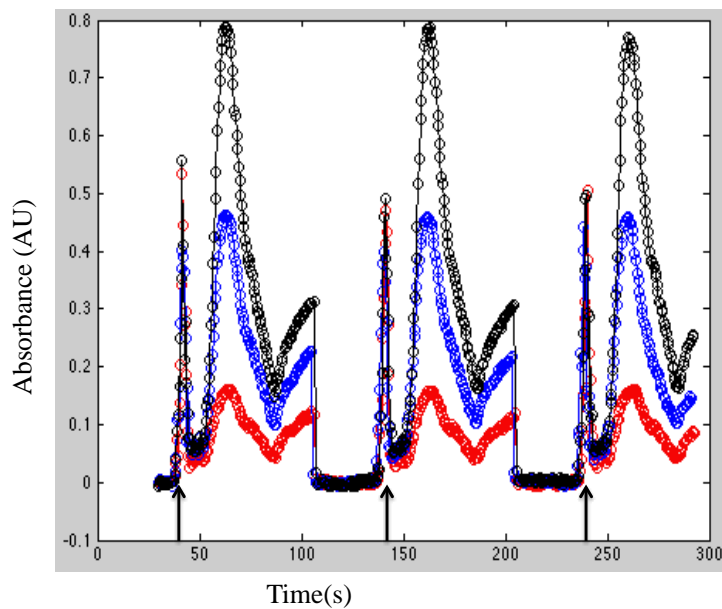
**Figure 3.1.2.** Absorbance profiles using the SHC protocol of +0nM (red), +12nM (blue), and +25nM (black) Fe standard additions to filtered seawater containing ~1.0nM Fe. Black arrows point to the time when the refractive index gradient enters the flow cell prior to the DPDQ peak.
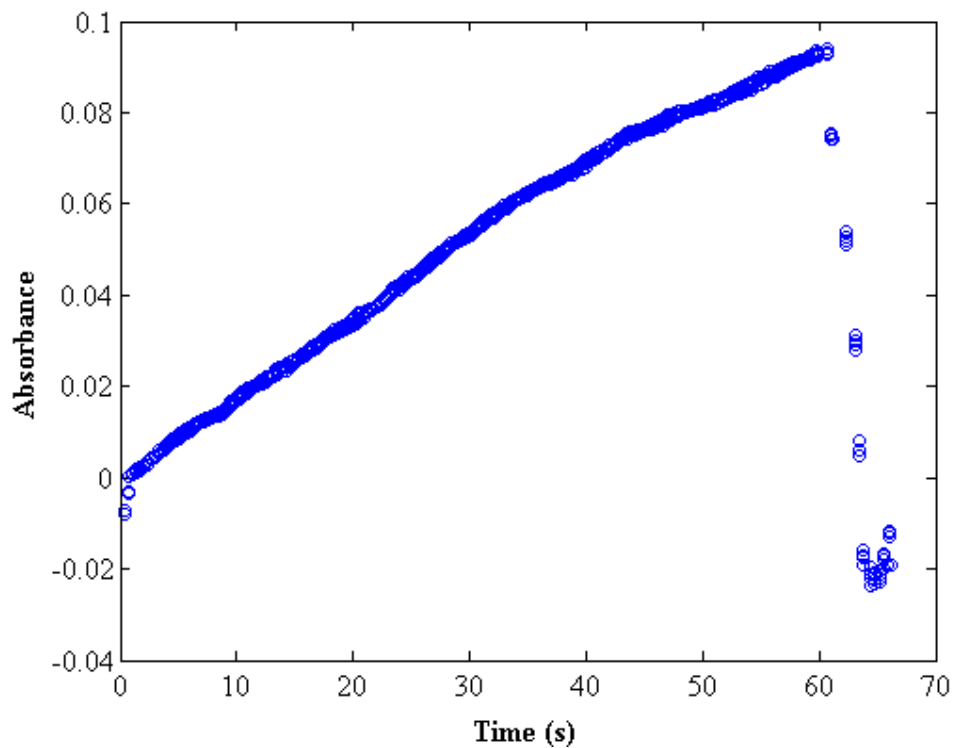
**Figure 3.1.3.** Typical SFC reaction progress signal for a ~6nM Fe seawater sample. The lower isolated blue dots after 60s result from values recorded as the flow cell is flushed.
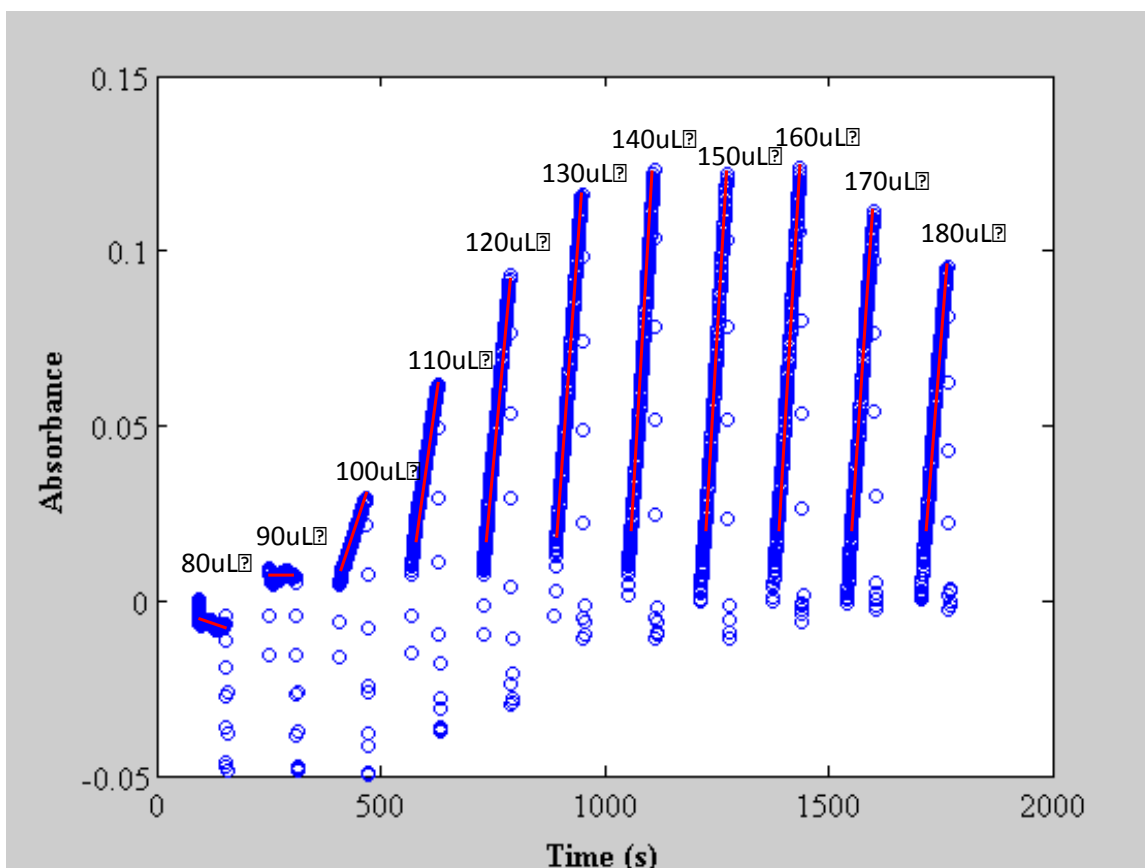
**Figure 3.1.4.** Effect on reaction progress (SFC) of varying the position of the reacting plug in the flow cell. The volume dispensed to the flow cell is indicated above each SFC profile. The high-resolution data (blue circles, O) over a 60s period are shown with their fitted slopes (red lines). The lower isolated blue circles after each SFC profile result from data points generated as the flow cell is flushed between these sequential runs.
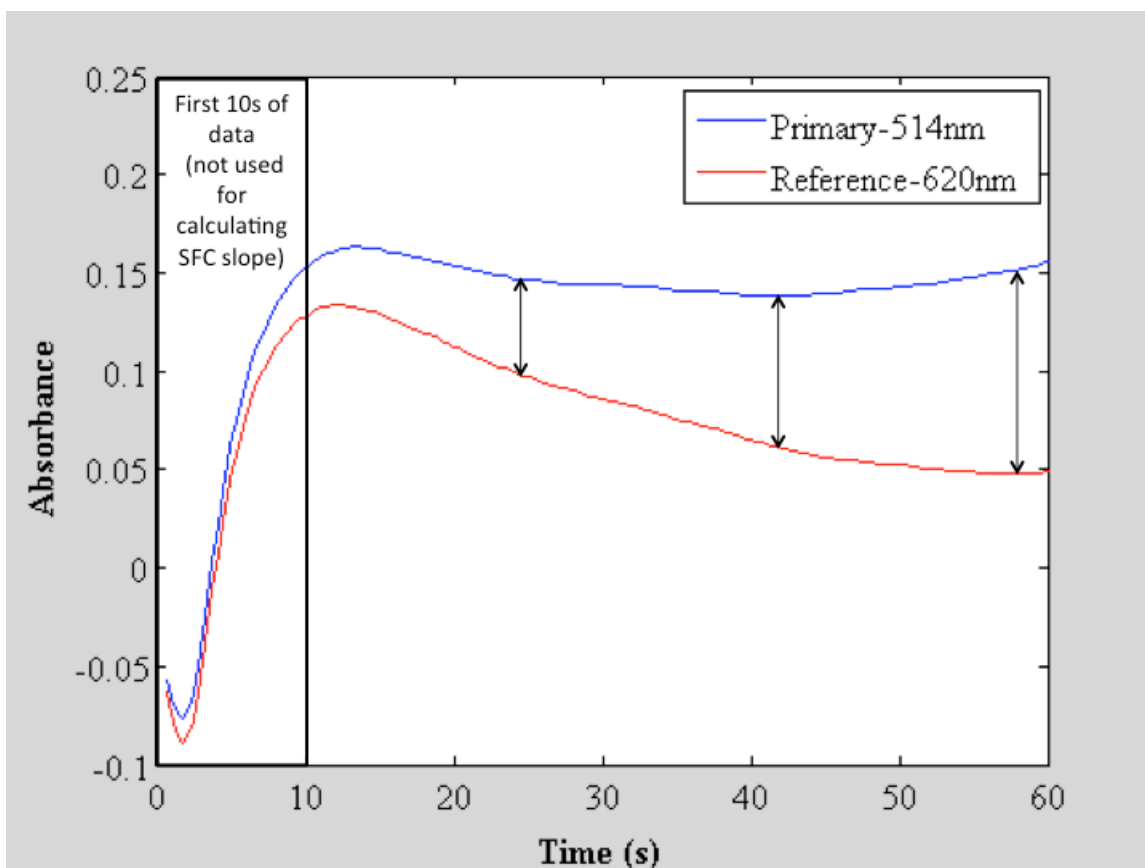
**Figure 3.1.5.** The uncorrected reaction progress absorbance monitored at 514nm (blue) and at 620nm (red), the reference wavelength, using the SFC technique.
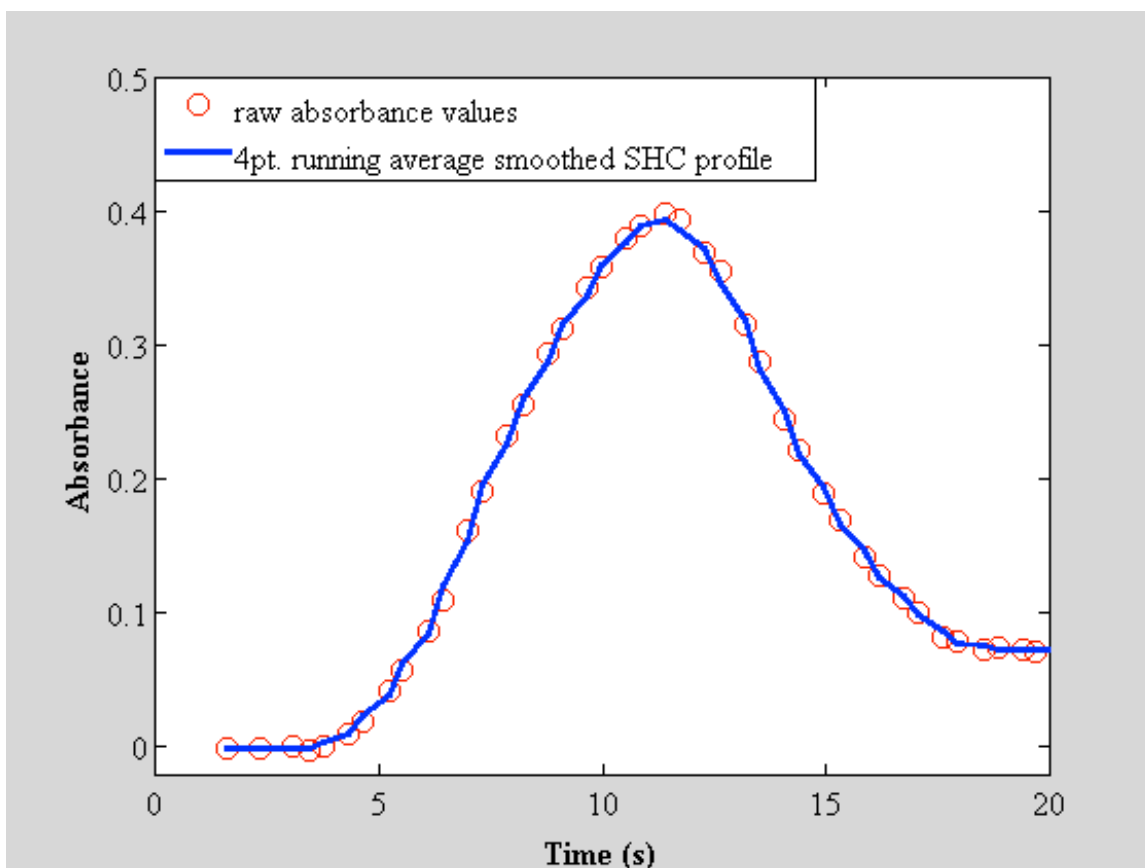
**Figure 3.1.6.** SHC absorbance profile from a 0.4nM Fe sample. The red circles are the corrected absorbance values at 514nm (see text for details). The blue line is the result of a four-point running average of the corrected raw data.
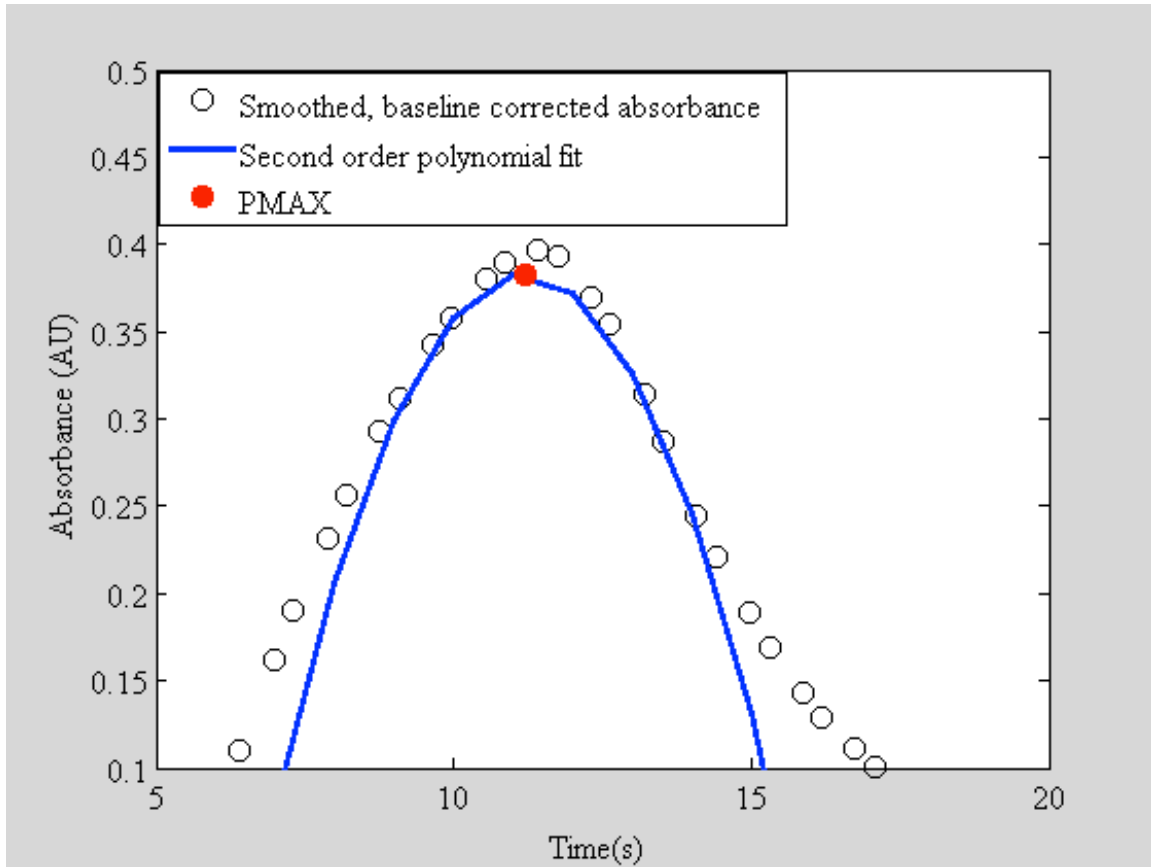
**Figure 3.1.7.** Matlab polynomial fitting of the corrected, smoothed absorbance signal at 514nm. -- Calculated 2nd order polynomial curve fit. • - Peak maxima identified from the curve fit.
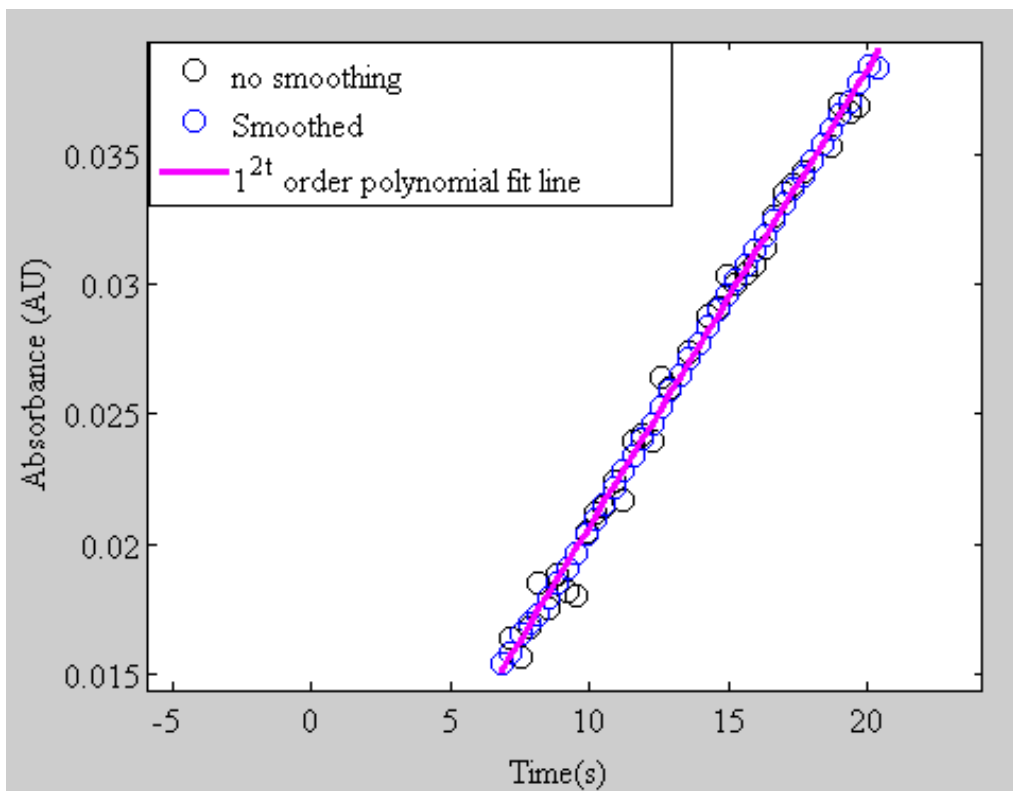
**Figure 3.1.8.** Example of a Matlab data fit for an SFC absorbance signal from a 0.4nM Fe seawater standard.
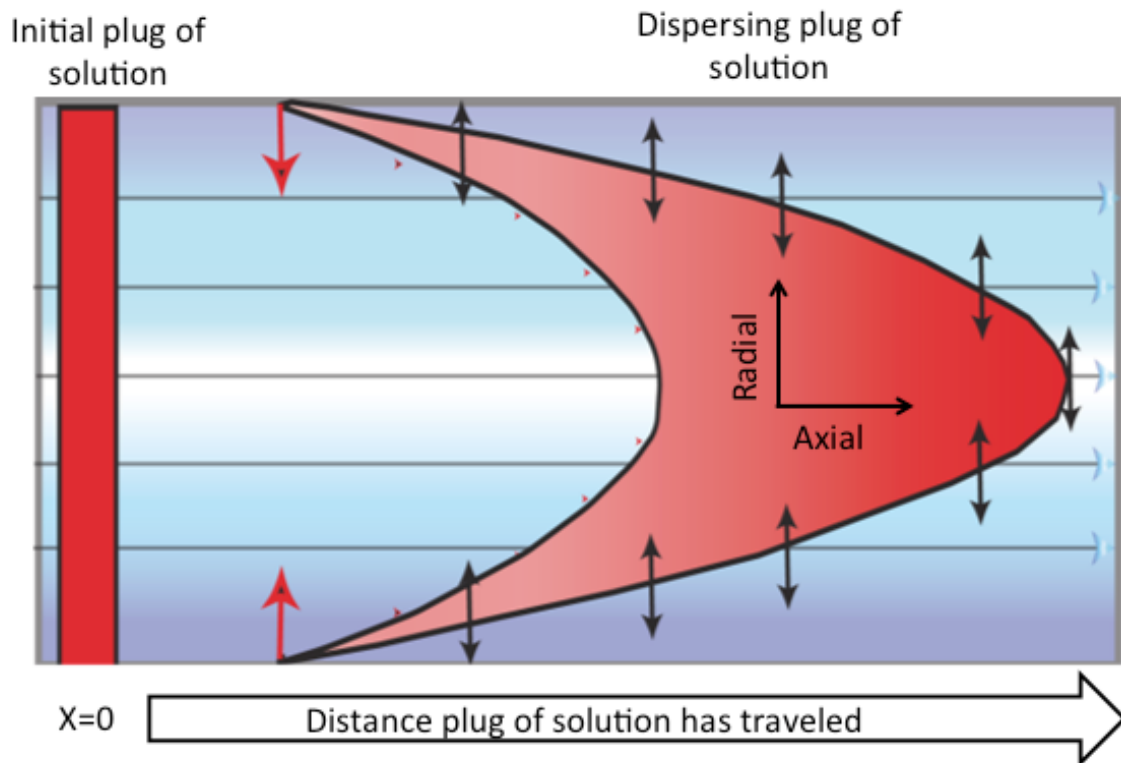
**Figure 3.2.1.** Visualization of dispersion in a unidirectional flow path (see text for details).
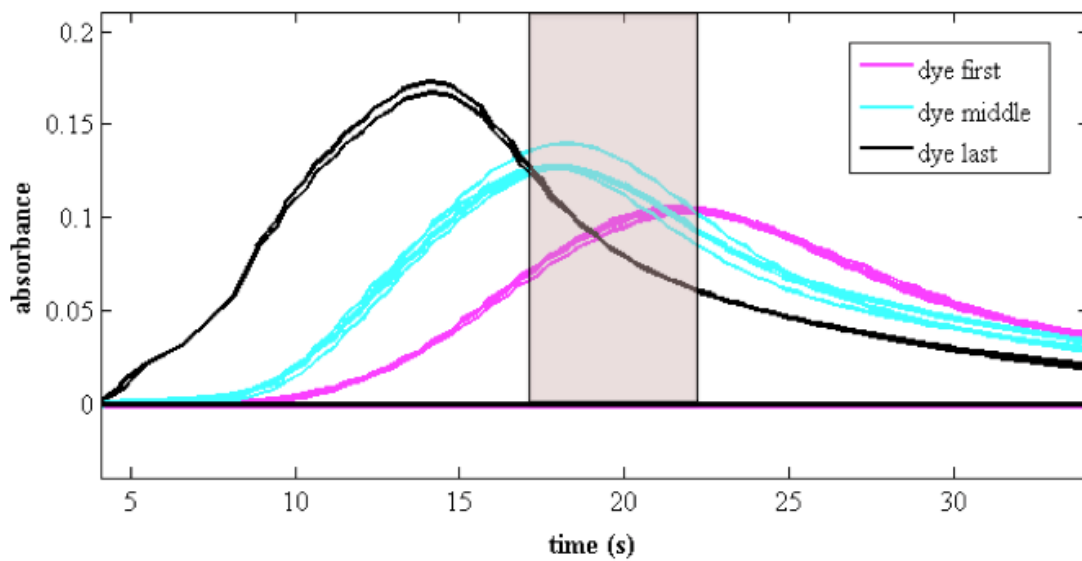


**Figure 3.2.2.** Dispersion of the dye when added separately to each of the 50µL aliquots of DI water in the aspiration sequence (see text for details).
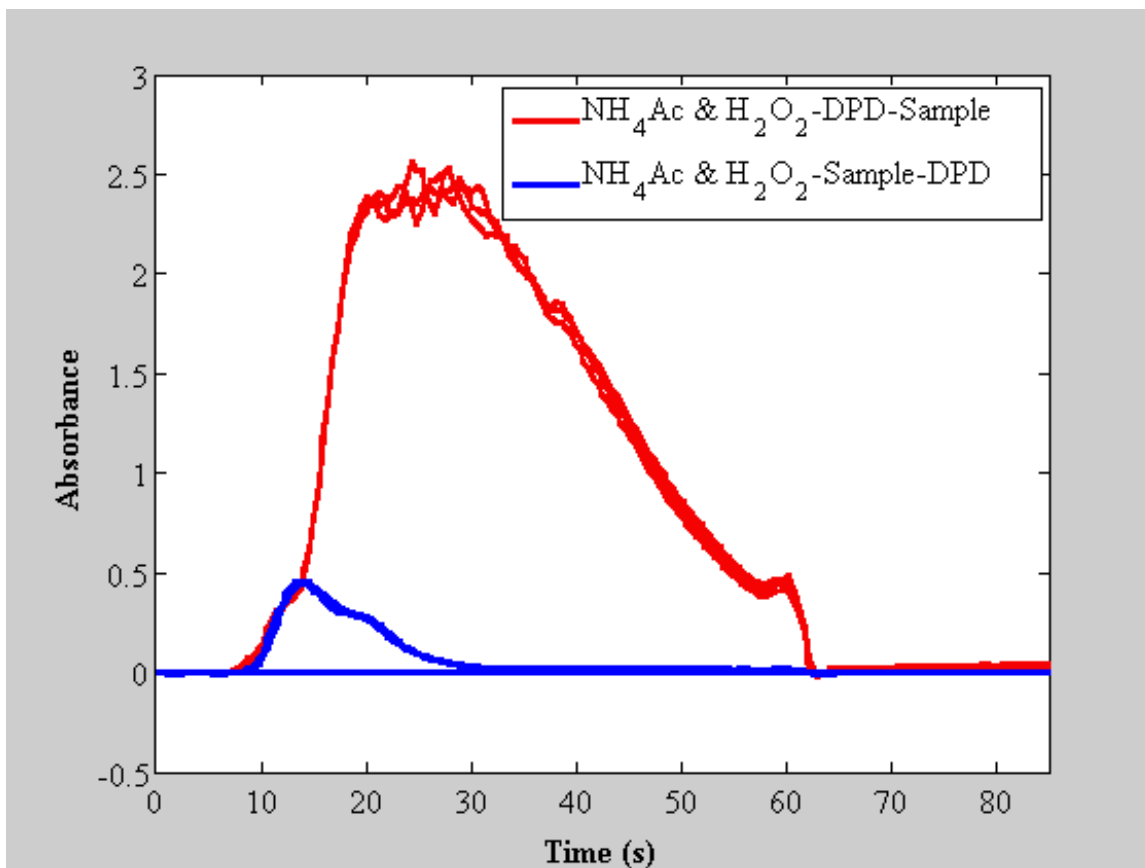
**Figure 3.2.3.** Comparison of SHC absorbance peaks from a 0.4nM seawater sample using different aspiration sequences (see text for details).
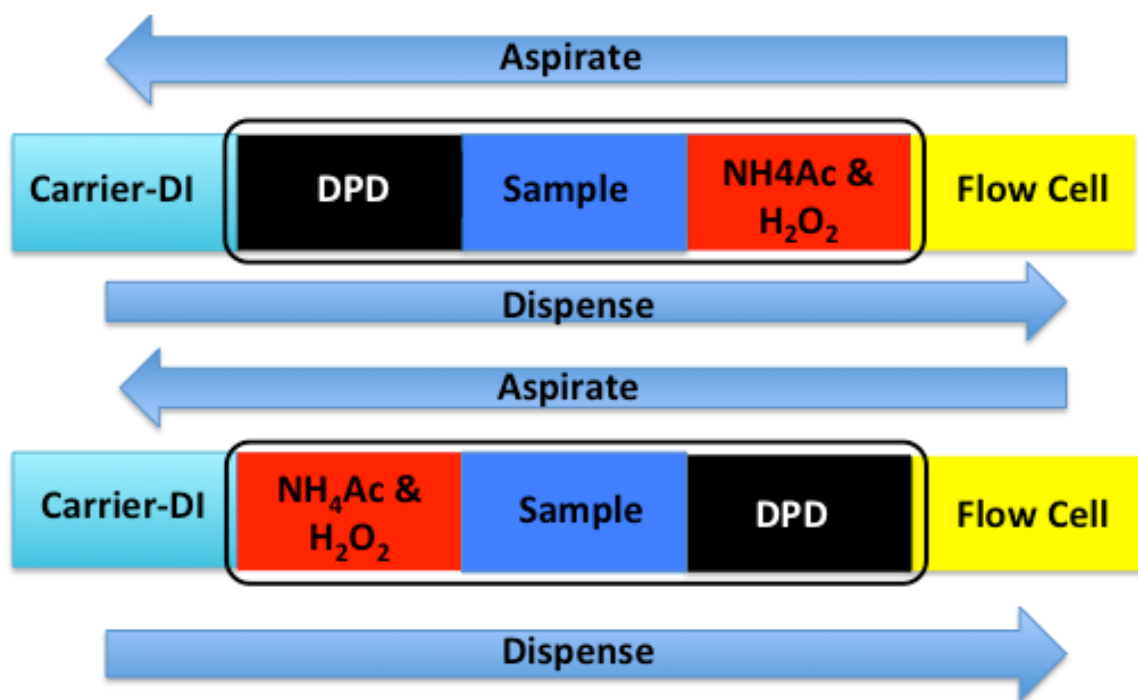
**Figure 3.2.4.** Schematic of the two aspiration sequences investigated for dFe determinations using the μSIA platform with DI water as a carrier.
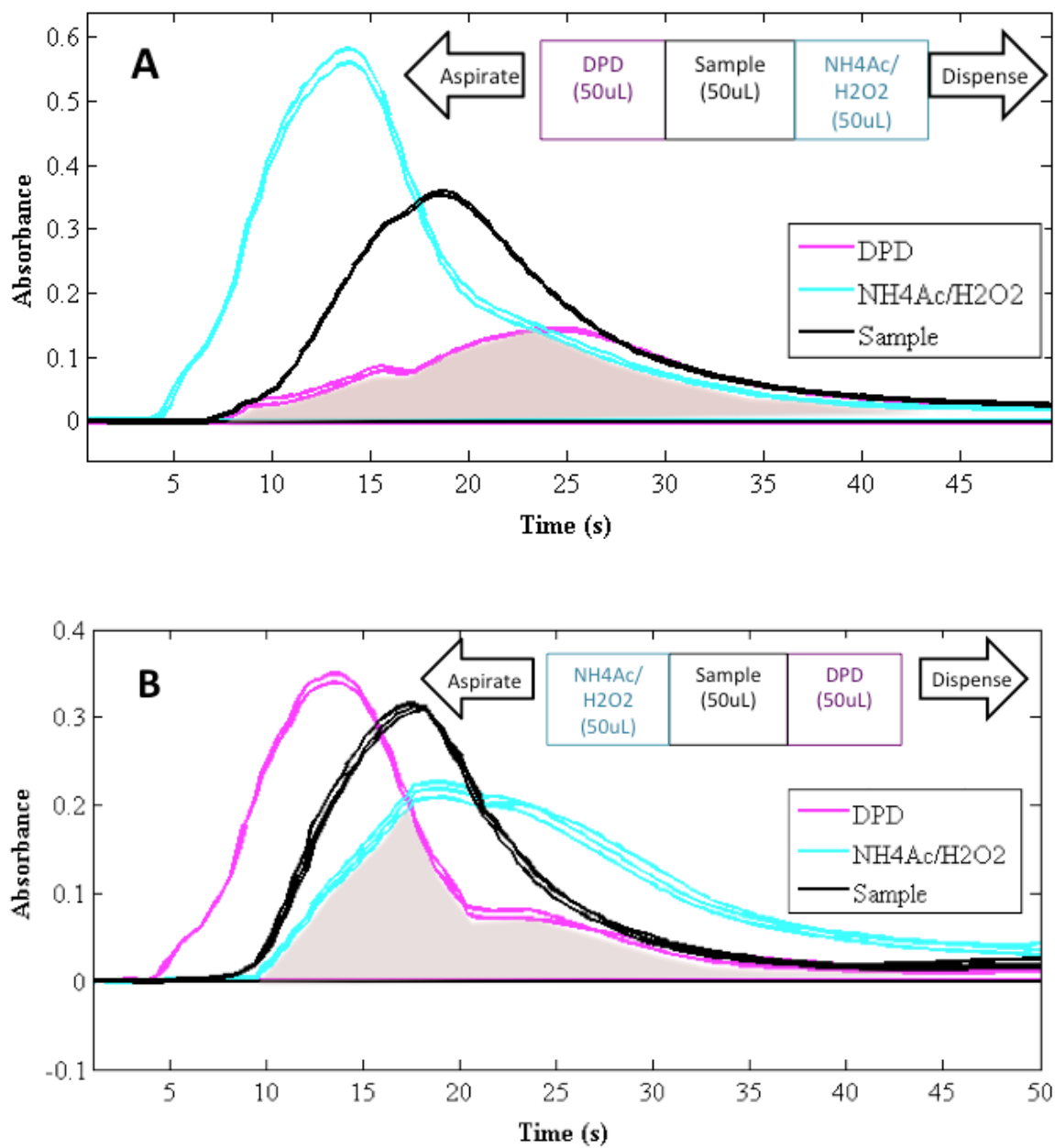
**Figure 3.2.5.** Comparison of the extent of dispersion for each plug of solution as a function of distance traveled and viscosity for two different aspiration sequences investigated; **A**) DPD- Sample- NH$_4$Ac & H$_2$O$_2$, **B)** NH$_4$Ac & H$_2$O$_2$- Sample- DPD (see text for details).
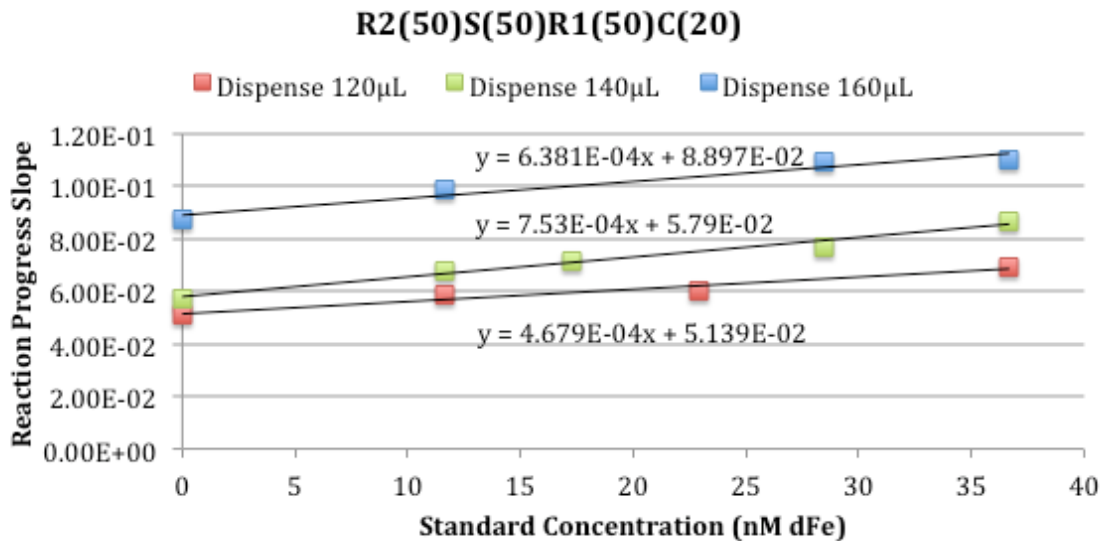
**Figure 3.2.6.** Comparison of calibration curves obtained using the aspiration sequence NH4Ac & H2O2 (50µL)- Sample (50µL)- DPD reagent (50µL)- carrier solution (20µL, DI water), with different volumes (in µL) dispensed to the flow cell for monitoring.
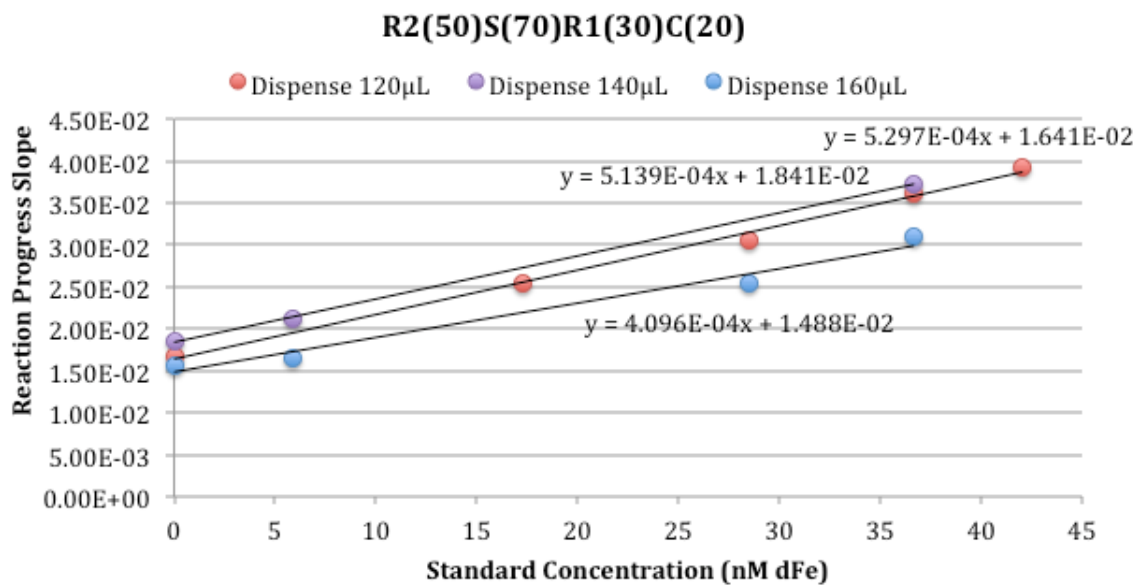
**Figure 3.2.7**. Calibration curves for monitoring the absorbance using the SFC technique with the aspiration sequence $NH_4Ac$ & $H_2O_2$ (50µL, 2.5% $H_2O_2$ in 0.6M $NH_4Ac$)- Sample (70µL)- DPD (30µL, 3.2mM)- Carrier (20µL, DI water), with different volumes (in µL) sent to the flow cell for monitoring.

**R2(50)S(80)R1(20)C(20)**

◆ Dispense 160μL  ◆ Dispense 140μL  ◆ Dispense 120μL

$y = 4.67E\text{-}04x + 1.03E\text{-}02$

$y = 3.51E\text{-}04x + 1.09E\text{-}02$

$y = 2.66E\text{-}04x + 7.64E\text{-}03$
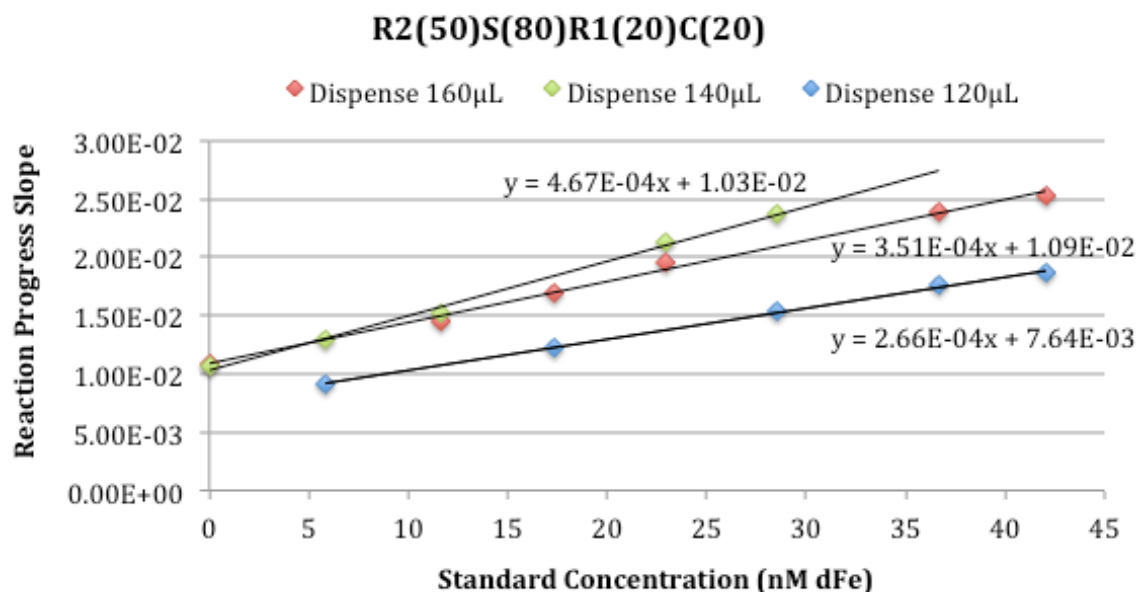
**Figure 3.2.8.** Calibration curves for the aspiration sequence $NH_4Ac$ & $H_2O_2$ (50μL, 2.5% $H_2O_2$ in 0.6M $NH_4Ac$)- Sample (80μL)- DPD (20μL, 3.2mM)- Carrier (20μL, DI water), 3.2mM DPD, with different volumes (in μL) sent to the flow cell for monitoring.
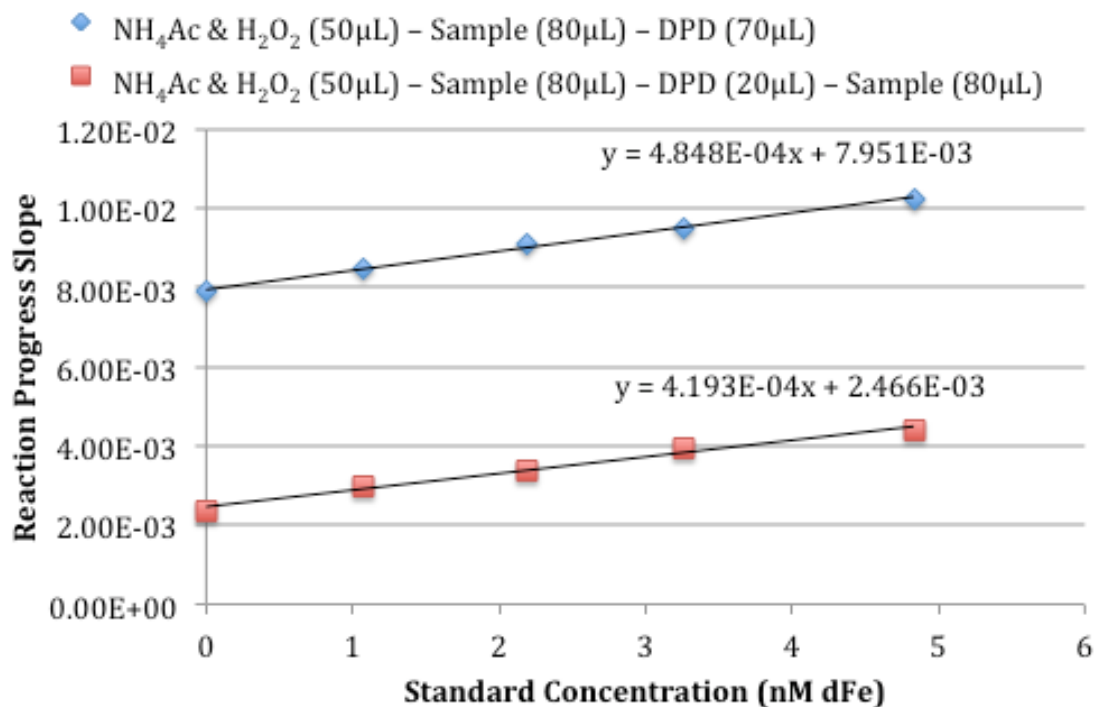
**Figure 3.2.9.** Comparison of the sensitivity and blank that result from the two aspiration sequences: 1) NH$_4$Ac & H$_2$O$_2$ (50µL)- Sample (80µL)- DPD (20µL)-Sample (50µL) & 2) NH$_4$Ac & H$_2$O$_2$ (50µL)- Sample (80µL)- DPD (70µL) using 0.45mM DPD and 0.6M NH$_4$Ac with 13% H$_2$O$_2$ (w/w).
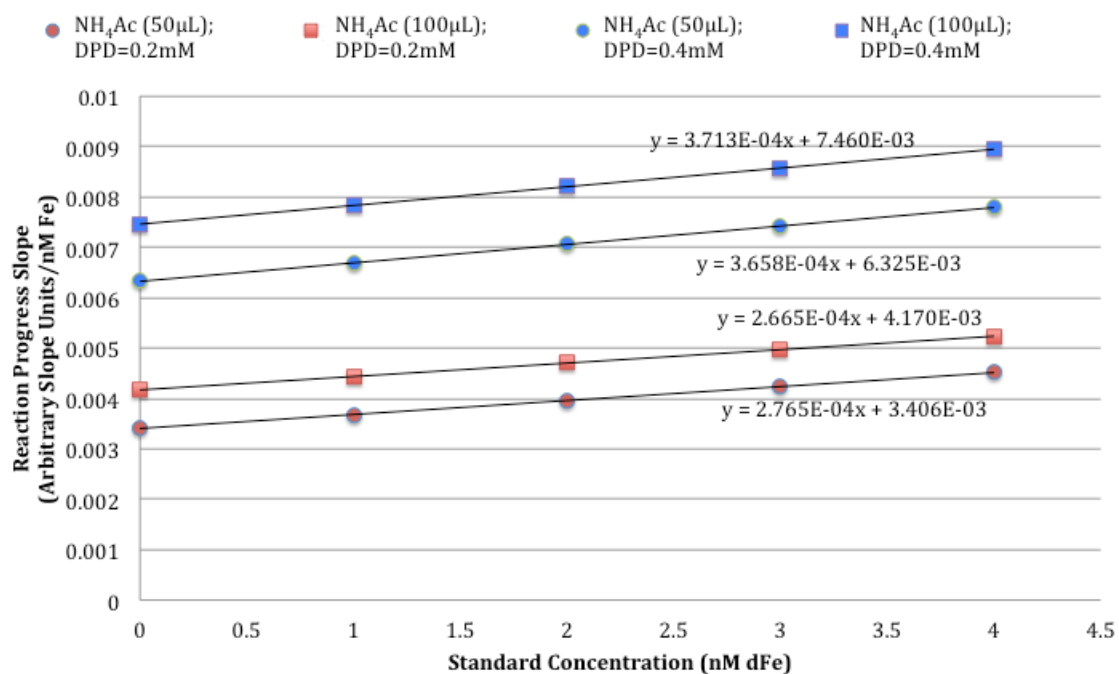
**Figure 3.2.10.** Sensitivity as a function of NH$_4$Ac & H$_2$O$_2$ volume with 0.4mM DPD and 0.6M NH$_4$Ac & 13% H$_2$O$_2$ (w/w).
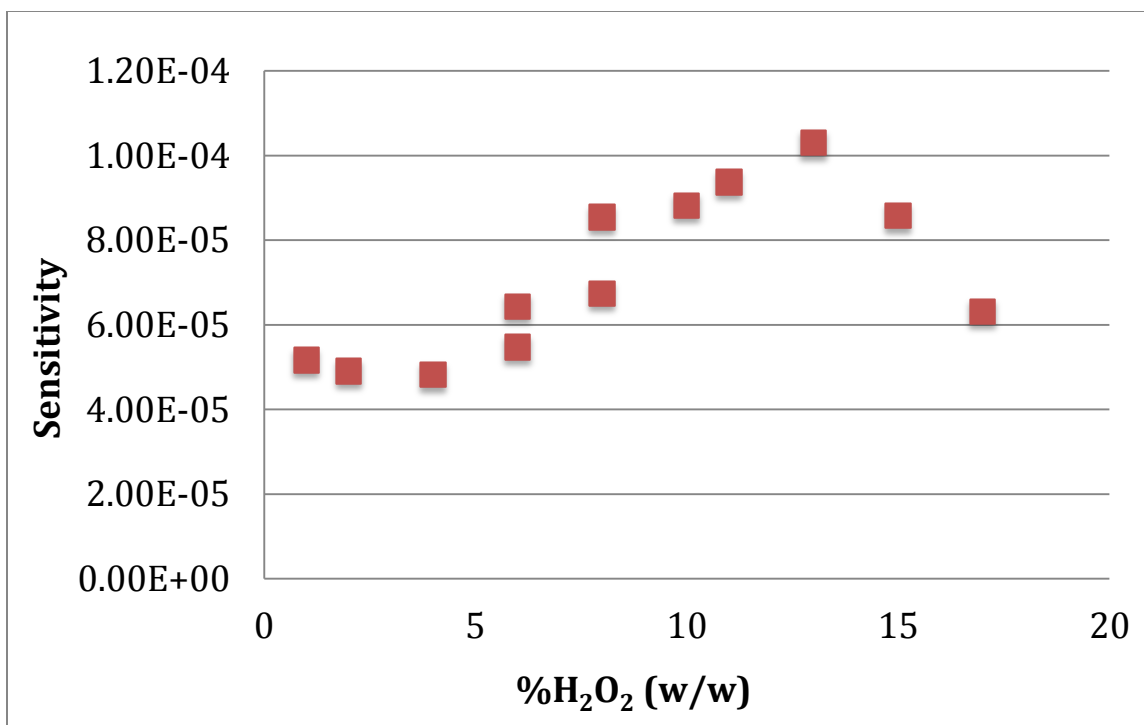
**Figure 3.2.11.** Sensitivity (defined as arbitrary slope units (gain in absorbance/time) per nM dFe) as a function of $H_2O_2$ concentration using 0.07mM DPD.
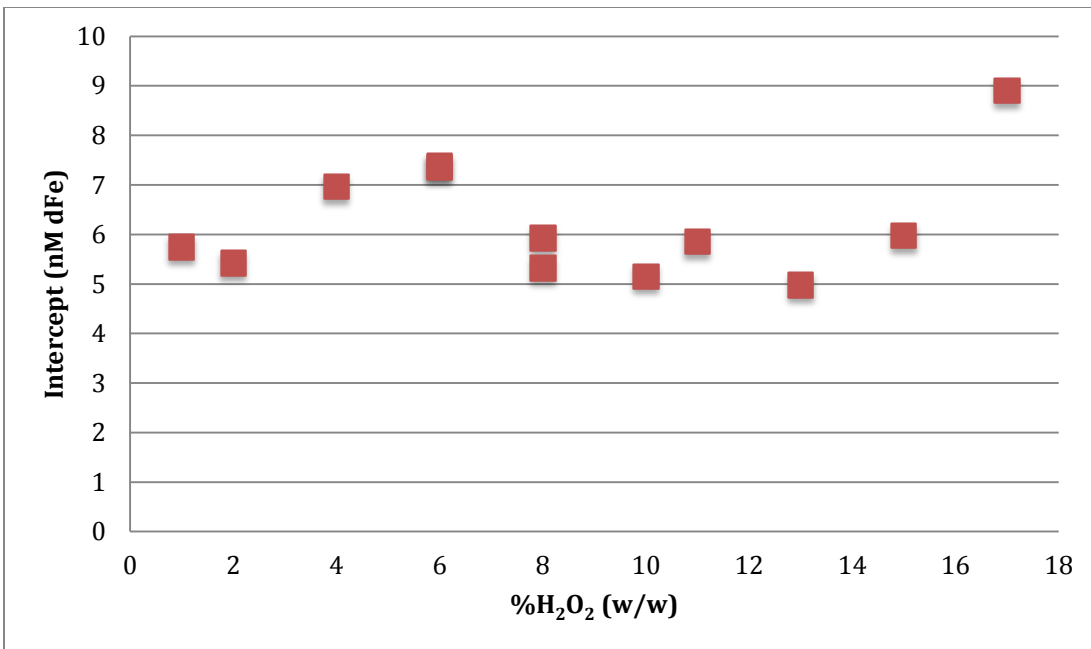
**Figure 3.2.12.** Calibration curve intercept values as a function of $H_2O_2$ concentration using 0.07mM DPD.
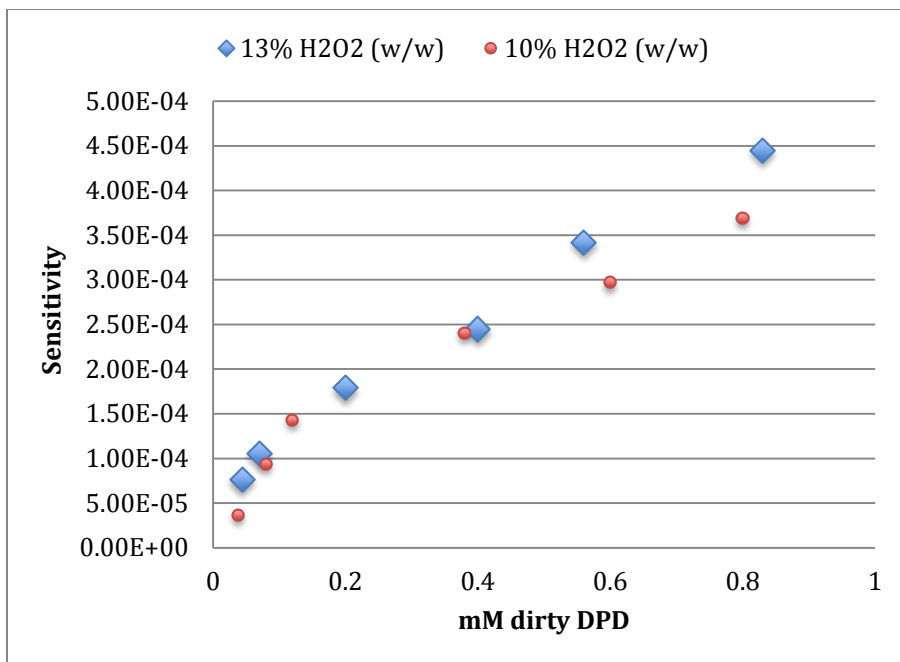
**Figure 3.2.13.** Sensitivity (defined as arbitrary slope units (gain in absorbance/time) per nM dFe) as a function of the concentration of DPD using either 10% $H_2O_2$ (w/w) (blue diamonds) or 13% $H_2O_2$ (w/w) (red circles) in the reagent mixture (see text for details).
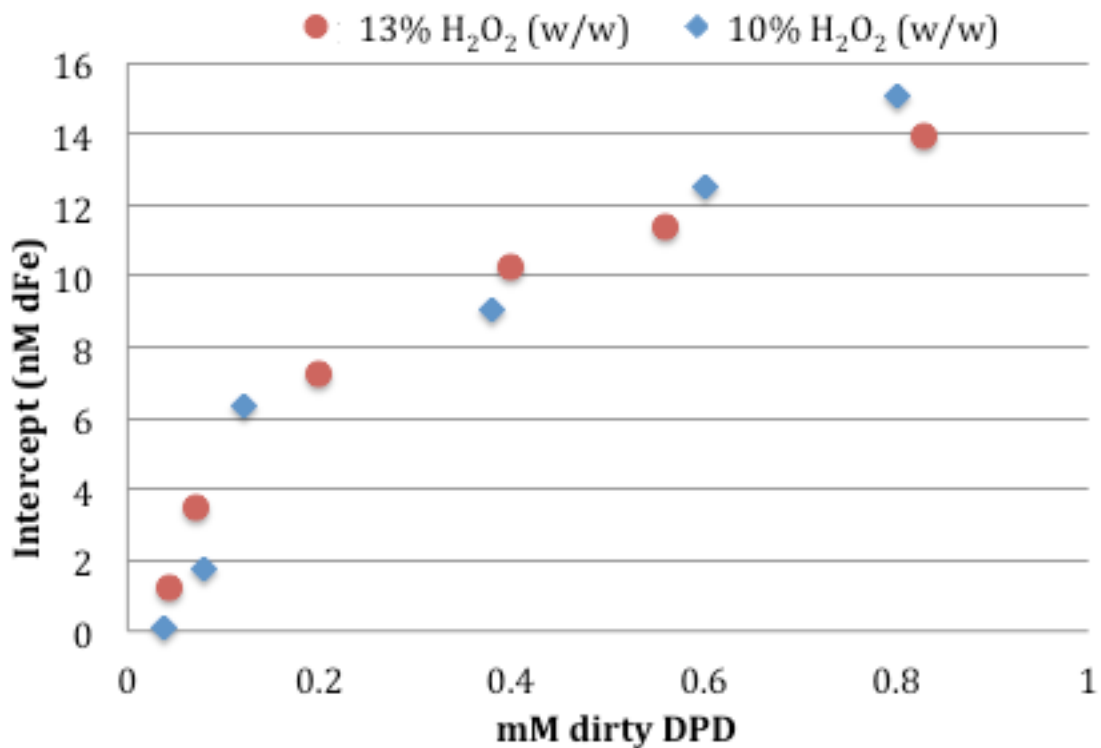
**Figure 3.2.14.** Calibration curve intercept as a function of DPD concentration using a set of seawater standards ranging from 0.4 to +5nM dFe using either 10% (w/w)(blue diamonds) or 13% $H_2O_2$ (w/w) (red circles) in the reagent mixture.
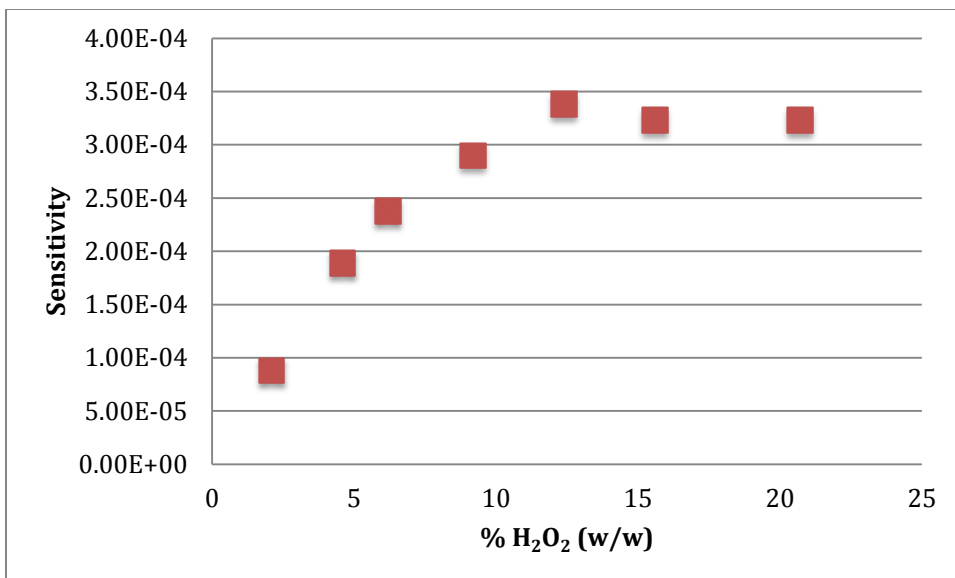
**Figure 3.2.15.** Sensitivity (defined as arbitrary slope units (gain in absorbance/time) per nM dFe) as a function of the concentration of $H_2O_2$ using ~0.4mM DPD.
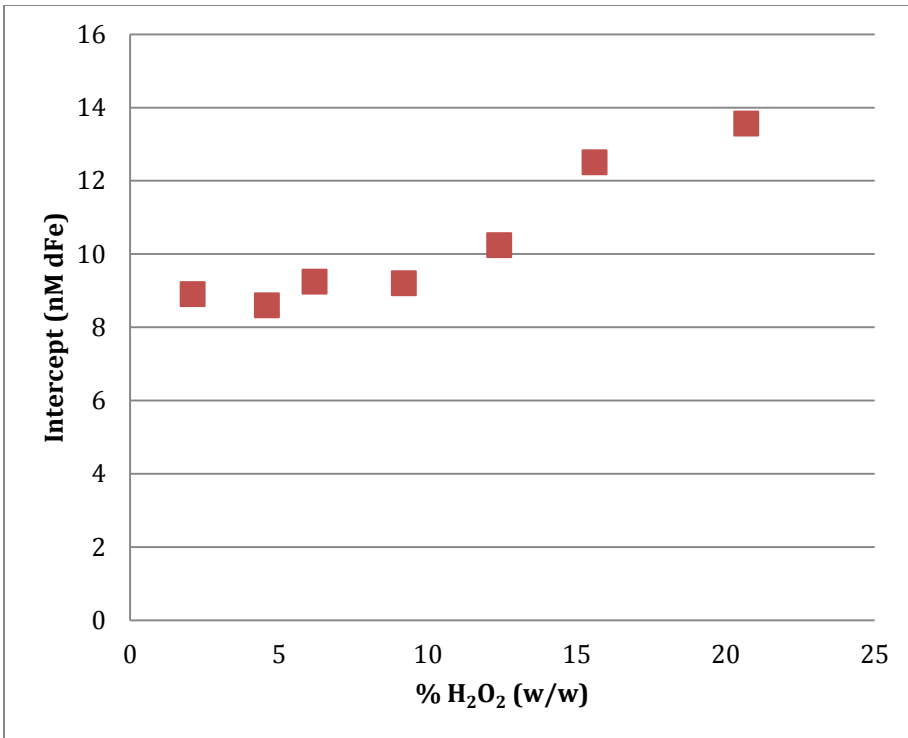
**Figure 3.2.16.** Calculated dFe intercept as a function of the concentration of $H_2O_2$ using a set of standards ranging from +0 to +5nM dFe made in filtered (0.2μm) Kaneohe bay seawater using 0.4mM DPD.
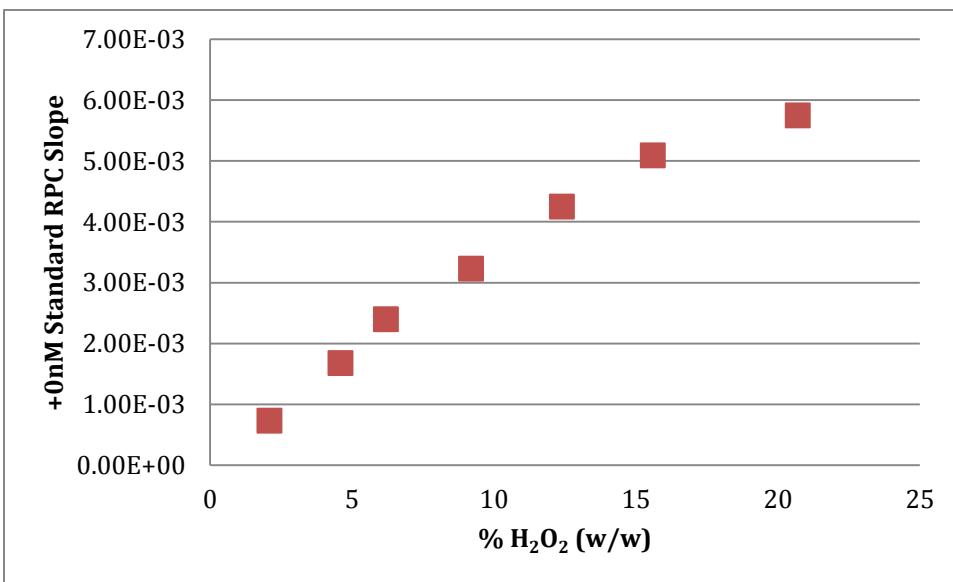


**Figure 3.2.17.** Stopped-flow slope of a 0.4nM standard as a function of % $H_2O_2$.
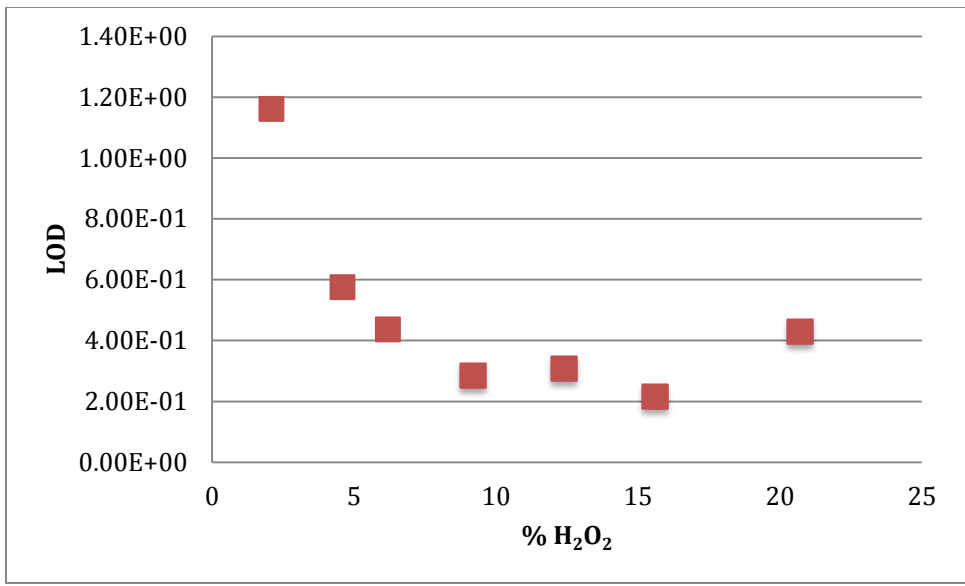
**Figure 3.2.18.** Limit of Detection (LOD) as a function of the concentration of $H_2O_2$ with 0.4mM DPD.
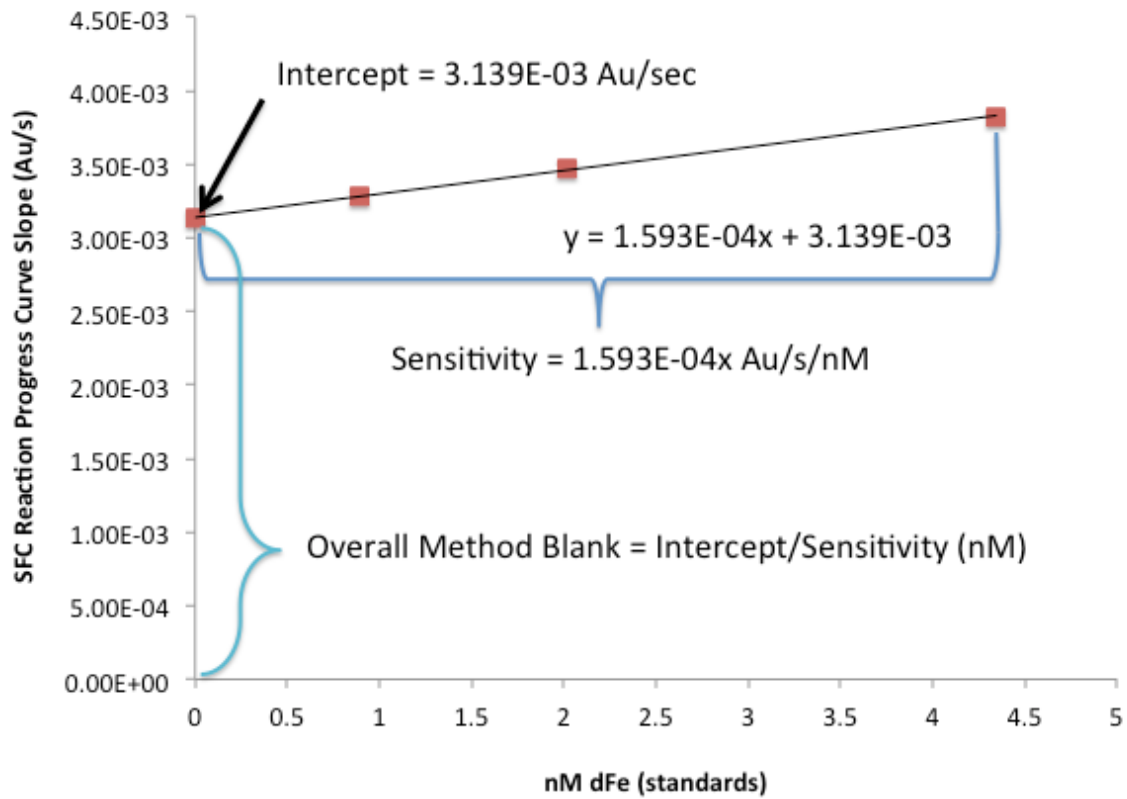
**Figure 3.3.1.** Calculating the overall method blank. This figure demonstrates how the overall method blank is calculated based on the intercept of the calibration curve and the sensitivity of the respective calibration curve.
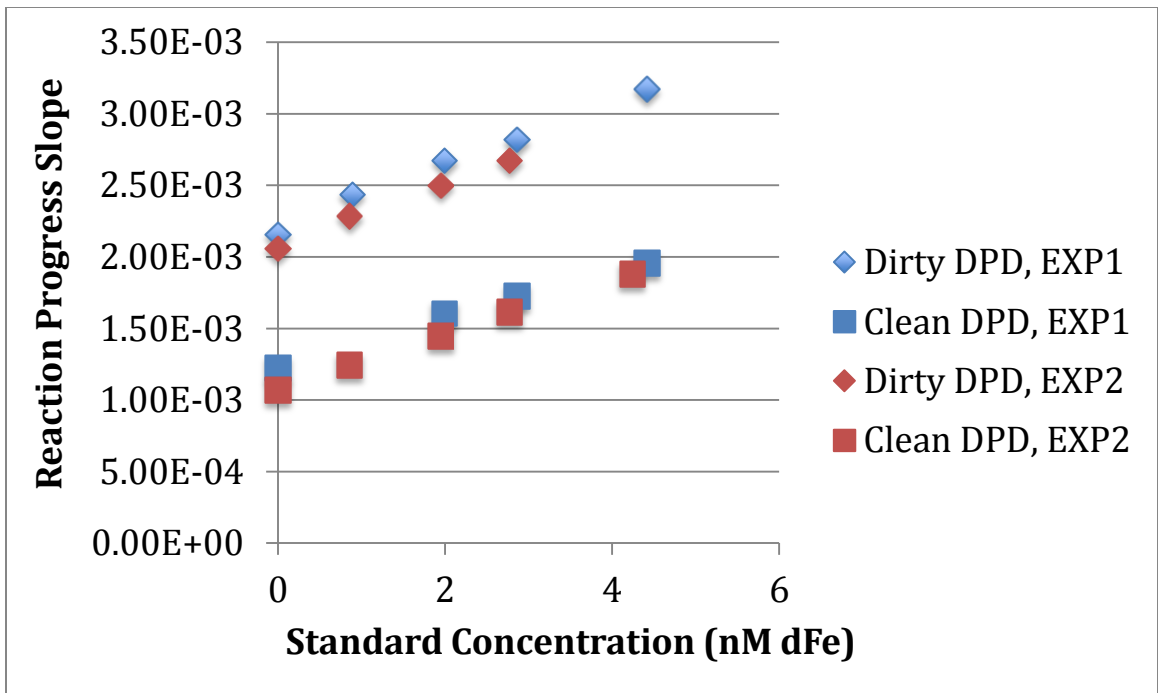
**Figure 3.3.2.** A comparison of calibration curves obtained using 0.2mM clean and

0.2mM dirty DPD acidified to pH 4.
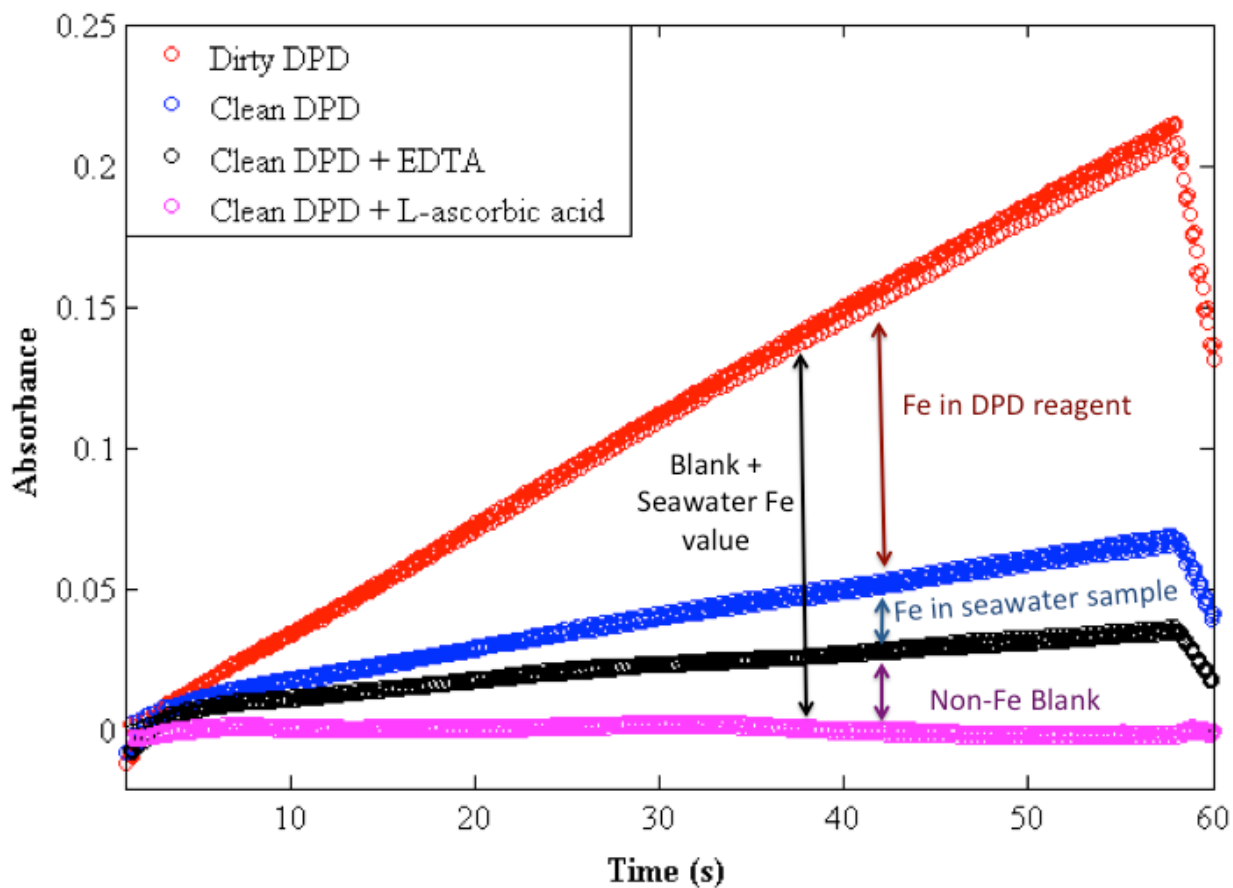
**Figure 3.3.3.** Components of the SFC absorbance signal for a seawater sample. The red reaction progress curve results from using 0.4mM DPD that has not been cleaned. The blue reaction progress curve is the absorbance using a 0.4mM DPD reagent passed over an 8-HQ column to remove Fe. The black reaction progress curve is the rate of DPDQ formation in the presence of EDTA (see text for details). The pink reaction progress curve is the absorbance in the presence of L- ascorbic acid (see text for details).
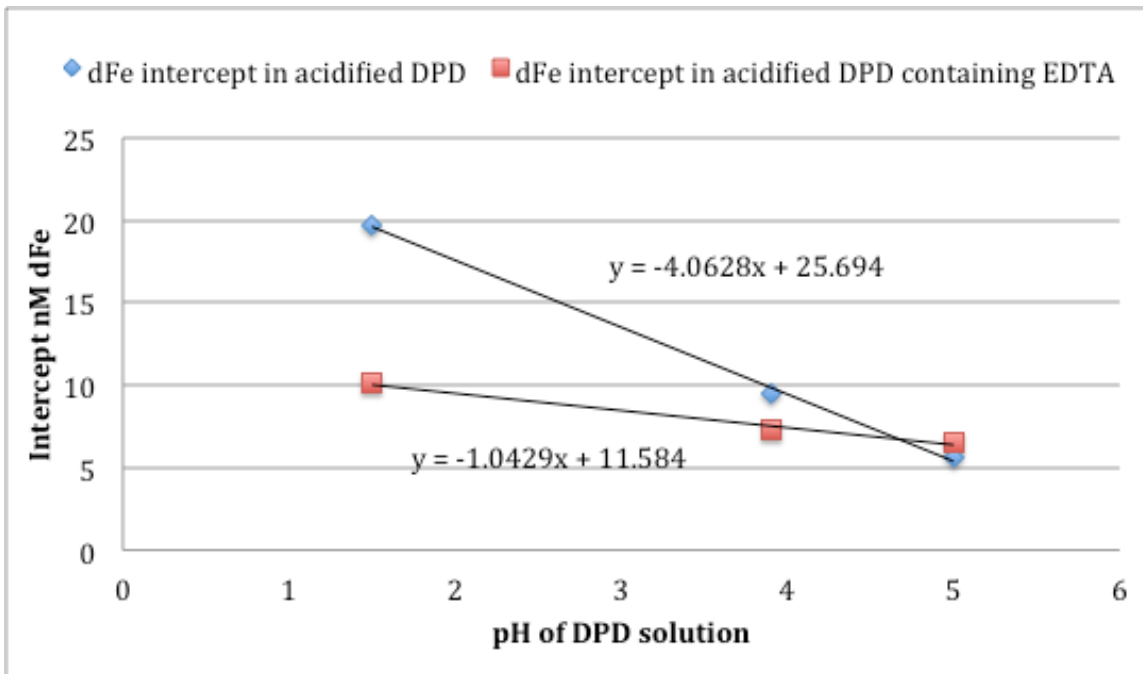
**Figure 3.3.4.** Calculated dFe intercept as a function of the pH of the DPD reagent acidified with HCl (see text for details).
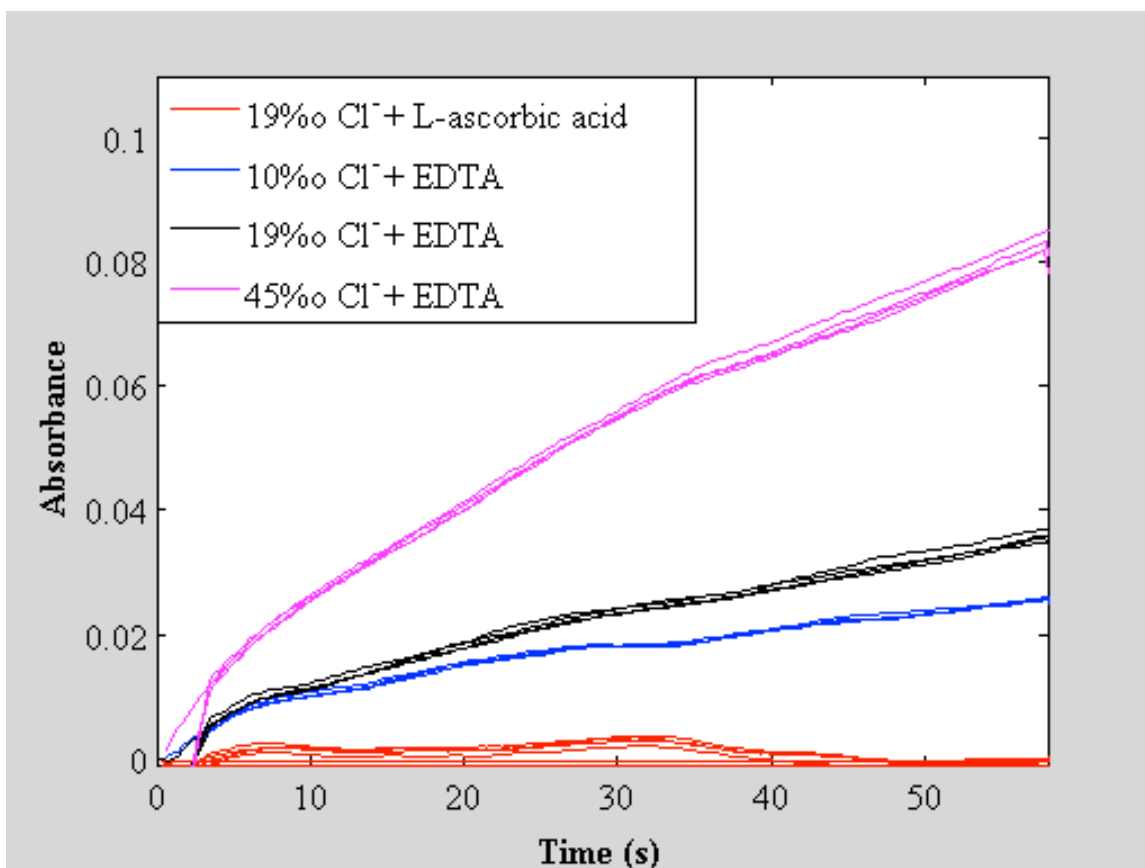
**Figure 3.3.5.** Reaction progress as a function of chloride concentration in the presence of EDTA using 0.4mM clean DPD reagent solution and a 0.6M $NH_4Ac$ & 13% $H_2O_2$ (w/w) reagent mixture (see text for details).
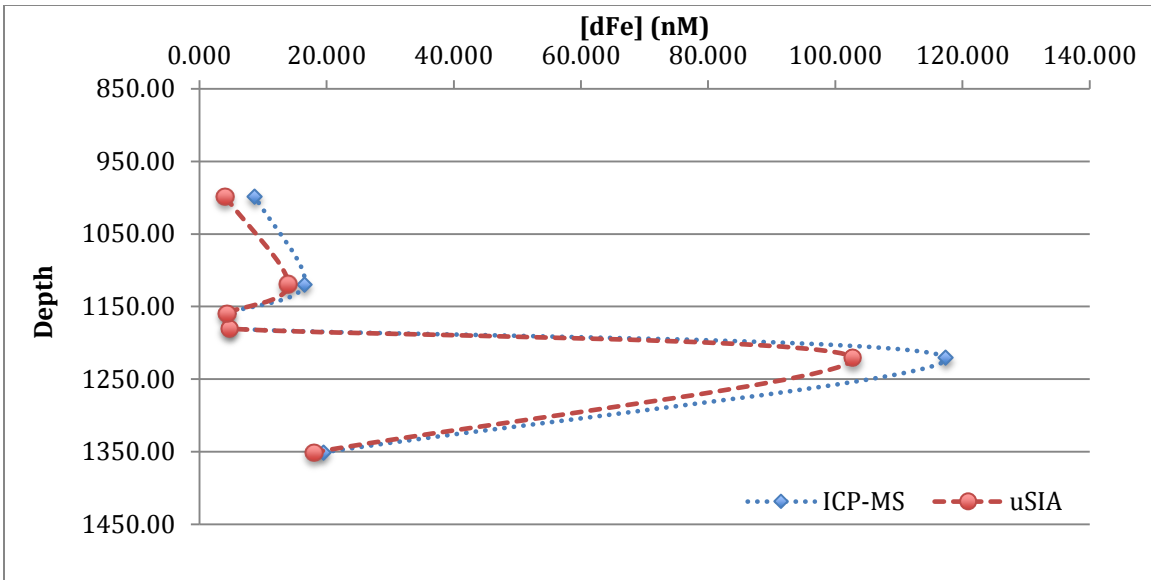
**Figure 3.4.1. µSIA vs. ICP-MS.** Vertical dFe profile from Loihi samples obtained

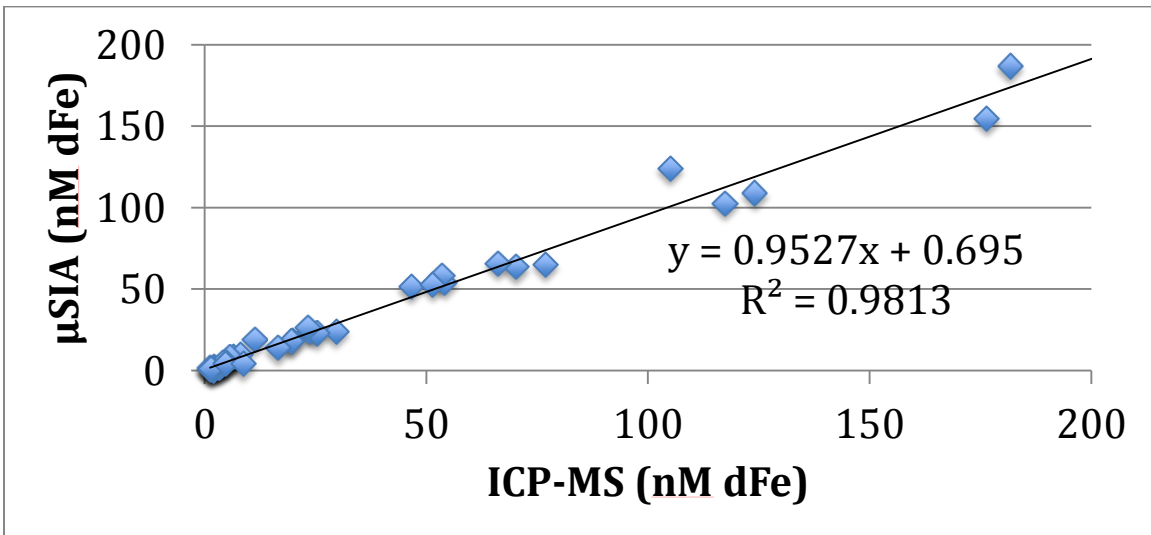using µSIA (red) and ICP-MS (Olivier Rouxel, pers. comm.) (blue).



**Figure 3.4.2.** Comparison of dFe concentrations determined by µSIA and ICP-MS

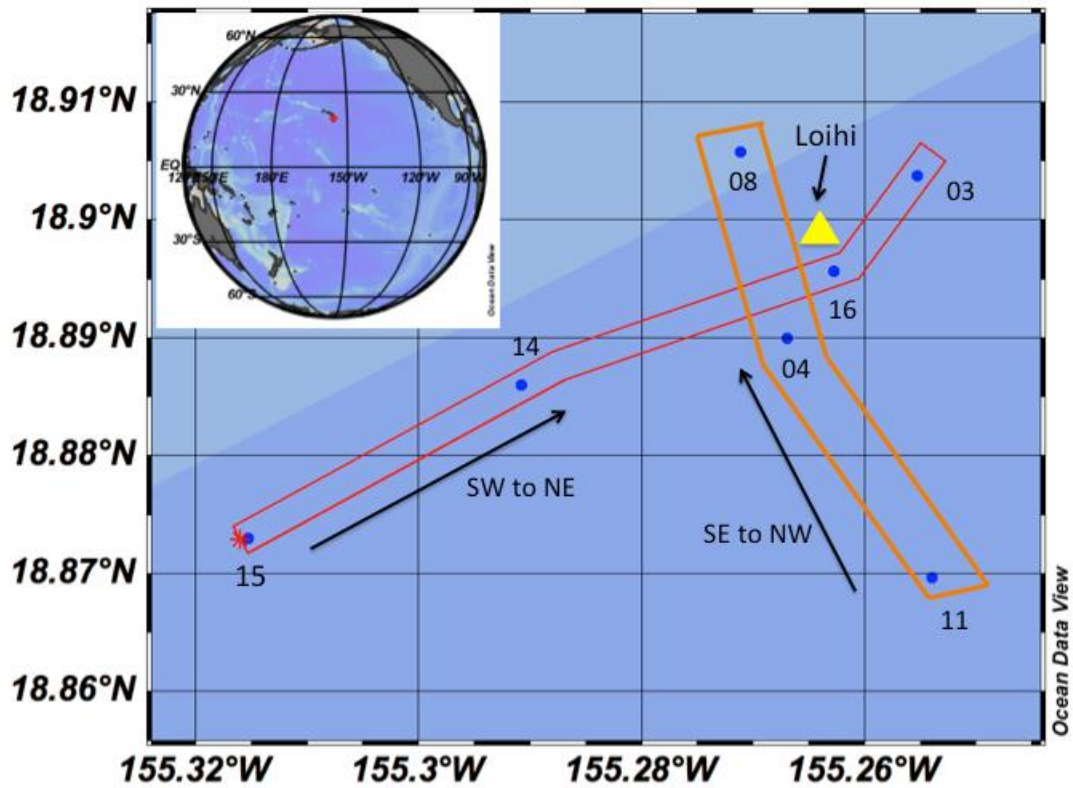(Olivier Rouxel, pers. comm.) for samples from Loihi.

**Figure 3.5.1.** The location and number of the CTD stations sampled for dFe analyses. The red box is the SW to NE, and the orange box is the SE to NW transect. The position of Loihi Seamount is shown by the yellow triangle.
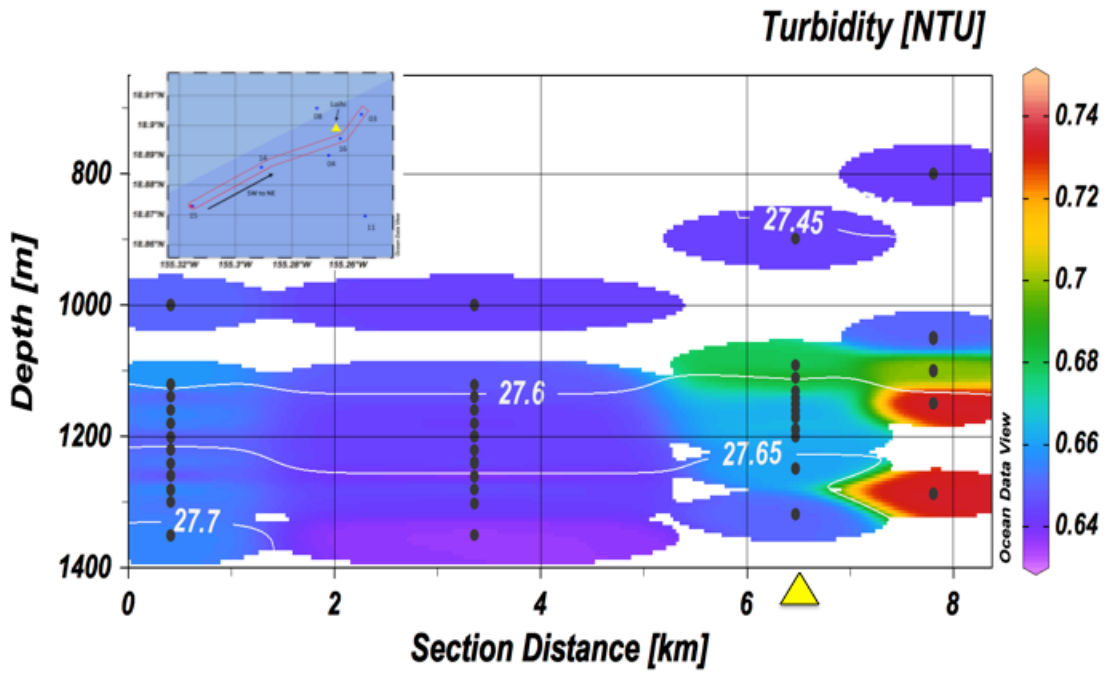
**Figure 3.5.2.** Turbidity from the hydrothermal plume dispersing from Loihi along the SW to NE transect with neutral density contours overlaid in white. The depths of the dFe samples are in black. The position of Loihi is indicated by the yellow triangle.
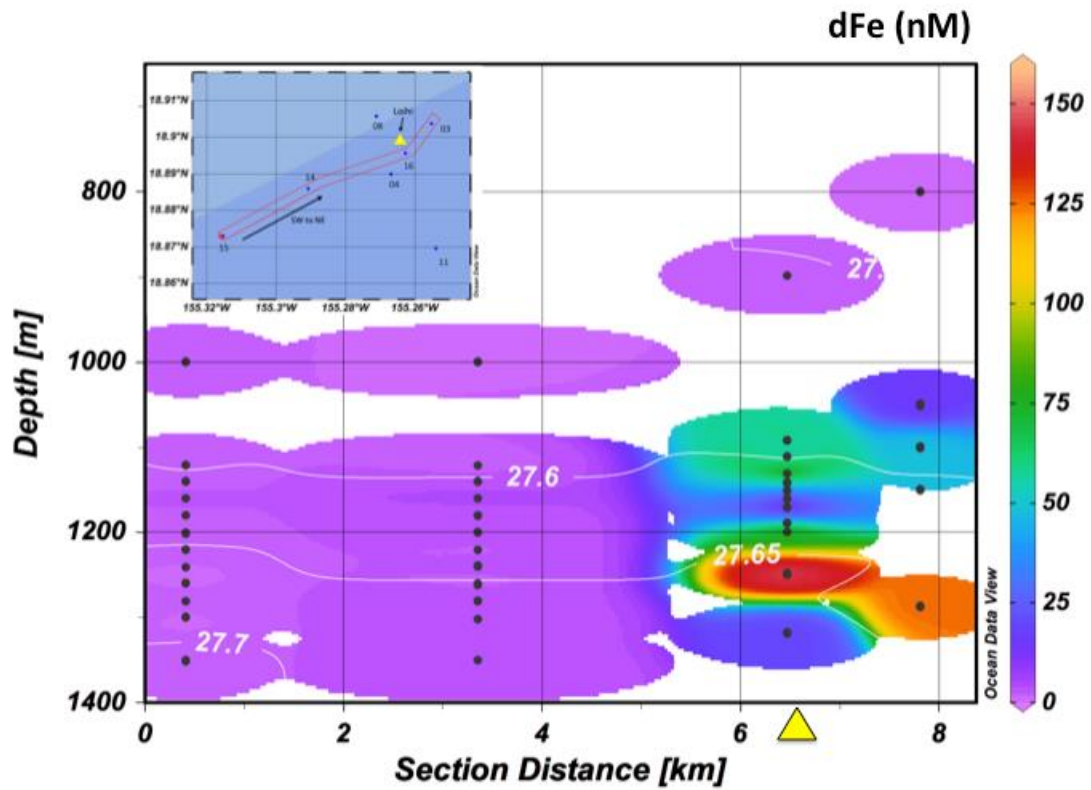
**Figure 3.5.3.** The distribution of dFe along the SW to NE transect (in color), with the neutral density contours overlaid in white. The depths of the dFe samples are in black and the position of Loihi is indicated by the yellow triangle.

**Figure 3.5.4.** Turbidity in the hydrothermal plume from Loihi along the SE to NW transect with neutral density contours overlaid in white. The depths of the dFe samples are in black and the position of Loihi is indicated by the yellow triangle.
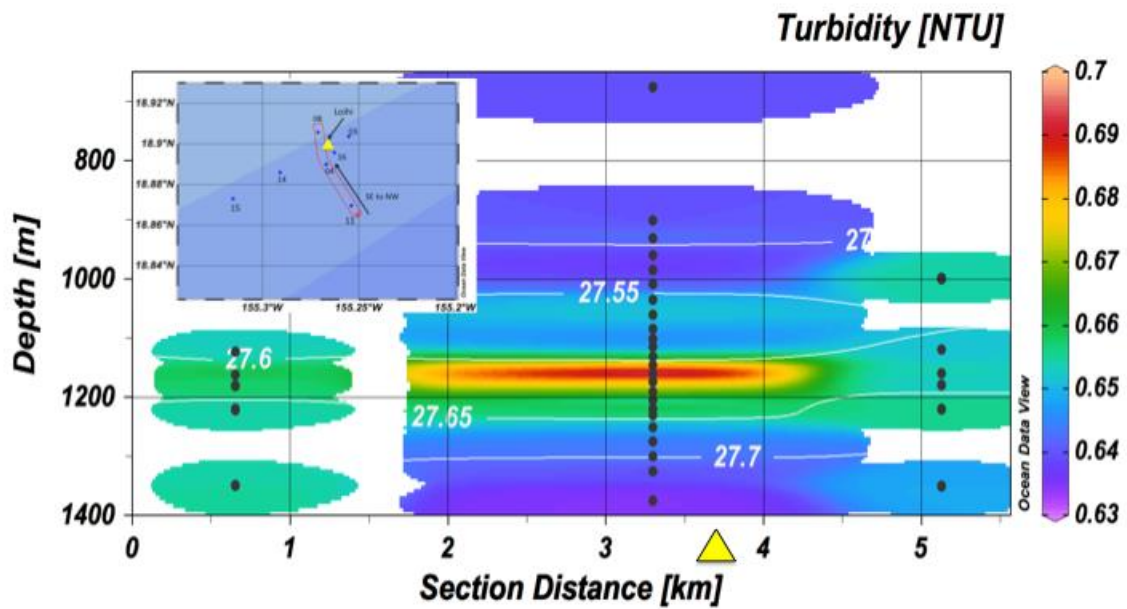
**Figure 3.5.5.** The distribution of dFe along the SW to NE transect (in color), with the neutral density contours overlaid in white.    The depths of the dFe samples are in black and the position of Loihi is indicated by the yellow triangle.
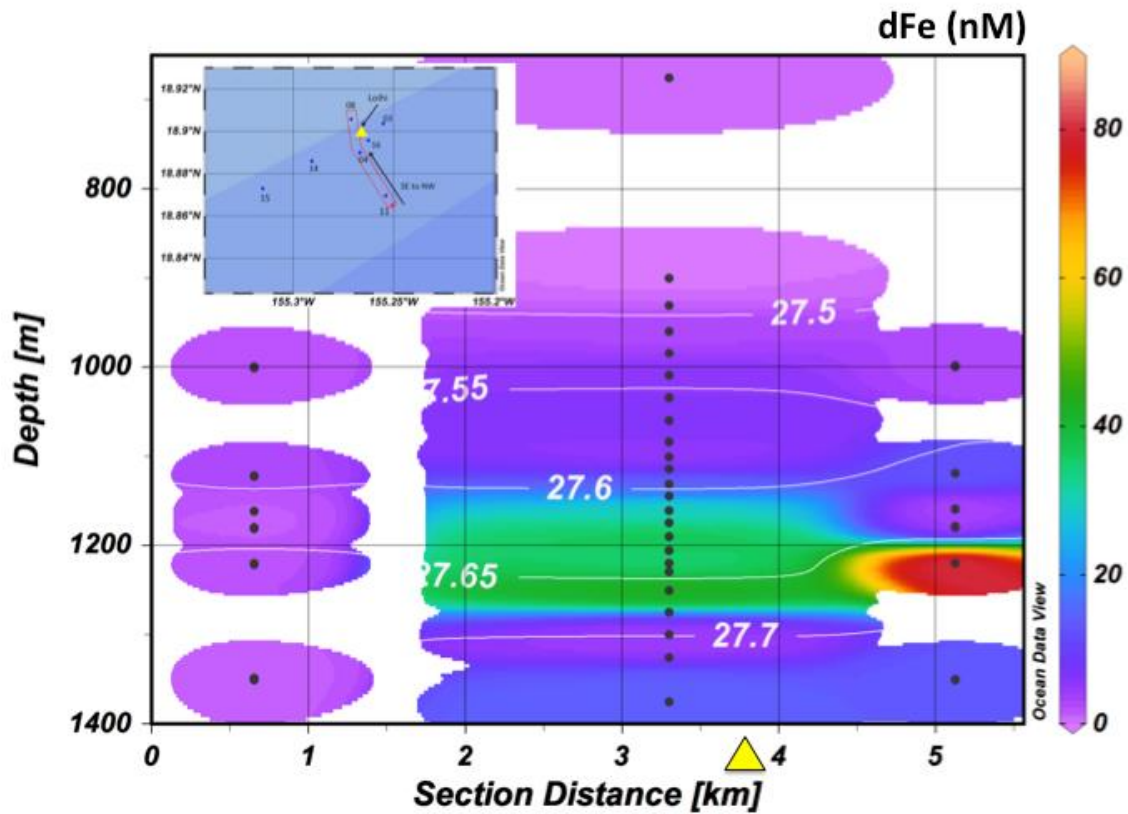
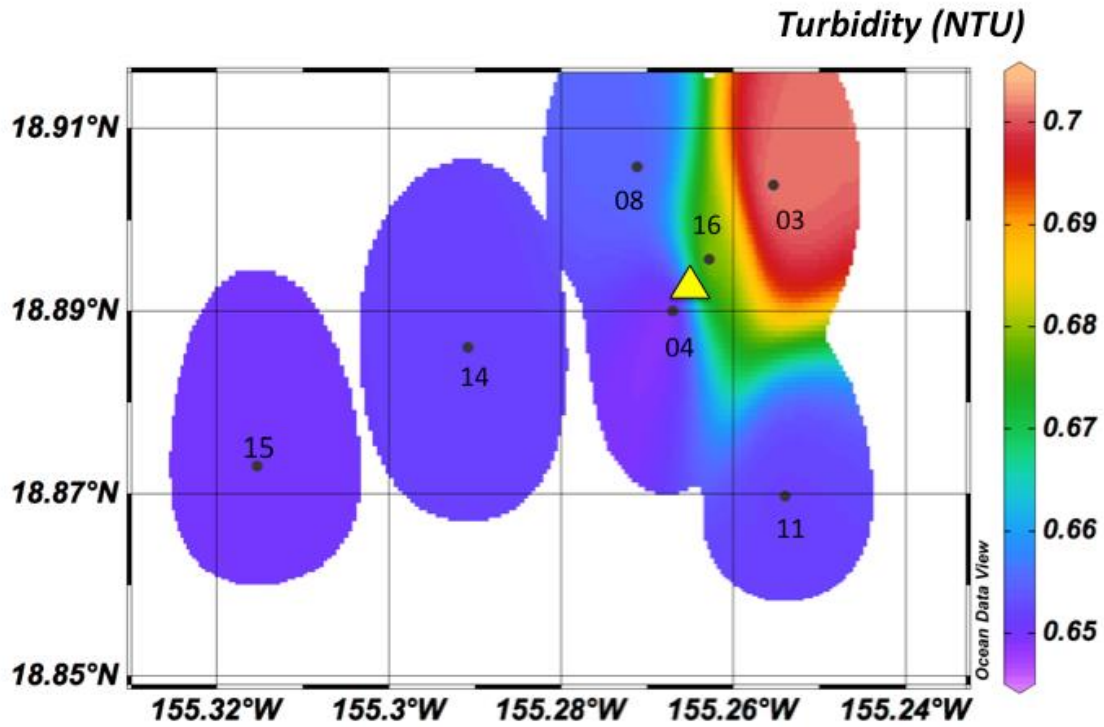**Figure 3.5.6.** Turbidity along a neutral density surface = 27.60kg/m³, ~1160m

 depth.  The corresponding station numbers are shown in black.  The yellow triangle

shows the position of Loihi.

**Figure 3.5.7.** Concentrations of dFe along a neutral density surface = 27.60 kg/m³, ~1160m depth. Station numbers are in black and the yellow triangle shows the position of Loihi.

**Figure 3.5.8.** Turbidity along a neutral density surface = 27.660kg/m³, ~1260m depth. Station numbers are in black and the yellow triangle shows the position of Loihi.
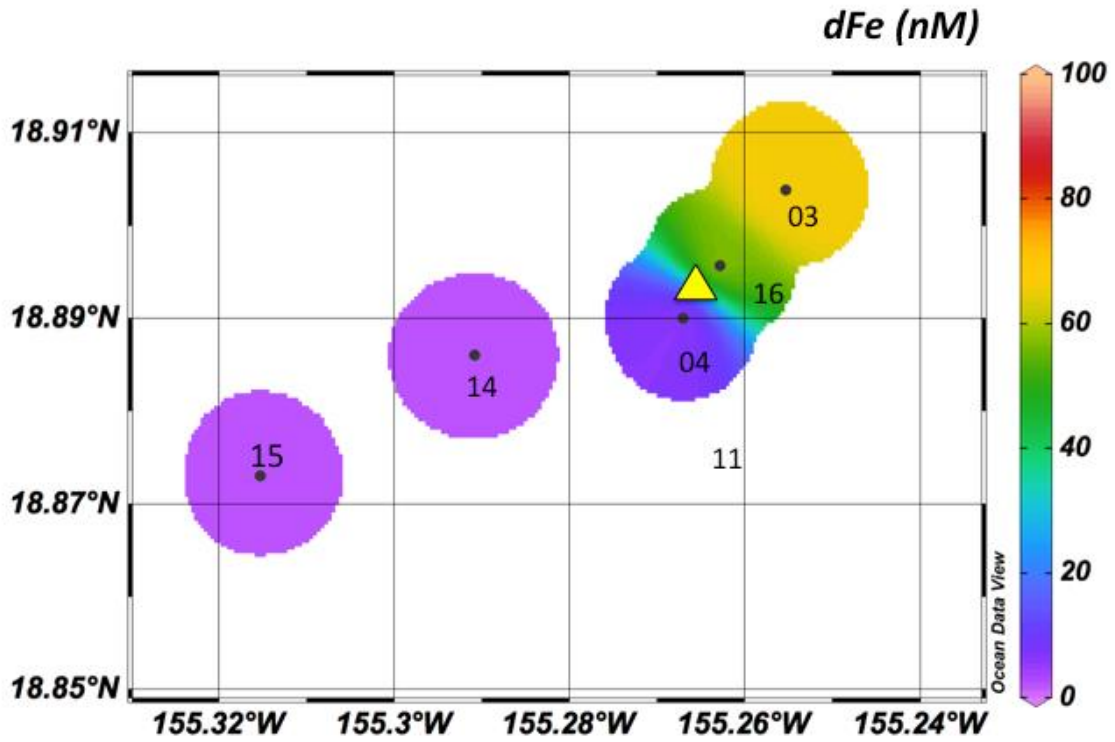
**Figure 3.5.9.** Concentrations of dFe determined along a neutral density surface = 27.660 kg/m³, ~1260m depth. Station numbers are in black and the yellow triangle shows the position of Loihi.
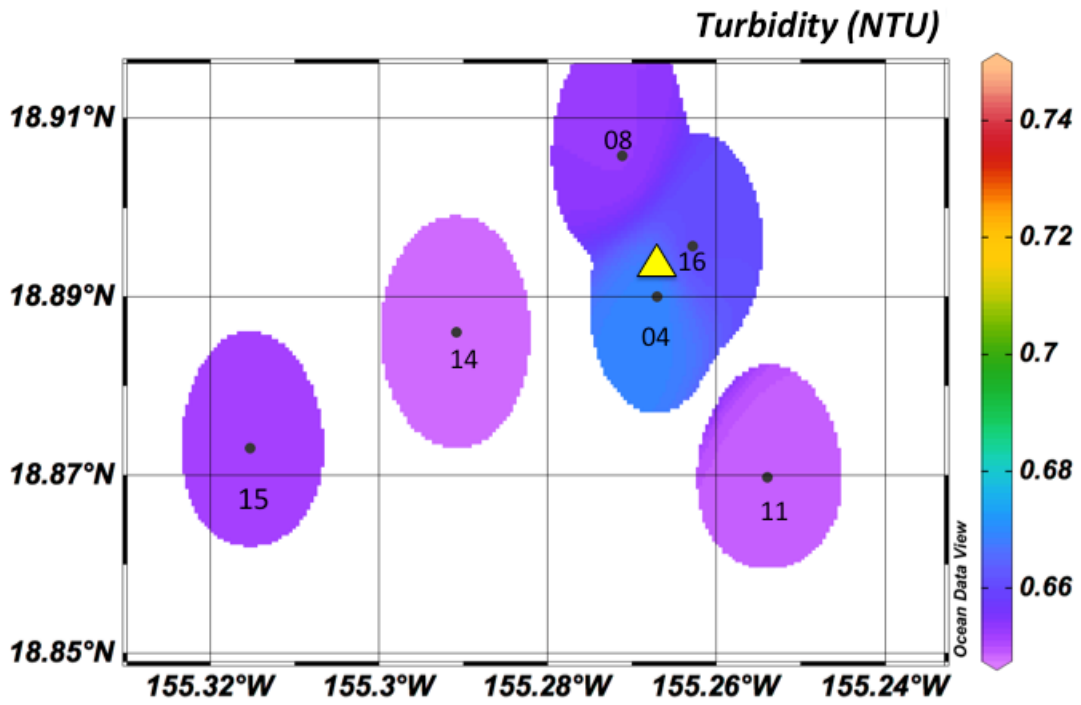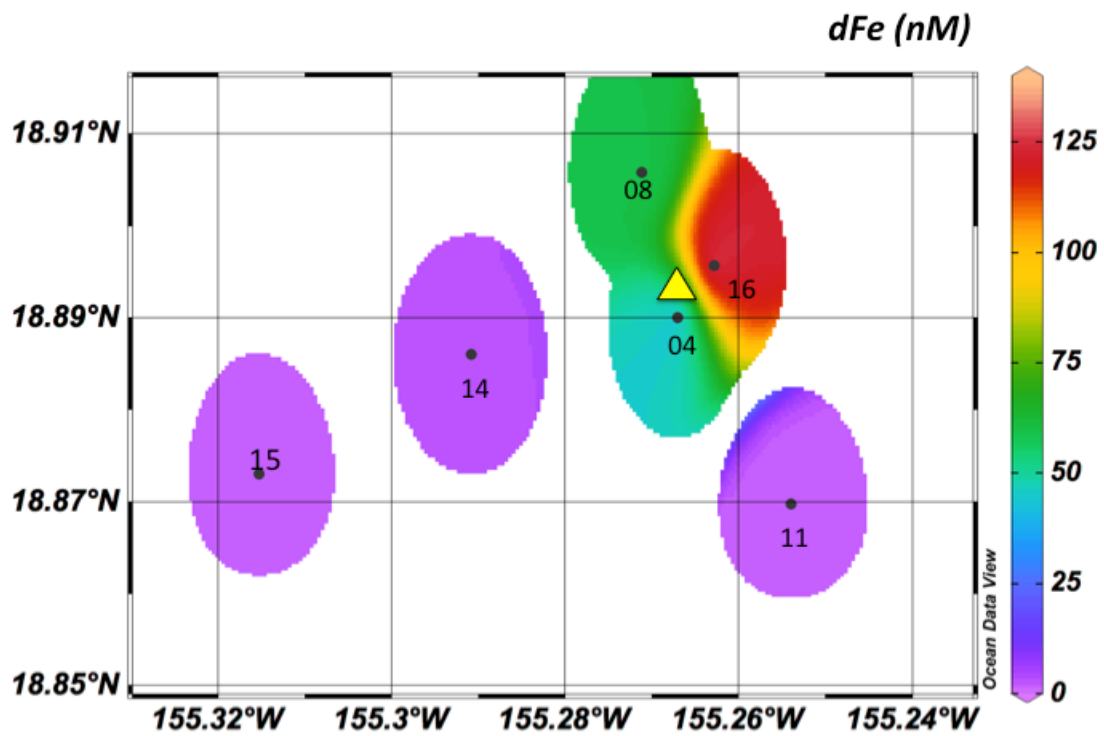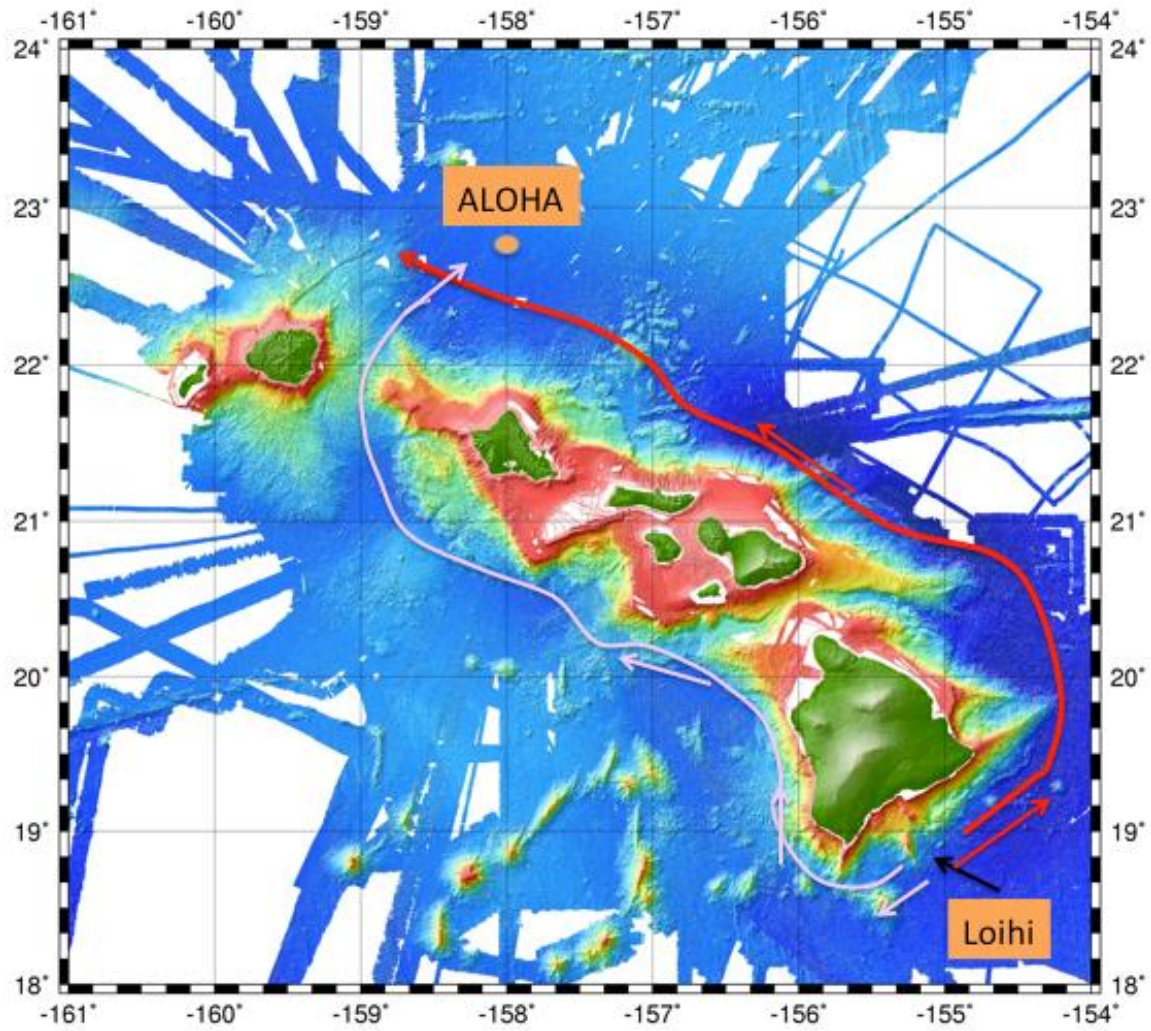
**Figure 3.5.10.** Possible hydrothermal plume transport paths from Loihi to Station ALOHA.

**REFERENCES**

Alfthan, K., & Jarvis, A. C. (1928). A new indicator for chlorine. *Journal*

    *(American Water Works Association)*, *20*(3), 407-411.

Aumont, O., & Bopp, L. (2006). Globalizing results from ocean in situ iron

    fertilization studies. *Global Biogeochemical Cycles*, *20*(2).

Bidigare, R. R. et al. (1999). Iron simulated changes in $^{13}C$ fractionation and export

    by equatorial Pacific phytoplankton: Toward a paleogrowth rate proxy.

    *Paleoceanography,* 14, 589-595.

Bishop, J. K., Wood, T. J., Davis, R. E., & Sherman, J. T. (2004). Robotic observations of

    enhanced carbon biomass and export at 55 S during SOFeX.

    *Science*, *304*(5669), 417-420.

Boyd, P. W., & Ellwood, M. J. (2010). The biogeochemical cycle of iron in the

    ocean. *Nature Geoscience*, *3*(10), 675-682.

Boyd, P. W., Law, C. S., Hutchins, D. A., Abraham, E. R., Croot, P. L., Ellwood, M., ... &

    Hare, C. (2005). FeCycle: Attempting an iron biogeochemical budget from a

    mesoscale SF6 tracer experiment in unperturbed low iron waters. *Global*

    *Biogeochemical Cycles*, *19*(4).

Boyle, E. (1997). What controls dissolved iron concentrations in the world ocean?—

    A comment. *Marine chemistry*, *57*(3), 163-167.

Boyle, E. A., Bergquist, B. A., Kayser, R. A., & Mahowald, N. (2005). Iron, manganese,

    and lead at Hawaii Ocean Time-series station ALOHA: Temporal variability

    and an intermediate water hydrothermal plume. *Geochimica et Cosmochimica*

    *Acta*, *69*(4), 933-952.

Bruland, K. W., & Rue, E. L. (2001). Iron: analytical methods for the determination of concentrations and speciation. *The Biogeochemistry of Iron in Seawater*, 255-289.

Buesseler, K. O., Andrews, J. E., Pike, S. M., Charette, M. A., Goldson, L. E., Brzezinski, M. A., & Lance, V. P. (2005). Particle export during the southern ocean iron experiment (SOFeX). *Limnology and Oceanography*, *50*(1), 311-327.

Coale, K. H., Johnson, K. S., Fitzwater, S. E., Blain, S. P. G., Stanton, T. P., and Coley, T. L. (1998). IronEx-I, an in situ iron-enrichment experiment: Experimental design, implementation and results. Deep Sea Res., Part II, 45, 919 – 945.

de Baar, H. J., & de Jong, J. T. (2001). Distributions, sources and sinks of iron in seawater. *IUPAC series on analytical and physical chemistry of environmental systems*, *7*, 123-254.

Dias, A. C. B., Borges, E. P., Zagatto, E. A., & Worsfold, P. J. (2006). A critical examination of the components of the Schlieren effect in flow analysis. *Talanta*, *68*(4), 1076-1082.

Edmond, J. M., Measures, C., Mangum, B., Grant, B., Sclater, F. R., Collier, R., ... & Corliss, J. B. (1979a). On the formation of metal-rich deposits at ridge crests. *Earth and Planetary Science Letters*, *46*(1), 19-30.

Edmond, J. M., Measures, C., McDuff, R. E., Chan, L. H., Collier, R., Grant, B., ... & Corliss, J. B. (1979b). Ridge crest hydrothermal activity and the balances of the major and minor elements in the ocean: the Galapagos data.*Earth and Planetary Science Letters*, *46*(1), 1-18.

Elrod, V. A., Berelson, W. M., Coale, K. H., & Johnson, K. S. (2004). The flux of iron

from continental shelf sediments: A missing source for global budgets.

*Geophysical Research Letters*, *31*(12).

Fitzsimmons, J. N., Hayes, C. T., Al-Subiai, S. N., Zhang, R., Morton, P. L., Weisend, R. E.,

... & Boyle, E. A. (2015). Daily to decadal variability of size-fractionated iron

and iron-binding ligands at the Hawaii Ocean Time-series Station

ALOHA. *Geochimica et Cosmochimica Acta*, *171*, 303-324.


Fitzsimmons, J. N., Zhang, R., & Boyle, E. A. (2013). Dissolved iron in the tropical

North Atlantic Ocean. *Marine Chemistry*, *154*, 87-99.

Grand, M., Oliveira, H. M., & Ruzicka, J. (2011). Determination of dissolved zinc in

seawater using micro-Sequential Injection lab-on-valve with fluorescence

detection. *Analyst*, *136*(13), 2747-2755.

Hawkes, J. A., Connelly, D. P., Gledhill, M., & Achterberg, E. P. (2013). The

stabilisation and transportation of dissolved iron from high temperature

hydrothermal vent systems. *Earth and Planetary Science Letters*, *375*, 280-

290.

Hedenquist, J. W., & Lowenstern, J. B. (1994). The role of magmas in the formation of

hydrothermal ore deposits. *Nature*, *370*(6490), 519-527.

Hirayama, K., & Unohara, N. (1988). Spectrophotometric catalytic determination of

an ultratrace amount of iron (III) in water based on the oxidation of N, N-

dimethyl-p-phenylenediamine by hydrogen peroxide. *Analytical*

*Chemistry*, *60*(23), 2573-2577.

Hudson, R. J., Morel, F. M., & Morel, F. M. M. (1990). Iron transport in marine phytoplankton: Kinetics of cellular and medium coordination reactions. *Limnol. Oceanogr*, *35*(5), 1002-1020.

Jickells, T. D., An, Z. S., Andersen, K. K., Baker, A. R., Bergametti, G., Brooks, N., ... & Kawahata, H. (2005). Global iron connections between desert dust, ocean biogeochemistry, and climate. *science*, *308*(5718), 67-71.

Johnson, K. S., Boyle, E., Bruland, K., Coale, K., Measures, C., Moffett, J., ... & Wu, J. (2007). The SAFe Iron Intercomparison Cruise: An International Collaboration to Develop Dissolved Iron in Seawater Standards. Eos,

Johnson, K. S., Gordon, R. M., & Coale, K. H. (1997). What controls dissolved iron concentrations in the world ocean?. *Marine Chemistry*, *57*(3), 137-161.

Kalnejais, L. H., Martin, W. R., & Bothner, M. H. (2010). The release of dissolved nutrients and metals from coastal sediments due to resuspension. *Marine Chemistry*, *121*(1), 224-235.

King, D. W., Lounsbury, H. A., & Millero, F. J. (1995). Rates and mechanism of Fe (II) oxidation at nanomolar total iron concentrations. *Environmental science & technology*, *29*(3), 818-824.

Kinnan, M. K. (2003). Determination of Iron (II) Concentrations in Seawater Using Flow Injection Analysis and Chemiluminescence.

Landing, W. M., Haraldsson, C., and Paxeus, N. (1986), Vinyl polymer agglomerate based transition metal cation chelating ion-exchange resin contaminant the 8-hydroxyquinoline functional group. *Anal. Chem., 58* (14), 3031-3035.

Lis, H., Shaked, Y., Kranzler, C., Keren, N., & Morel, F. M. (2015). Iron bioavailability

to phytoplankton: an empirical approach. *The ISME journal*, *9*(4), 1003-1013.

Lohan, M. C., Aguilar- Islas, A. M., & Bruland, K. W. (2006). Direct determination of iron in acidified (pH 1.7) seawater samples by flow injection analysis with catalytic spectrophotometric detection: Application and intercomparison, *Limnology and Oceanography*: Methods, 4, 164-171.

Lohan, M. C., Aguilar-Islas, A. M., Franks, R. P., and Bruland, K. W. (2005), Determination of iron and copper in seawater at pH 1.7 with a new commercially available chelating resin. NTA Superflow, *Analytica Chimica Acta*, 530, 121-129.

Malahoff, A., Kolotyrkina, I. Y., Midson, B. P., & Massoth, G. J. (2006). A decade of exploring a submarine intraplate volcano: Hydrothermal manganese and iron at Lōʻihi volcano, Hawaiʻi. *Geochemistry, Geophysics, Geosystems*, *7*(6).

Martin, J.H. (1990) Glacial-interglacial CO2 change: The iron hypothesis. *Paleoceanography, 5*(1):1–13, http://dx.doi.org/10.1029/PA005i001p00001.

Martin, J.H, Coale, K.H., Johnson, K.S., Fitzwater, S.E., Gordon, R.M., Tanner, S.J., … & Tindale, N.W. (1994) Testing the iron hypothesis in ecosystems of the equatorial Pacific Ocean. Nature, 371, 123-129. doi:10.1038/371123a0.

Martin, J.H., and Fitzwater, S.E. (1988). Iron deficiency limits phytoplankton growth in the north-east Pacific subarctic. *Nature,* 331:341–343, http://dx.doi.org/ 10.1038/331341a0.

Martin, J. H., Fitzwater, S. E., and Gordon, M. (1990) Iron deficiency limits phytoplankton growth in Antarctic waters. *Global Biogeochemical Cycles*, *4*(1), 5-12.

Martin, J.H., Fitzwater, S.E., Gordon, R.M., Hunter, C.N., and Tanner, S.J. (1993) Iron, primary production and carbon-nitrogen flux studies during the JGOFS North Atlantic bloom experiment. *Deep-Sea Res. II Top. Stud. Oceanogr.*, *40* (1–2), pp. 115–134.

Measures, C.I., J. Yuan and J.A. Resing, 1995. Determination of iron in seawater by flow injection analysis using in-line preconcentration and spectrophotometric detection. Mar. Chem., 50, 3-12.

Measures, C.I., M. Hatta, and M.M. Grand. 2012. Bioactive trace metal distributions and biogeochemical controls in the Southern Ocean. *Oceanography,* 25(3), 122–133, http://dx.doi.org/10.5670/oceanog.2012.85.

Millero, F. J., Yao, W., & Aicher, J. (1995). The speciation of Fe (II) and Fe (III) in natural waters. *Marine Chemistry*, *50*(1), 21-39.

Moore, J. K. & O. Braucher (2007) Observation of dissolved iron concentrations in the World Ocean: implications and constraints for ocean biogeochemical models, Biogeosciences Discuss., 4, 1241-1277.

Morel, F. M., Kustka, A. B., & Shaked, Y. (2008). The role of unchelated Fe in the iron nutrition of phytoplankton. *Limnology and Oceanography*, *53*(1), 400-404.

Obata, H. and van den Berg, C. M. G. (2001). Determination of picomolar levels of iron in seawater using catalytic cathodic stripping voltammetry. *Anal. Chem.* 73, 2522-2528.

Oliveira, H. M., M. M. Grand, J. Ruzicka, C. I. Measures (2015). Towards chemiluminescence detection in micro-sequential injection lab-on-valve

format: A proof of concept based on the reaction between Fe(II) and luminol in seawater. *Talanta*, 133, 107-111.

Palin, A. T. (1945). The determination of free chlorine and of chloramine in water using p-aminodimethylaniline. *Analyst*, *70*(831), 203-207.

Petri, B. G., Watts, R. J., Teel, A. L., Huling, S. G., & Brown, R. A. (2011). Fundamentals of ISCO using hydrogen peroxide. In *In situ chemical oxidation for groundwater remediation* (pp. 33-88). Springer New York.

Rijkenberg MJA, Middag R, Laan P, Gerringa LJA, van Aken HM, et al. (2014) The Distribution of Dissolved Iron in the West Atlantic Ocean. *PLoS ONE,* 9(6).

Rue, E. L., and K. W. Bruland (1995) Complexation of iron(III) by natural organic ligands in the Central North Pacific as determined by a new competitive ligand equilibration/adsorptive cathodic stripping voltammetric method. *Mar. Chem.,* 50 (1–4), pp. 117–138.

Ruzicka, J. (2009), Flow Injection Analysis, 4th Edition, *E-monograph DVD*, self–published at www.flowinjection.com. Available from: jarda@flowinjection.com.

Ruzicka, J., & Hansen, E. H. (1988). Homogeneous and heterogeneous systems: Flow injection analysis today and tomorrow. *Analytica Chimica Acta*, *214*, 1-27.

Sakai, H., Tsubota, H., Nakai, T., Ishibashi, J., Akagi, T., Gamo, T., ... & Nakamura, S. (1987). Hydrothermal activity on the summit of Loihi Seamount, Hawaii. *Geochemical Journal*, *21*(1), 11-21.

Seyfried, W. E., & Mottl, M. J. (1982). Hydrothermal alteration of basalt by seawater under seawater-dominated conditions. *Geochimica et Cosmochimica Acta*, *46*(6), 985-1002.

Shaked, Y., & Lis, H. (2012). Disassembling iron availability to phytoplankton. *Environmental Bioinorganic Chemistry of Aquatic Microbial Organisms*, 28.

Sholkovitz, E. R., E. A. Boyle, and N. B. Price (1978) The removal of dissolved humic acids and iron during estuarine mixing, Earth and Planetary Science Letters, 40, 130-136.

Stookey, L. L. (1970) Ferrozine- A new spectrophotometric reagent for iron. Anal. Chem., 42(7), 779-781.

Sunda W.G. and Huntsman S.A. (1997). Interrelated influence of iron, light and cell size on marine phytoplankton growth. *Nature* **390**: 389–392.

Sunda, W. G., & Huntsman, S. A. (2015). High iron requirement for growth, photosynthesis, and low-light acclimation in the coastal cyanobacterium *Synechococcus bacillaris. Frontiers in Microbiology*, *6*, 561. http://doi.org/10.3389/ fmicb.2015.00561.

Tagliabue, A., Bopp, L., Dutay, J. C., Bowie, A. R., Chever, F., Jean-Baptiste, P., ... & Aumont, O. (2010). Hydrothermal contribution to the oceanic dissolved iron inventory. *Nature Geoscience*, *3*(4), 252-256.

Tarvin, D., Todd, H. R., & Buswell, A. M. (1934). The determination of free chlorine. *Journal (American Water Works Association)*, *26*(11), 1645-1662.

Tivey, M. K. (2007). Generation of seafloor hydrothermal vent fluids and associated mineral deposits.

Von Damm, K. L. (1995). Controls on the chemistry and temporal variability of seafloor hydrothermal fluids. *Seafloor Hydrothermal Systems: Physical, Chemical, Biological, and Geological Interactions*, 222-247.

Watson A.J., Bakker D.C.E., Ridgwell A.J., Boyd P.W. and Law C.S. (2000). Effect of iron supply in Southern Ocean CO2 uptake and implications for glacial atmospheric CO2. *Nature*, 407 (12 October) 730-733.

Wells, M. L, N. M. Price, and K. W. Bruland (1995) Iron chemistry in seawater and its relationship to phytoplankton: a workshop report, Marine Chemistry, 48, 157-182.

Wu J, Wells ML, Rember R. (2011) Dissolved iron anomaly in the deep tropical-subtropical Pacific: Evidence for long-range transport of hydrothermal iron. *Geochim Cosmochim Acta, 75*(2): 460–468.